

THEORETICAL AND EXPERIMENTAL INVESTIGATIONS
OF THE FLOCCULATION OF CHARGED PARTICLES
IN AQUEOUS SOLUTIONS BY POLYELECTROLYTES
OF OPPOSITE CHARGE

Thesis by
Dennis Robert Kasper

In Partial Fulfillment of the Requirements
For the Degree of
Doctor of Philosophy

California Institute of Technology

Pasadena, California

1971

(Submitted May 18, 1971)

ACKNOWLEDGMENTS

To Professor James J. Morgan, my deepest appreciation and most sincere gratitude. His patience, encouragement and guidance were invaluable to the completion of this work. I wish also to thank Professor Jack E. McKee and the many other members of the faculty who have aided me in my work.

The author was supported during this work by a U. S. Public Health Service Training Grant. This financial support is gratefully acknowledged.

I wish to thank all of the graduate students in the group, and in particular Daniel P.-Y. Chang and Francois M. Morel, for numerous discussions and suggestions.

The help of the following is also appreciated: Miss Jasenka Vuceta for her aid in performing some of the experiments; Mr. Elton Daly and Mr. Robert Greenway for their aid in design and construction of apparatus; Mr. Carl Green for the preparations of some of the drawings; and Mrs. Marge Connely for her expert typing of this manuscript. A debt of gratitude is owed to my parents who have always supplied encouragement.

Finally, and with most affection, I thank my wife, Jeanne, for her indulgence, encouragement and devotion given throughout the course of this study.

ABSTRACT

An electrostatic mechanism for the flocculation of charged particles by polyelectrolytes of opposite charge is proposed. The difference between this and previous electrostatic coagulation mechanisms is the formation of charged polyion patches on the oppositely charged surfaces. The size of a patch is primarily a function of polymer molecular weight and the total patch area is a function of the amount of polymer adsorbed. The theoretical predictions of the model agree with the experimental dependence of the polymer dose required for flocculation on polymer molecular weight and solution ionic strength.

A theoretical analysis based on the Derjaguin-Landau, Verwey-Overbeek electrical double layer theory and statistical mechanical treatments of adsorbed polymer configurations indicates that flocculation of charged particles in aqueous solutions by polyelectrolytes of opposite charge does not occur by the commonly accepted polymer-bridge mechanism.

A series of 1,2-dimethyl-5-vinylpyridinium bromide polymers with a molecular weight range of 6×10^3 to 5×10^6 was synthesized and used to flocculate dilute polystyrene latex and silica suspensions in solutions of various ionic strengths. It was found that with high molecular weight polymers and/or high ionic strengths the polymer dose required for flocculation is independent of molecular weight. With low molecular weights and/or low ionic strengths, the flocculation dose decreases with increasing molecular weight.

TABLE OF CONTENTS

Part	Title	Page
Chapter I	Introduction	1
A.	General background	1
B.	Water composition and polymer properties	2
C.	Purpose of the present work	4
Chapter II	Theoretical analysis of polymer bridging in terms of the diffuse electrical double layer theory and adsorbed polymer configurations	5
A.	Polyelectrolytes in solution	5
1.	Definitions	5
2.	Solution configurations	7
B.	Mechanisms for polymer aggregation of particles	9
C.	Particle stability	15
1.	Potential energy of interaction between particles	15
2.	Stern corrections	19
3.	Specific ion adsorption and reversal of zeta potential	21
4.	Distance of closest approach	24
a.	Definition	24
b.	Dependence of DCA on system parameters	27
D.	Adsorbed polymer configuration	39
1.	Configurations based on empirical adsorption data	41
2.	Measurement of adsorbed layer thickness	44
3.	Statistical mechanical treatments	45
a.	Thermodynamics of adsorption	45
b.	Adsorbed configuration	46
E.	The improbability of a bridging mechanism in polyelectrolyte flocculation of particles of opposite charge	58

Part	Title	Page
Chapter III	An electrostatic patch model of polymer flocculation	62
A.	Description	62
	1. Polymer configuration	62
	2. Electrical double layers	62
	3. Effect of molecular weight on patch size	67
	4. Effect of solution composition on patch model	70
B.	Mathematical modeling of the electrostatic patch mechanism	71
	1. Computer program	71
	2. Effects of molecular weight and ionic strength	73
Chapter IV	Experimental materials and methods	81
A.	Polymer synthesis	81
	1. Radioactive methyl bromide	81
	2. Monomer synthesis	84
	3. Polymerization	85
	a. Reactions	85
	b. Procedure	86
	c. Concentrations of initiator and monomer	87
B.	Polymer characterization	89
	1. Molecular weight	89
	2. Viscosity	92
	3. Ultraviolet absorbance	94
C.	Particle characteristics	94
D.	Scintillation system	101
E.	Flocculation-Adsorption experiments	103
	1. Mixing procedure	103
	2. Electrophoretic mobility	106
	3. Polymer adsorption	106
	4. Optical density	108
F.	Adsorption experiments	109

Part	Title	Page
Chapter V	Results of polymer and particle characterizations	110
A.	Polymers	110
1.	Molecular weight	110
2.	Branched polymers	113
3.	Polymer configuration in solution	113
B.	Particles	117
1.	PSL	119
2.	Min-U-Sil	122
Chapter VI	Kinetics of polymer adsorption and particle aggregation	126
A.	Theory	126
1.	Collision rates	126
a.	Diffusion transport	127
b.	Laminar velocity gradient transport	128
2.	Collision efficiency factors	134
B.	Experimental results	135
1.	Non-aggregating systems	135
2.	Aggregating systems	139
Chapter VII	Flocculating systems: experimental results and discussion	143
A.	Residual turbidity	145
1.	Min-U-Sil particles	145
a.	pH effects	145
b.	Effects of polymer molecular weight and NaHCO_3 concentration	145
c.	Solution composition effects	151
2.	Polystyrene latex (PSL)	154
a.	pH effects	154
b.	Effects of NaCl concentration and polymer molecular weight	156
B.	Electrophoretic mobility data	156
1.	Zero mobility	156
2.	OFD mobility	164
C.	Adsorption data	166
1.	Saturation	166
a.	Ionic strength effects	166
b.	Molecular weight effects	169

Part	Title	Page
	2. Adsorption at optimum flocculation conditions	171
	a. Flocculation mechanism	171
	b. Residual polyelectrolyte concentrations	175
Chapter VII	Summary and conclusions	178
A.	Rationale of this research	178
B.	Research objectives	178
C.	Qualitative description of the flocculation process	179
D.	Principal results	180
	1. Improbability of flocculation by polymer bridges	180
	2. Electrostatic patch model for flocculation	181
	3. Kinetics	181
	4. Experimental effects of polymer molecular weight and solution ionic strength on flocculation	182
E.	Applications	182
	1. Treatment plant operation	182
	2. Polymer manufactures	183
F.	Suggestions for further research	184
Appendices		186
Nomenclature		191
References		193

LIST OF FIGURES

Number	Title	Page
II-1	Influence of ionic strength on configuration of polyelectrolyte molecule in aqueous solution.	10
II-2	Polymer adsorption configuration and the resulting aggregate configuration.	12
II-3	Variations of interaction energies with separation distance. Particle diameter = 0.2 microns, $\psi_0 = 50$ mv, and Hamaker constant = 10^{-12} ergs.	18
II-4	Stern's model of potential distribution in the electric double layer.	22
II-5	Reversal of zeta potential, ζ , by adsorption of ions in Stern layer.	22
II-6	(a) Interaction energy between particles versus distance from surface. (b) Normalized particle concentrations corresponding to interaction energies illustrated in (a).	26
II-7	Effect of the energy value defining the DCA on the DCA-ionic strength relationship. Particle diameter = 1 micron and $A = 10^{-12}$ ergs.	30
II-8	Dependence of the 5 kT DCA on ionic strength for particles with various surface potentials. Particle diameter = 1 micron, $A = 10^{-12}$ ergs.	33
II-9	Variation of the DCA with surface potential at several ionic strengths. Particle diameter = 1.3 microns and $A = 10^{-12}$ ergs; $I =$ moles/liter.	34
II-10	Effect of A , the Hamaker constant (ergs), on the DCA variation with ψ_0 . Particle diameter = 1 micron.	36
II-11	Influence of particle size on the DCA variation with ionic strength. $\psi_0 = 50$ mv and $A = 10^{-12}$ ergs.	37
II-12	Effect of counterion valence (Z) on the DCA. Particle diameter = 1 micron, $A = 10^{-12}$ ergs and $\psi_0 = 50$ mv.	38

Number	Title	Page
II-13	Variation of DCA- ψ_0 relationship with counterion valence (Z) at a constant counterion concentration of 3×10^{-3} moles/liter. Particle diameter = 1 micron.	38
II-14	Two-dimensional models of adsorbed polymer configurations for various values of	43
II-15	Dependence of the average number of segments per loop (N_L) on the adsorption energy per segment. Adapted from Motomura and Matuura ⁴² .	49
II-16	Variation of the average number of segments per loop (N_L) with adsorption energy per segment. Adapted from Silberberg ⁶³ .	49
II-17	Distribution of density of polymer segments $\rho(Z)$ with distance from surface (Z) for various adsorption energies (ϵ). From DiMarzio and McCrackin ¹⁸ .	52
II-18	The average distance (Max. Z) to the segment farthest from the surface. The distance is given vs adsorption energy (ϵ) for three different degrees of polymerization. Adapted from McCrackin ³⁸ .	52
II-19	The average number of segments per loop (N_L) plotted against adsorption energy for flexible (solid lines) and stiff polymer chains (broken lines). The numbers on the lines indicate degrees of polymerization. From Roe ⁵⁵ .	54
II-20	The same as Fig. II-19, except that here the number of segments (N_T) of the desorbed sequence at the polymer ends is plotted. From Roe ⁵⁵ .	54
II-21	Plot of Θ , the fraction of the total number of segments which are attached directly to the surface, against adsorption energy in the limit molecular weight $\rightarrow \infty$. From Motomura and Matuura ⁴¹ .	56
II-22	The fraction of attached segments (θ) against adsorption energy for flexible (solid line) and stiff polymer chains (broken line). Adapted from Roe ⁵⁵ .	56

Number	Title	Page
II-23	A plot of Θ , the attached fraction of segments against the adsorption energy (ϵ). A, B and C correspond to degrees of polymerization of 10^2 , 10^3 , and 10^4 , respectively. Adapted from Higuchi ²⁸ .	57
II-24	Regions of particle stability, particle instability and polymer bridging. Maximum polymer extension = 60 \AA , Hamaker constant = 10^{-12} ergs, particle diameter = 1 micron and DCA based on interaction energy of 5 kT.	60
III-1	Adsorbed polymer configurations.	63
III-2	Schematic models of double layers and the corresponding potential diagram. (a) Free surfaces, (b) surface with adsorbed cationic polyion.	66
III-3	Effects of molecular weight and degree of surface coverage on adsorbed polymer patch distributions. Degrees of surface coverage: A - 17%, B - 33% and C - 50%.	68
III-4	Polymers patch distributions at 25% surface coverage for polymers of various molecular weights.	74
III-5	Particle-particle orientations resulting in maximum attraction and maximum repulsion for a given polymer patch distribution.	76
III-6	Percent surface coverage at zero F versus S, the separation between the surfaces of one-micron spheres. Polymer molecular weight = 1.6×10^5 .	78
III-7	The effect of polymer molecular weight on the percent surface coverage required for zero F. Systems: 40 \AA^2 / polymer segment, $M_0 = 214$ and $S = 30 \text{ \AA}$ & 100 \AA for 10^{-2} molar & 10^{-4} molar solutions, respectively.	79
IV-1	Synthesis reaction of poly (DMVPB).	82
IV-2	Vacuum manifold for preparation of tritium-tagged methyl bromide.	83

Number	Title	Page
IV-3	The effect of initiator concentration on molecular weight. Monomer concentration = 1.17 molar.	88
IV-4	Effect of monomer concentration on molecular weight.	88
IV-5	Typical Zimm plot of light scattering data.	91
IV-6	Typical viscosity data for poly (DMVPB) obtained by dilution at various constant NaCl concentrations.	95
IV-7	Ultraviolet absorbance of aqueous polymer and monomer solutions at $10 \mu\text{g/l}$.	96
IV-8	Electron micrograph of 1.3 micron polystyrene latex particles.	98
IV-9	Electron micrograph of Min-U-Sil 5 particles.	99
V-1	Relationship between the intrinsic viscosity and the molecular weight determined by light scattering. Aqueous polymer solutions in 0.3 molar NaCl.	111
V-2	Effect of NaCl ionic strength on intrinsic viscosity (deciliters/gram).	115
V-3	Effect of anion valence on viscosity-salt concentration relationships for cationic polyelectrolytes.	116
V-4	The effects of ϵ' and δ on ψ_0 , the surface potential, for a constant charge surface. $\sigma = 5.32 \times 10^4 \text{ esu/cm}^2$, $N_1 = 10^{15}/\text{cm}^2$.	121
V-5	Dependence of Stern potential on ϵ' and δ for constant potential surface. $\psi_0 = 338 \text{ mv}$, ionic strength = $10^{-3} \text{ moles/liter}$ and $N_1 = 10^{15}/\text{cm}^2$.	124
V-6	Dependence of surface charge density, σ , on ϵ' and δ for constant potential surface. $\psi_0 = 338 \text{ mv}$, ionic strength = $10^{-3} \text{ moles/liter}$ and $N_1 = 10^{15} \text{ cm}^2$.	124

Number	Title	Page
VI-1	Dependence of B, the collision ratio factor, on particle diameter and on solution polymer size for $G=0$ and $G=100 \text{ sec}^{-1}$.	131
VI-2	Effect of $G(\text{sec}^{-1})$ on B, the collision ratio factor. $dp = 0.01$ microns.	132
VI-3	Effect of NaHCO_3 concentration on adsorption of poly (DMVPB) ₃ to Pyrex glass surfaces.	136
VI-4	Effect of molecular weight on adsorption of poly (DMVPB) to Pyrex glass surfaces.	137
VI-5	Time variations of: (A) polymer adsorption from solutions of various initial polymer concentrations and (B) supernatant turbidity.	140
VII-1	Typical results illustrating the dependencies of residual turbidity, electrophoretic mobility and polymer adsorption on the initial polymer dose.	144
VII-2	Effect of pH on the OFD's of 50 mg/l Min-U-Sil suspensions in 5×10^{-4} molar ionic strength solutions. $M = 6 \times 10^3$.	146
VII-3	Effect of polymer molecular weight on relative residual turbidity-polymer dose relationship for 50 mg/l Min-U-Sil suspensions in 5×10^{-5} molar NaHCO_3 . $\text{pH} = 8.3$	147
VII-4	Effect of polymer molecular weight on relative residual turbidity-polymer dose relationship for 50 mg/l Min-U-Sil suspensions in 10^{-2} molar NaHCO_3 . $\text{pH} = 8.3$	149
VII-5	Dependence of OFD on polymer molecular weight and concentration of NaHCO_3 . System: $\text{pH} = 8.3$ and Min-U-Sil at 50 mg/l.	150
VII-6	Flocculation regions defined by position of "limiting molecular weights". In Region I the OFD is independent of molecular weight. In Region II the OFD decreases with increasing molecular weight.	150

Number	Title	Page
VII-7	Effect of pH on the OFD's of 20 mg/l PSL suspensions in 10^{-3} molar ionic strength solutions. $M = 5.5 \times 10^6$.	155
VII-8	Effect of NaCl concentration on flocculation of 20 mg/l PSL suspensions. pH = 6.0 and $M = 6 \times 10^3$.	157
VII-9	Effect of NaCl concentration on flocculation of 20 mg/l PSL suspensions. pH = 6.0 and $M = 5.5 \times 10^6$.	157
VII-10	Variation of OFD with polymer molecular weight and NaCl concentration. System: pH = 6.0 and PSL at 20 mg/l.	158
VII-11	Electrophoretic mobility versus polymer adsorption. (A) 50 mg/l Min-U-Sil in 5×10^{-5} molar NaHCO_3 . (B) 20 mg/l PSL in 5×10^{-4} molar NaCl.	160
VII-12	Illustration of general trends in data of Table VII-3 showing the effects of salt concentration and polymer molecular weight on the polymer adsorption required for zero mobility.	162
VII-13	Effect of molecular weight on polymer adsorption at the OFD for Min-U-Sil suspensions. Particle surface coverage values based on two specific surface area values of Min-U-Sil are illustrated.	174
VII-14	Comparison of PSL experimental OFD surface coverage data (points) with theoretical patch model results (solid lines).	176

LIST OF TABLES

Number	Title	Page
II-1	DCA values at interaction energies of 10, 5 and kT. System: 1 micron diameter spherical particles, Hamaker constant = 10^{-12} ergs, temperature = 20°C	29
II-2	DCA values at temperatures of 0°, 20° and 40°C. System parameters: 1 micron diameter spherical particles, Hamaker constant = 10^{-12} ergs, DCA interaction energy = 5 kT.	40
IV-1	Particle characteristics	97
IV-2	Suspension characteristics	105
V-1	Characteristics of tritium labeled (1,2 dimethyl-5-vinylpyridinium bromide) polymers	112
V-2	Values of PSL Stern potentials for various Stern layer adsorption site densities (N_1).	120
V-3	Double layer characteristics of PSL particles.	123
V-4	Double layer characteristics of Min-U-sil particles.	123
VI-1	Particle-polymer number ratios for various flocculating systems.	133
VII-1	Effects of solution composition of OFD of Min-U-Sil.	152
VII-2	Values of polymer adsorption at zero particle mobility.	161
VII-3	Electrophoretic mobility values at optimum flocculation dose.	165
VII-4	Saturation values of polymer adsorption and resulting areas per adsorbed segment.	167
VII-5	Values of polymer adsorption and degree surface coverage at OFD.	172
VII-6	Residual polymer in solution at OFD and at 2 x OFD.	177

Chapter I

INTRODUCTION

A. General Background

A substantial portion of municipal water treatment involves the removal of negatively-charged suspended particles ranging in size from approximately 0.01 to 10 microns. These colloidal particles have been removed from water primarily because they impart a turbidity which is aesthetically unacceptable. The particles include metal oxides and hydroxides, clays and minerals resulting from soil weathering, and biological matter such as bacteria and algae cells.

Recent studies have placed a new emphasis on particulate removal. It has been found that pesticides, herbicides, radio-nuclides, dissolved trace metals, and other substances potentially detrimental to human life are associated with the particulate matter in waters. Particle removal can no longer be considered simply "aesthetically desirable". The increased need of producing particulate-free waters requires that the present techniques of particulate removal be improved and that new methods be developed.

The water treatment industry has removed colloidal material from waters for over eighty years by chemical coagulation with multivalent inorganic salts⁸. Extensive use has been made of soluble aluminum and iron (II) and (III) salts. In recent years it has been found that synthetic organic polymers can act as coagulating agents. Polymers, in addition to increased effectiveness and lower required doses, have the inherent advantage over traditional salts of not

significantly increasing the volume of settled material to be disposed of. With use of inorganic salts, up to 95 percent of the volume of settled material is the precipitate formed by the coagulating agent.

Organic polymers have been used for almost a decade to dewater sludges, thicken slurries, and coagulate solids in industrial treatment processes. Polymer treatment of potable waters is just coming of age as can be seen by the fact that in the last six years over one hundred synthetic polymers have been approved by the United States Public Health Service for use in public water supplies².

Both organic and inorganic polymers can be divided into three classifications, depending on the net charge of the polymer chain: anionic, cationic, and nonionic. Each type of polymer is suited to particular applications. A recent review of the use of all three types in water treatment has been made by Hawkes²⁷. An early review of the physical processes believed to be involved in polymer flocculation was presented by LaMer and Healy³⁷.

Adequate knowledge of the effects of certain key variables on the flocculation of dilute suspensions by polymers is lacking. One such variable is water composition. The ionic strength of a water should affect the polymer flocculation process since the properties of both particles and polymer depend on ionic strength.

B. Water Composition and Polymer Properties

Natural waters of the United States vary greatly in both type and concentration of ions present. Based on data published by the

United States Geological Survey⁷², the ionic strength of public water supplies for forty of the largest cities in the United States varies between 4×10^{-4} and 4×10^{-2} moles per liter. There are smaller cities using waters having ionic strengths outside these limits. It can also be expected that in the future as the water demand increases, water supplies of more widely ranging salt content will be used. An average ionic strength value of 6×10^{-3} is obtained using the U. S. potable water composition data published by Davis and DeWiest¹⁵.

In the polymer flocculation of dilute suspensions an important polymer parameter which has received little attention is molecular weight. Dilute suspensions have a solids volume fraction of less than 5×10^{-5} . For clay and bacterial suspensions this corresponds to approximate weight concentrations of 125 mg/l and 50 mg/l, respectively. Most natural waters have suspended particle concentrations less than these values.

The effect of polymer molecular weight on the flocculation of concentrated suspensions or slurries has been studied by several investigators (Dixon and Zielyk¹⁹, Dixon et al²⁰, Walles⁷⁵, and Sakaguchi and Nagase⁵⁷). It is impossible to use the results of these investigations to determine the fundamental characteristics of the flocculation mechanism because the experimental systems studied were poorly defined.

Gregory²⁴ has investigated the effects of molecular weight variation on the destabilization of well-defined, dilute suspensions using two commercially available polyamines (Primaflor C-3 and

Primafloc C-7, products of Rohm and Haas Co.). In Gregory's work, however, it is difficult to attribute differences in flocculation behavior solely to variation in molecular weight since the polymers used also have different chemical structures¹⁶.

C. Purpose of the Present Work

It is the purpose of the present research to investigate the effects of polymer molecular weight and solution composition on the polymer flocculation of dilute suspensions. The use of well-defined systems is necessary if a better understanding of the fundamental mechanisms involved in polymer flocculation is to be gained. Because of the basic differences in the various polymer-particle systems it was decided to limit the investigation to systems of negatively charged particles and a positively charged polyelectrolyte. The research was accomplished by synthesizing and characterizing a homologous series of linear cationic polymers. These polymers were then used to flocculate particles having negative surface charge.

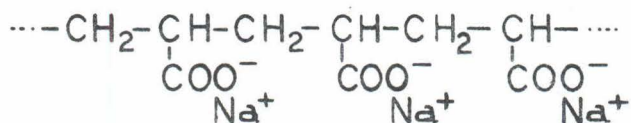
An electrostatic flocculation model is developed to describe the mechanism by which a polyelectrolyte flocculates particles of opposite charge. The model was then used to analyze the results from the well-defined experimental system. It is shown that the commonly assumed polymer bridging mechanism does not apply to systems of polyelectrolytes and particles of opposite charge.

Chapter II

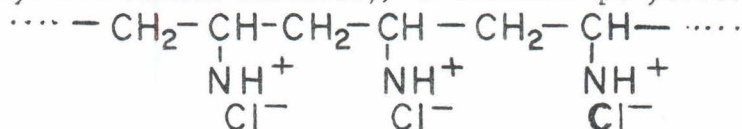
THEORETICAL ANALYSIS OF POLYMER BRIDGING IN TERMS
OF THE DIFFUSE ELECTRICAL DOUBLE LAYER THEORY
AND ADSORBED POLYMER CONFIGURATIONS

A. Polyelectrolytes in Solution

If the subunit (segment) of a linear polymer contains an ionic group, the macromolecule has the properties of both polymers and electrolytes and is known as a linear polyelectrolyte. Examples are sodium polyacrylate, an anionic polyelectrolyte,



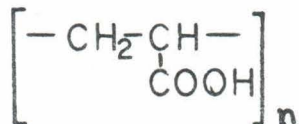
and poly(vinylammonium chloride), a cationic polyelectrolyte,



A description of the solution properties of polyelectrolytes requires the use of certain terms which characterize polymers. For a more detailed treatment than the one presented below, the reader is referred to one of several polymer texts^{22, 70}.

1. Definitions. The degree of polymerization, n , of a given polymer molecule is the number of structural units in the polymer chain. Usually n is simply the number of monomer units per polymer molecule. The molecular weight, M , is the sum of the molecular weights of all atoms in the macromolecule. For large n , M is equal to nM_0 where M_0 is the molecular weight of a monomer segment.

The degree of ionization is the fraction of ionizable groups which are dissociated. The degree of ionization of the polymer is determined primarily by the ionization constant of the individual functional groups and the dielectric constant of the solvent. Poly (acrylic acid),



is a weakly ionized polymer because of the relatively weak tendency of the carboxyl groups to dissociate. In contrast is sodium polyacrylate which consists mainly of ionized carboxylate groups and sodium counter ions.

Ions dissociated from the polymer are referred to as gegenions or counterions and the resulting charged macromolecule is considered the polyion. The charge density of the polyion may be expressed as the number of ionized groups per unit length or per monomer unit.

The contour length is the length of the stretched out polymer, and is the length of each monomer unit in the macromolecule multiplied by the number of such units.

The radius of gyration, R_G' , characterizes the size of a macromolecule. R_G' is defined as the square root of the weight average of r_i^2 , the distance between the i -th segment and the center of mass; i. e.

$$R_G'^2 = \frac{\sum_i m_i r_i^2}{\sum_i m_i} \quad \text{II-1}$$

In order to characterize polymer solutions containing many macromolecules, R_G , the root-mean-square average of R_G' over all configurations is used:

$$R_G = (R_G'^2)^{1/2} = \left(\frac{\sum_i m_i r_i^2}{\sum_i m_i} \right)^{1/2} \quad \text{II-2}$$

Since the structural units of a polymer usually have identical masses, the radius of gyration can be expressed as

$$R_G = \left(\frac{\sum_i r_i^2}{n} \right)^{1/2} \quad \text{II-3}$$

The hydrodynamic volume, V_h , is the volume of the macromolecule and the solvated ions. The hydrodynamic volume of a polymer having a coiled configuration includes the solvent molecules which fill the voids of the coil. The hydrodynamic volume of polyelectrolytes is slightly more complicated since it is the volume of the neutral macromolecule component which includes the polyelectrolyte itself, small counter ions and solvent. A length characteristic of the hydrodynamic volume is defined as the radius, R_e , of a sphere having a volume equal to the hydrodynamic volume of the macromolecule.

2. Solution Configuration. Some of the processes involved in flocculation are influenced by the solution configuration of the polymer. The diffusion and transport rates depend on the size and shape of the polymer molecule. Under certain conditions the configuration of the polymer adsorbed at the solid-solution interface

is influenced by the configuration of the polymer in solution.

An uncharged, flexible linear polymer may, by rotation about its single bonds, take on any configuration compatible with its fixed bond lengths and angles and any other steric restrictions which may exist. From a consideration of the random-walk process, it is usually reasonable to expect the linear chain to assume a random coil configuration with a spherically symmetrical mass distribution.

When groups of a linear polymer ionize, that is, when the flexible polymer becomes a polyion, all configurations compatible with its geometric characteristics are still possible. However, repulsion between like charges on the polyion cause the free energy to vary for different configurations. The free energy of compact configurations is relatively high in comparison to the free energy of extended molecules. In a solution having high dielectric constant, polyelectrolytes favor an extended configuration; nonionic polymers in the same solution assume a more compact, random-coil configuration.

The effective range of the repulsion forces between the different ionized groups on a polyion depends on the ionic strength of the solution. This dependence is caused by the existence of a diffuse layer of oppositely charged simple ions (counter) around the polyion. Such systems have been described in terms of the electrical double layer^{70, 74}.

The counterions of the diffuse double layer act as a shield which reduces the effective range of the repulsive forces between the like-charged segments of a polyion. At low, bulk solution

concentrations the absolute number of counterions close to the polyion small and shielding is inadequate to prevent repulsion between the ionized groups of the polyion. This lack of shielding results in an extended configuration. At relatively high ionic strengths, the number of counterions close to the polyion is large and the effective range of the repulsive forces is reduced. Ionized segments are then able to approach each other more closely and a compact configuration results.

Fig. II-1 is an attempt to depict qualitatively the above described ionic strength influence on the configuration of poly-electrolytes. The polyion models are analogous to the models used to describe the double layer at the surface of a flat plate⁷⁴. In Fig. II-1(a) the counterion distribution around a segment of the polymer backbone is shown. The segment is short enough to be approximated as linear. In addition to the counterions shown, there are, in the same area, co-ions present at a concentration less than the bulk solution co-ion concentration. In part (b) the repulsive force between two segments is shown as a function of the distance separating the segments. At high ionic strengths the repulsive forces decrease rapidly and segments can approach each other. Part (c) illustrates schematic polymer solution configurations for the two ionic strength conditions.

B. Mechanisms for Polymer Aggregation of Particles

The aggregation of suspended particles occurs in two steps: (i) the transport of particles resulting in collisions and, (ii) the destabilization or successful sticking together of the particles⁶⁹.

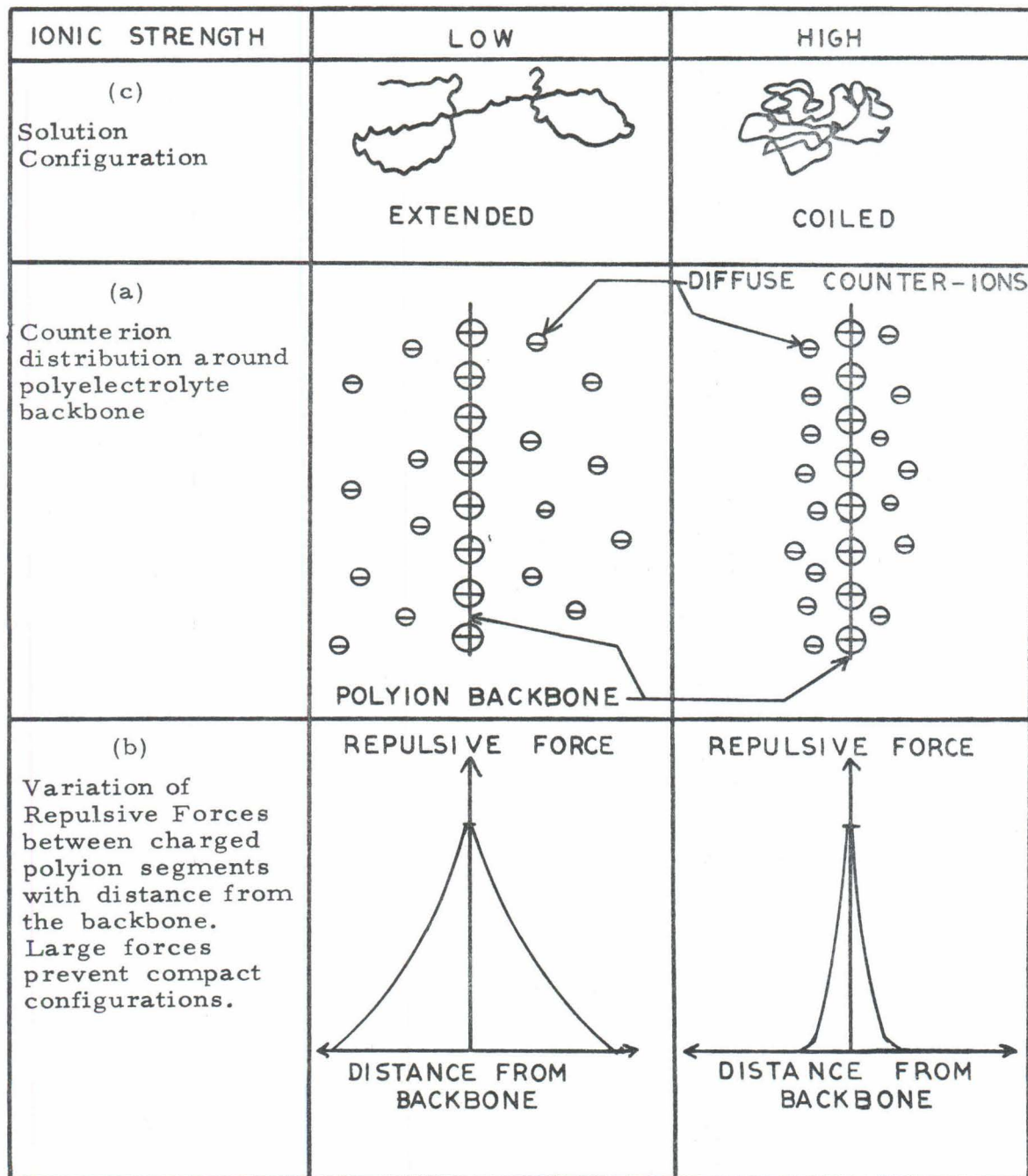


Fig. II-1. Influence of ionic strength on configuration of Polyelectrolyte molecule in aqueous solution.

Particles are transported by velocity gradients arising from energy dissipation in the solution (orthokinetic aggregation) and by Brownian motion (perikinetic aggregation). The parameters influencing the rate of collisions are the intensity of agitation, particle size, particle concentration and temperature.

Particle destabilization is controlled by the chemical and electrical parameters of the system. The turbidity-producing particles in aqueous solution do not aggregate into larger, settleable flocs because successful collisions are prevented by the repulsive forces between particles due to charges on the surfaces of the particles. A collision efficiency factor α , is defined as the ratio of the number of successful collisions to the total number of collisions⁷. The overall rate of aggregation can be expressed as the product of the collision efficiency factor and the rate of particle-particle collisions.

Polymer flocculation of charged particles can occur by two mechanisms: (i) reduction of the electrostatic repulsion between particles and, (ii) formation of polymer bridges between particles. The aggregation mechanism for a particular suspension is determined by the physical and electrochemical surface characteristics of the particles and the physical and chemical nature of the polymer. In Fig. II-2 the adsorbed configuration of polymer and the corresponding aggregation configuration is illustrated. It is possible to separate the polymer adsorption process and the particle aggregation process because of their different time scales. As will be developed in a following section, the rate of polymer adsorption is

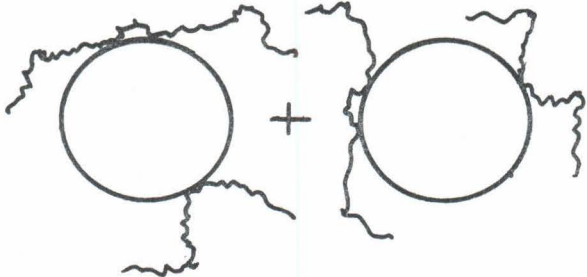
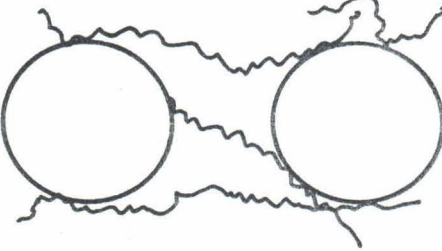
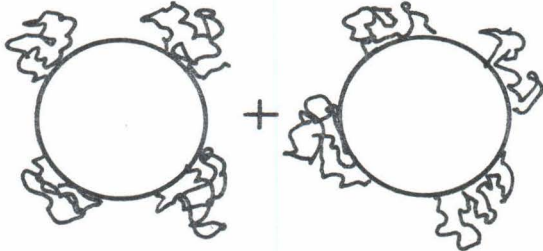
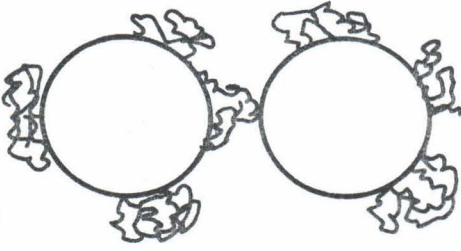
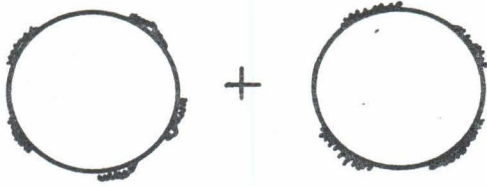

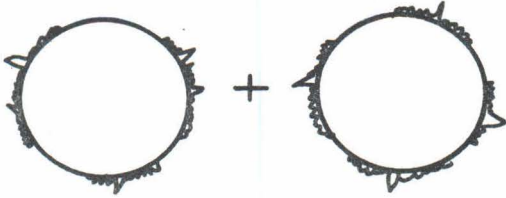
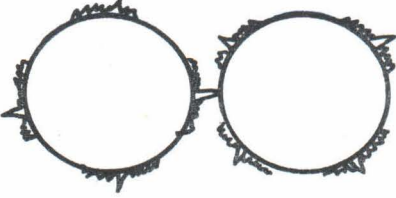
ADSORBED POLYMER CONFIGURATION ON PARTICLE	AGGREGATE CONFIGURATION
 <p>(a) "dangling ends"</p>	 <p>bridging</p>
 <p>(b) looped</p>	 <p>bridging</p>
 <p>(c) flat</p>	 <p>shielding</p>
 <p>(d) combination</p>	 <p>combination</p>

Fig. II-2. Polymer adsorption configuration and the resulting aggregate configuration

fast in comparison to the aggregation rate of particles in the majority of systems.

In Fig. II-2(a), long, stretched-out polymer molecules attach to two or more particles. Characteristics of this model are: (a) attachment of relatively few segments of the polymer molecule to the particles and, (b) relatively great length of polymer molecules in comparison to the size of the particles. The effectiveness of flocculation by this model is very dependent on the size or molecular weight of the polymer.

In Fig. II-2(b) polymer molecules are shown adsorbed with looped configurations on the surfaces of individual particles. Collisions between particles result in aggregation if a looped polymer segment of one particle can attach to an available site on another particle. In the aggregated state the particles cannot approach each other more closely because electrostatic repulsion between the like-charged surfaces still exists. For successful aggregation by this bridging mechanism it is necessary for: (1) the loops of the adsorbed polymer to be larger than the interaction distances of the repulsive forces and, (2) for adsorption sites to be available.

The availability of adsorption sites depends upon the degree of surface coverage or the amount of polymer already adsorbed on the particles. An almost universal characteristic of polymer flocculation is that excessive doses of polymer result in reversal of surface charge and restabilization of the suspension⁶⁹. Restabilization is caused by the saturation of the surface by polymer

which may: (a) reverse the charge of the surface or, (b) leave no sites available for bridge formation.

The electrostatic or shielding model is illustrated in Fig. II-2 (c). Oppositely charged polyelectrolytes adsorb to the charged surfaces of the particles in a flat configuration and shield the surface charge from the solution and from other particles. Destabilization then occurs as a result of the universal London-van der Waal's attractive forces or by simple electrostatic attraction. That is, aggregation occurs when the repulsive forces have been reduced to a level that enables particles to approach each other closely enough for the short-ranged van der Waal's attractive forces to act, or when a polymer coated surface comes in contact with an uncoated, oppositely charged surface. A looped configuration of adsorbed polymer on the surface will not prevent aggregation by the electrostatic mechanism if the loops are able to collapse and lie flat between two surfaces.

Fig. II-2(d) illustrates aggregation by the combination of the bridging and shielding mechanisms. Polymer adsorbs in a relatively flat configuration with small loops. The repulsive forces in the polymer-free system prevent the particles from approaching each other closely enough for the small loops to form bridges. That is, the loops are not long enough to bridge the "gap" between particles. However, the polyion segments attached directly to the surface shield the surface charge and the "gap" between the particles is reduced until the loops can form bridges. As in the case of pure bridging the particles cannot approach each other more closely

because of repulsion between surfaces and yet the particles cannot move apart because of the polymer bridges between their surfaces.

The particular destabilization mechanism actually operative will be determined primarily by: (1) the configuration of the adsorbed polymer, or the length of a loop; and (2) the magnitude of the repulsion forces between the particles. In terms of the models presented these two parameters may be interpreted respectively as the length of the available bridge and the size of the gap between particles which must be bridged if flocculation is to occur.

In order to determine the flocculation mechanism the distance between particles and the size of polymer loops are investigated in the following sections of this chapter.

C. Particle Stability

1. Potential Energy of Interaction Between Particles.

The interaction energies between charged particles in aqueous solution are described by the Derjaguin-Landau, Verwey-Overbeek (DLVO) theory of the diffuse electrical double layer. No attempt is made here to review double layer theory and the reader is referred to Verwey and Overbeek⁷⁴, Kruyt³⁶, and Adamson¹. In order to account for the effects of specific adsorption of polyions the Stern correction to the Gouy-Chapmann model of the double layer is used.

The energy of repulsion (V_R) between two spheres having surface potential ψ_0 can be calculated by the relationship

$$V_R = \frac{ea\psi_0^2}{2} \log_e \{1 + \exp(-\kappa H)\} \quad \text{II - 4}$$

where ϵ is the dielectric constant of the bulk solution; a is the radius of the spheres; κ^{-1} is the double layer thickness* ; and H is the distance between the surfaces of the particles.

The approximations used in the derivation of Eq. II-4 are valid when the double layer thickness is small in comparison to the size of the particle and when the surface potential is not too great. When κa is greater than 2.5 the error in the repulsive energy is less than one percent. In a system of one micron particles Eq. II-4 is valid for ionic strengths greater than 2×10^{-6} moles/liter.

In the DLVO theory the attraction between particles is entirely due to the London-van der Waal forces. Hamaker²⁵ derived the following relationship for the London-van der Waal attraction (V_A) between two spherical particles:

$$V_A = - \frac{A}{6} \left\{ \frac{2}{s^{2.4}} + \frac{2}{s^2} + \log_e \left(\frac{s^2 - 4}{s^2} \right) \right\} \quad (\text{II-5})$$

where A is the Hamaker constant and $s = (H + 2a)/a$. The

* $\kappa = ez \sqrt{\frac{8\pi n}{\epsilon k T}} = 3.27 \times 10^7 z \sqrt{C} \text{ cm}^{-1} \text{ at } (25^\circ\text{C})$ where e is

the elementary charge, z is the valence of the ions, n is the solution ion concentration in ions/cm³, k is the Boltzmann constant, T is the absolute temperature and C is the solution ion concentration in moles/liter.

major difficulty in using Eq. II-5 is determining the correct value for the Hamaker constant. Values of A have been estimated from fundamental atomic properties and have been experimentally determined from measurements of the stability of various colloids as a function of ionic strength. Watillon and Petit⁷⁶ have described the method they used to determine A for polystyrene latices.

The total interaction energy (V_T) between two charged spheres is the sum of the repulsive energy and the London-van der Waal attractive energy. That is $V_T = V_R + V_A$. Positive values of V_T indicate net repulsive energies. Fig. II-3 illustrates the variation of the attractive, repulsive and total energies with the distance between two spherical particles having surface potentials of 50 mv, diameters of 0.2 microns and Hamaker constants of 10^{-12} ergs. Several curves are shown for different values of ionic strength. The van der Waal attractive forces are independent of solution composition and particle surface potential.

To illustrate the dependence of the interaction energy on surface separation distance a hypothetical process bringing two particles together is described. Following the 10^{-3} molar ionic strength curve in Fig. II-3, the total interaction energy varies as follows:

At distances (between surfaces) greater than 0.05 microns there is no interaction between the particles. However as the particles approach more closely the repulsive energy increases until a maximum is reached at 0.005 microns; at distances less than 0.001 microns the particles are attracted to each other by van der Waals attraction.

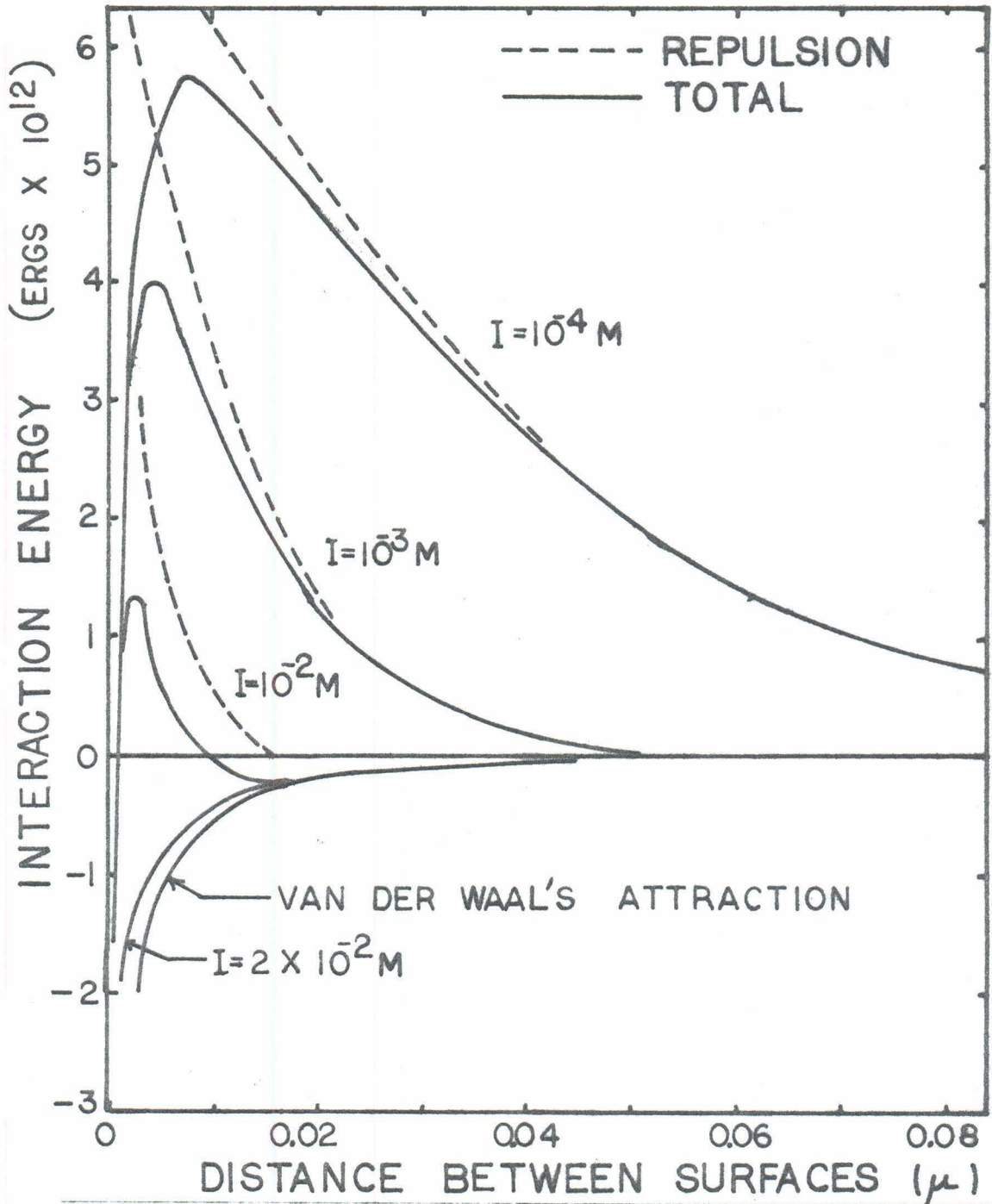


Fig. II-3. Variations of interaction energies with separation distance. Particle diameter = 0.2 microns, $\psi_0 = 50$ mv, and Hamaker constant = 10^{-12} ergs.

Colloidal suspensions are thermodynamically unstable since the free energy of the aggregated state is lower than the free energy of the dispersed state, which because of its disperseness, has large surface free energies. Non-coagulating suspensions are the result of electrostatic repulsion barriers which cause particles to exist in metastable states. Systems remain in metastable, dispersed states if the repulsion barrier is large with respect to the energy of the particles. If, however, the interaction barrier is lowered to the point where it is less than the energy of the particles, coagulation occurs irreversibly since the aggregated state has minimum free energy.

Particles have an average energy of kT due to thermal or Brownian motion (k is the Boltzmann constant and T is the absolute temperature). The energy distribution of the particles is described by the Boltzmann equation. Since coagulation is prevented only when the repulsive barrier is effectively unsurpassable to all particles, suspension stability requires interaction barriers of several kT . A barrier height of $10 kT$, determined empirically, is usually sufficient to prevent coagulation⁷⁴. Even though there is no detectable coagulation in systems with $10 kT$ energy barriers, 4×10^{-3} percent of the particles have energies greater than $10 kT$ and are capable of coagulating. The time for coagulation of a system with a $10 kT$ barrier might be on the order of years.

2. Stern Corrections. Several assumptions are made in the Gouy-Chapman model of the double layer which are unrealistic. Stern⁶⁷ proposed two corrections to account for the finite size of

the ions in the layer nearest the solid surface and for the possibility of specific adsorption of ions. Stern divided the region near the surface into two parts, the first consisting of ions adsorbed at the surface and forming an inner, compact double layer, and the second consisting of a diffuse Gouy-Chapman layer. The inner layer is referred to as the Stern layer and is enclosed by the surface plane and the plane of the centers of the closest counter-ions. In the Stern layer, which acts as a molecular condenser, the electric potential drops linearly with the distance from a value ψ_0 at the surface to a value of ψ_δ ; ψ_δ is called the Stern potential. The Stern model is illustrated in Fig. II-4.

The quantitative treatment of the diffuse layer of the Stern model is the same as the treatment of the Gouy-Chapman layer except that the addition of electrolyte causes a compression of the diffuse layer and some shifting of counter-ions from the diffuse layer to the Stern layer. The increased concentration of ions in the Stern layer lowers the Stern potential.

A mathematical treatment of the Stern layer is given by Verwey and Overbeek⁷⁴. The major difficulty in quantitatively using the Stern model is the lack of certain information. The thickness of the Stern layer δ , the dielectric constant in the Stern layer ϵ' , the number of adsorption sites on the surface N_1 , and the specific interaction energy ϕ are all needed for a mathematical treatment. Values of the capacity of the compact layer, $\epsilon' / 4\pi\delta$, have been estimated from electrocapillarity measurements and related studies for a few systems.¹

δ is estimated as 3 to 10 Å, depending on the adsorbing ions; ϵ' , the local dielectric constant, is less than the bulk solution value. N_1 is related to the surface area occupied by the adsorbed ions; usually each ion will occupy between 5 and 50 Å² depending on the size of the ion. The specific interaction energy ϕ depends on the chemical nature of the adsorbing ions.

As discussed in section II-D-3A, ϕ is related to the adsorption energy. When calculating the energy of interaction between two surfaces it is possible to replace the Gouy-Chapman potential by the Stern potential and perform the calculations in the manner derived for interacting Gouy layers⁷⁴. This substitution is justifiable since the Stern layers influence each other only when the distances between the surfaces are on the order of atomic dimensions. It is the diffuse double layers which interact with each other. All Stern corrections are effectively accounted for by using the Stern Potential instead of ψ_0 in Eq. II-4.

The mathematical dependence of the Stern potential on the Stern parameters (ϵ' , δ , N_1 , ϕ) is given in Appendix 1.

3. Specific Ion Adsorption and Reversal of Zeta Potential.

The zeta potential has received considerable attention in colloid chemistry. It is defined as the electric potential in the double layer at the interface between a particle moving in an electric field and the surrounding solution. The zeta potential is computed from the experimentally-measured electrophoretic mobility. The concept of the zeta potential is illustrated in Fig. II-5.

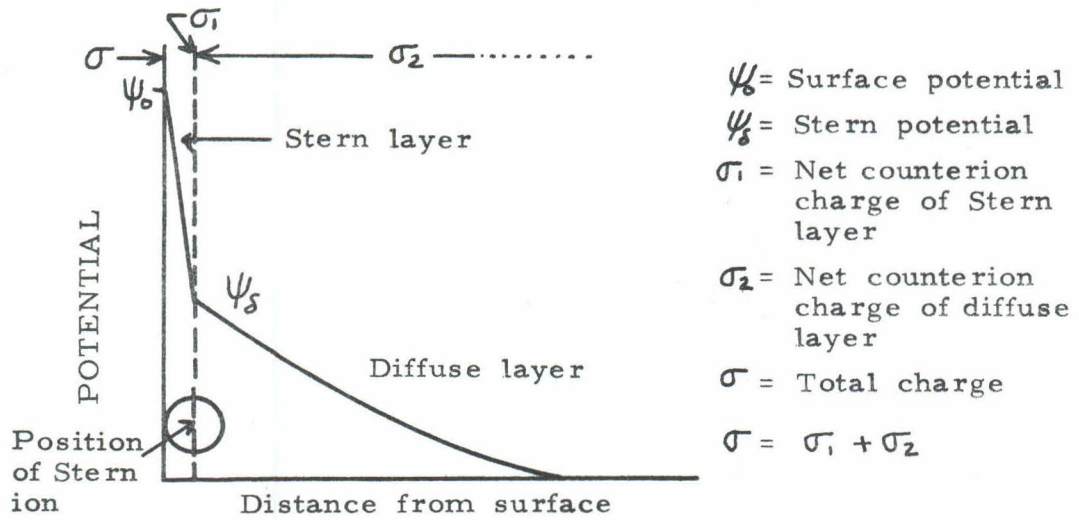


Fig. II-4 Stern's model of potential distribution in the electric double layer.

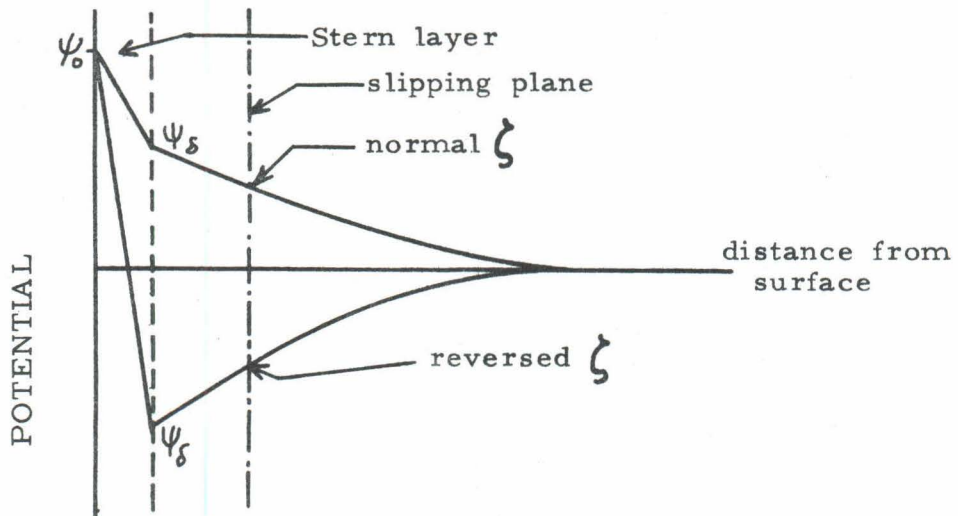


Fig. II-5 Reversal of zeta potential, ζ , by adsorption of ions in Stern layer.

The interface at which the zeta potential occurs is the slipping or shear plane between the bulk liquid and the liquid which moves with the particle. The major difficulty in quantitatively computing double layer parameters from zeta potential values is that the position of the shear plane is unknown. That is, the zeta potential represents the potential at an unknown distance from the surface. The zeta potential is less than the surface potential since some counter-ions are carried along with the particle. The zeta potential has been equated to the Stern potential by some investigators but it is more accurate to consider the zeta potential less than the Stern potential since the shear plane is further from the surface than the Stern layer.

The zeta potential can be reversed if enough ions adsorb in the Stern layer. Charge reversal requires the existence of specific adsorption forces between the adsorbing ions and the surface to overcome the Coulombic repulsion involved in adsorbing ions to a like-charged surface. Zeta potential reversal is illustrated in Fig. II-5.

In a system in which the zeta potential can be reversed, the Stern potential is zero when the zeta potential is zero. No assumptions concerning the position of the shear plane are needed at zero zeta potential if the zeta potential truly reverses its polarity. This Stern potential characteristic of systems having a reversible zeta potential allows quantitative analysis of the adsorption of polyions into the Stern layer.

Polyelectrolyte molecules adsorbed to surfaces can lie in either the Stern layer or the diffuse layer. It is possible for different segments of a single macromolecule to be adsorbed in different layers. It is assumed that the segments contained in loops lie in the diffuse layer and the segments attached directly to the surface lie in the Stern layer. The potential used to compute interaction energies (Stern potential) is reduced only by the segments of the polyions in the Stern layer; the looped portions result only in the compression of the double layer.

4. Distance of Closest Approach.

a. Definition. The polymer-flocculation-bridging-model is based on the formation of polymer bridges between particles which are stable in terms of the DLVO theory. That is, particles which cannot approach each other because of repulsion barriers are aggregated by polymer bridges which extend beyond the repulsion barrier. A length characteristic of the shortest distance between stable particles can be defined. This characteristic distance represents the length of polymer loops required if bridging is to occur.

The distribution of particles with distance from a central particle can be approximated by the use of Fuch's theory⁷⁴ for the rate of coagulation in a field of force. The flux of particles, J , reaching a central particle is

$$J = 4 \pi x^2 \left(D \frac{\partial n}{\partial x} + \frac{n}{f} \frac{dV_T}{dx} \right) \quad \text{II-6}$$

where x is the distance between centers of the particles, V_T is the total interaction energy between particles, n is the concentration of particles, D is the Einstein diffusion coefficient, and f is Stokes friction coefficient. In a stable system the flux is very small and can be approximated as zero. This assumes steady state and enables Eq. II-6 to be rewritten as:

$$0 = D \frac{dn}{dx} + \frac{n}{f} \frac{dV_T}{dx} \quad \text{II-7}$$

The solution to Eq. II-7 with the boundary condition $n = n_B =$ bulk particle concentration at $V_T = 0$ is

$$n = n_B \exp\left(-\frac{V_T}{Df}\right) = n_B \exp\left(-\frac{V_T}{kT}\right) \quad \text{II-8}$$

since $D = kT/f$. The distribution of ions with distance is a direct function of the interaction energy variation with distance. In Fig. II-6 two interaction curves and the corresponding particle concentration distributions are illustrated. The slope of the interaction energy curve between 0 and 10 kT controls the width of the distribution zone.

While Fig. II-6(b) shows that there is a distribution of distances between particles in a stable suspension, a single distance characteristic of the system can nonetheless be defined. This characteristic distance is referred to as the "distance of closest approach" (DCA) and is based on the notion of two particles being able to approach each other until some particular interaction energy value is reached. In this and the following analyses 5 kT is the

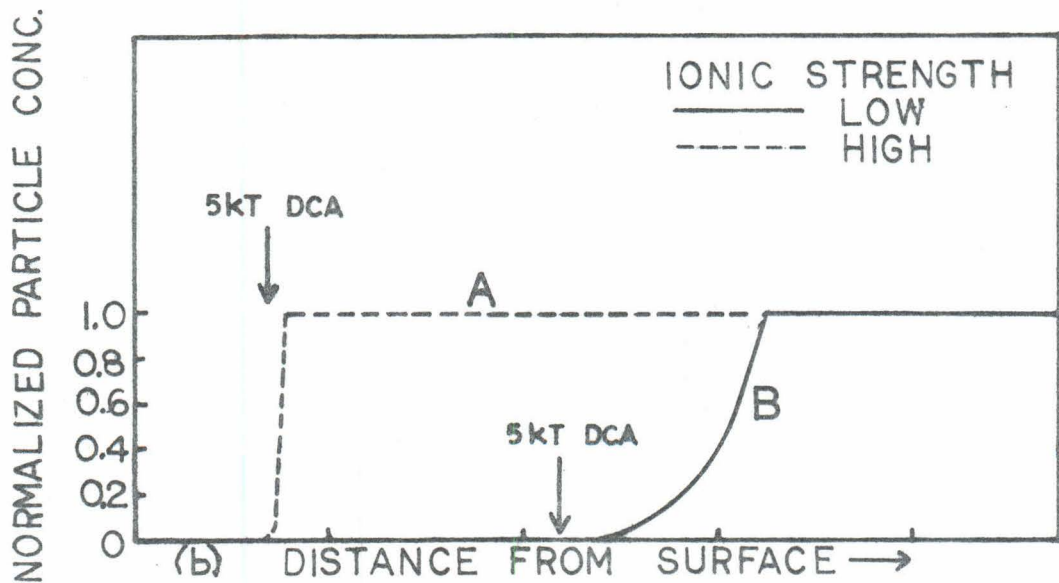
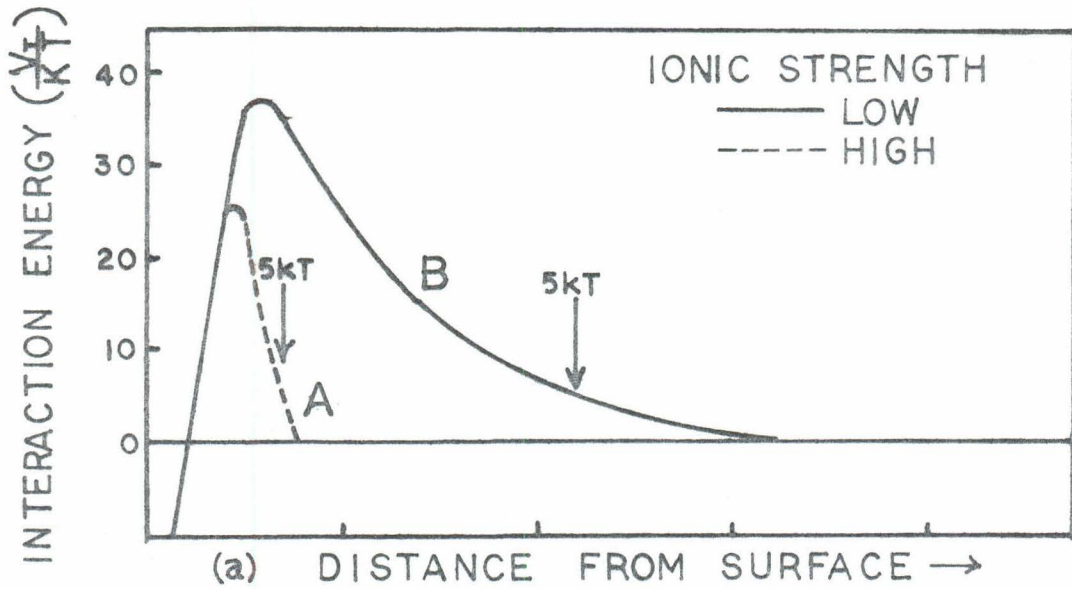


Fig. II-6. (a) Interaction energy between particles versus distance from surface. (b) Normalized particle concentrations corresponding to interaction energies illustrated in (a).

particular energy value defining the DCA unless otherwise noted. Approximately 0.6 percent of the particles are separated by distances less than that corresponding to a 5 kT energy. A DCA based on an interaction energy of 10 kT, results in separation distances which are almost never attained.

The DCA is defined as the distance between the surfaces of particles experiencing a total repulsive interaction energy of 5 kT in the region where the repulsive energy decreases with increasing distance between particles; if the maximum of the energy barrier is less than 5 kT, the DCA is zero since the particles are then able to coagulate.

DCA's are evaluated by determining the interaction energy as a function of distance. The 5 kT energy barrier shown in Fig. II-3 defines DCA's of 0.04, 0.008, and zero microns for ionic strengths of 10^{-3} , 10^{-2} , and 2×10^{-2} moles/liter, respectively. Fig. II-6 illustrates both the 5 kT DCA (arrows) and the entire distribution of distances between particles. The normalized concentration value of the 5 kT DCA, 0.006, is too small to be seen in Fig. II-6.

b. Dependence of DCA on System Parameters. The DCA, as defined in the previous section, depends on the following parameters:

- a) DCA energy barrier
- b) surface potential
- c) Hamaker's constant
- d) dimensions and shape of particles
- e) concentration of solution ions
- f) valence of bulk solution ions
- g) dielectric constant of bulk solution
- h) temperature

In order to investigate polymer bridging as a flocculation mechanism the response of the DCA to the above parameters must be known. The large variation in possible sizes of polymer bridges, 10 \AA for small loops to over $10,000 \text{ \AA}$ for completely stretched-out molecules, makes it necessary to investigate the parameters on two scales.

Within certain limits the value of the repulsion energy defining the DCA only slightly affects the value of the DCA. In Table II-1 the DCA's defined by energy values of kT , $5 kT$ and $10 kT$ are compared for various surface potentials at two ionic strengths. There is only a small dependence of DCA on the energy value used to define it at 10^{-2} molar ionic strengths because the interaction curves have relatively steep slopes (see curve A of Fig. II-6). For the 10^{-3} molar ionic strength system the DCA variation increases since the gradients of the interaction energy curves are smaller (see curve B of Fig. II-6). The variation is less than 15 percent for all cases listed in Table II-1.

In Fig. II-7 the variation of the $2 kT$ DCA and the $10 kT$ DCA with ionic strength is illustrated for one micron spherical particles having a surface potential of 50 mv and a Hamaker constant of 10^{-12} ergs. With decreasing ionic strength the double

Table II-1. DCA values at interaction energies of 10, 5 and kT. System: 1 micron diameter spherical particles, Hamaker constant = 10^{-12} ergs, temperature = 20°C.

(a) Ionic Strength = 10^{-2} moles/liter

Surface Potential (mv)	DCA (Å)		
	10 kT	5 kT	1 kT
40	0	0	0
45	49	52	54
50	66	68	70
60	86	88	90
70	101	103	105

(b) Ionic Strength = 10^{-3} moles/liter

Surface Potential (mv)	DCA (Å)		
	10 kT	5 kT	1 kT
20	0	0	0
25	150	178	201
30	230	251	276
40	318	340	367

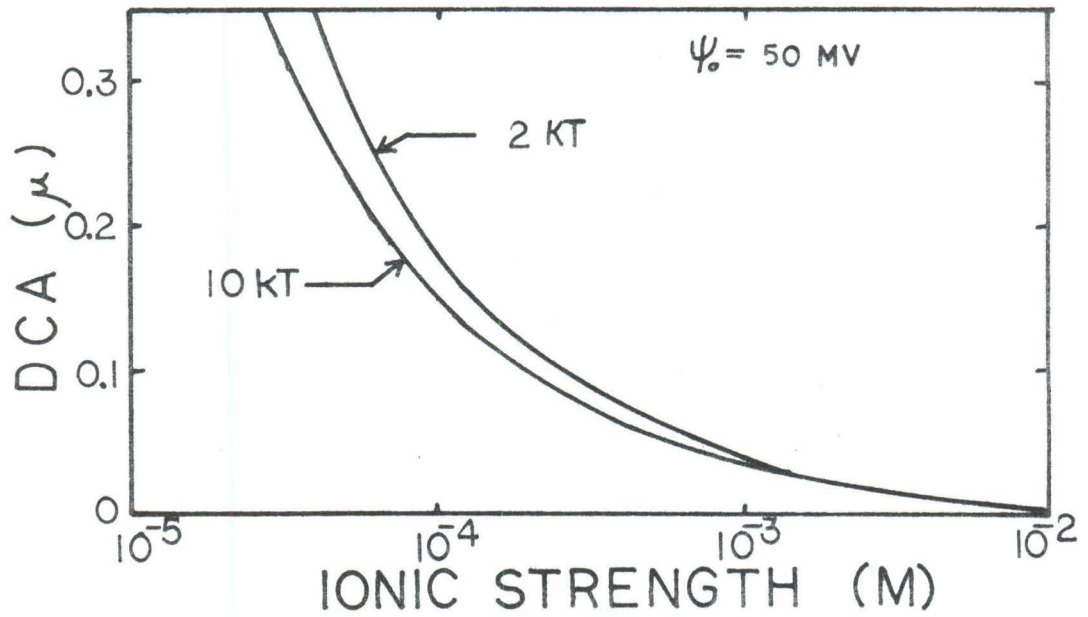


Fig. II-7. Effect of the energy value defining the DCA on the DCA-ionic strength relationship. Particle diameter = 1 micron and $A = 10^{-18}$ ergs.

layer expands and the DCA increases. At 10^{-4} molar ionic strength the difference between the DCA's defined at energies of 2 kT and 10 kT is less than 20 percent. From this and the previous observation it can be concluded that the value of the interaction energy defining the DCA is not critical.

For the relationships shown between the DCA and the ionic strength certain limitations must be placed on the composition of electrolytes in solution or the usual ionic strength definition must be modified. In the derivation of the double layer repulsion energy relationship, Eq. II-4, the solution was assumed to consist of symmetrical electrolytes. Verwey and Overbeek later showed that the capacity of the double layer is actually almost completely determined by the valency of the ions having charge opposite to that of the surface⁷⁴. This enables the double layer relationships to be used for systems containing unsymmetrical electrolytes if the valence and concentration used in the equations are those of the counter-ions.

Expression of the double layer relationships in terms of ionic strengths is straightforward for solutions of symmetric electrolytes; for solutions of unsymmetric electrolytes the usual ionic strength definition* must be modified to

$$I = \sum_i c_i z_i^2 \quad \text{II-9}$$

* $I = \frac{1}{2} \sum c_i z_i^2$, where i refers to all ions.

where C is the molar concentration, Z is the valency, and i refers only to counter-ions.

The relationship of the surface potential, ψ_0 , to the 5 kT DCA is illustrated in Figs. II-8 and II-9. At constant ionic strength the DCA increases with increasing surface potential. For systems having maximum interaction energies less than 15 kT, the shape of the curves in Fig. II-8 near zero DCA and the almost horizontal portions of the curves in Fig. II-9 are due to the fact that the DCA is defined as zero for all systems having total repulsion energies less than 5 kT.

If the maximum polymer loops extend 50 Å from the surface bridging can occur in a 10^{-2} molar ionic strength system only if the surface potential is between 42 and 49 mv. If ψ_0 is below 42 mv the particles coagulate by van der Waal's attraction; if ψ_0 is greater than 49 mv the particles cannot approach close enough to each other for the loops to form bridges.

The total interaction energy is the sum of the double layer repulsion (Eq. II-4) and the van der Waal's attractive energy (Eq. II-5). The van der Waal's attraction, equal to the product of the Hamaker constant and a separation distance factor, is directly proportional to the Hamaker constant. At distances between surfaces greater than 0.05 microns the attractive energy contributes little to the total interaction energy since the separation distance factor decays rapidly with increasing separation. The DCA is therefore essentially independent of the Hamaker constant for surface separations greater than 0.05 microns.

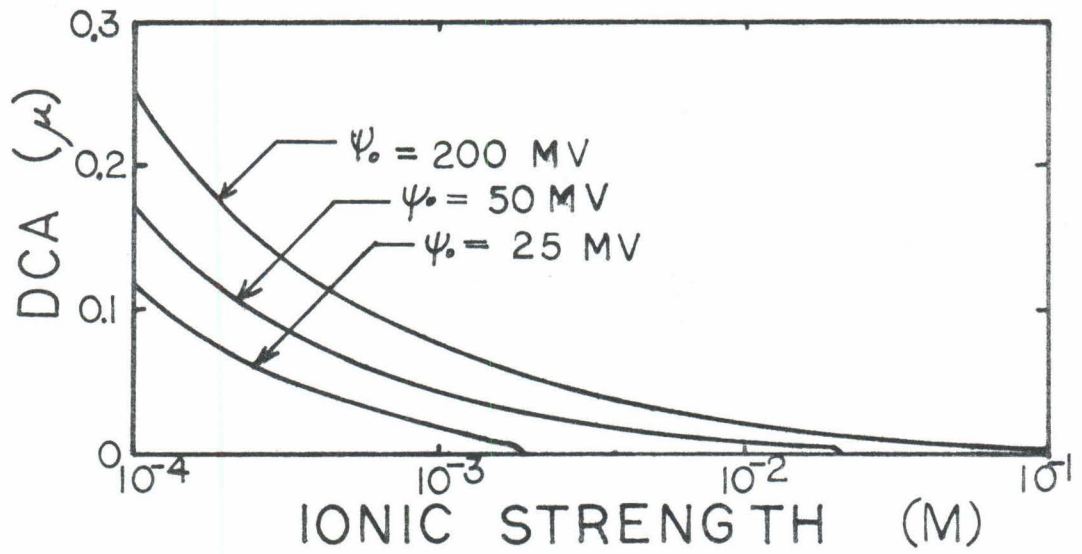


Fig. II-8. Dependence of the 5 kT DCA on ionic strength for particles with various surface potentials. Particle diameter = 1 micron, $A = 10^{-12}$ ergs.

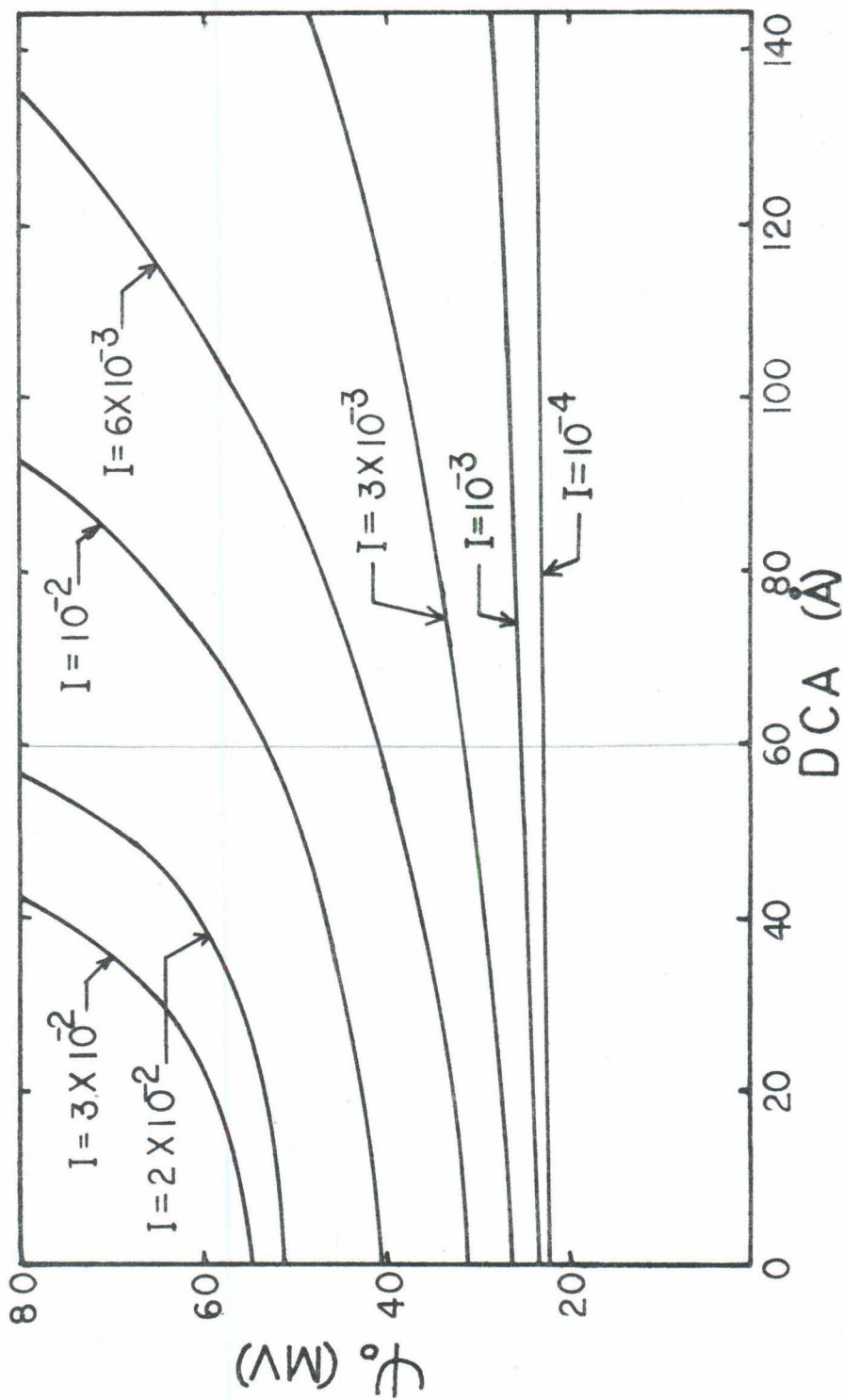


Fig. II-9. Variation of the DCA with surface potential at several ionic strengths. Particle diameter = 1.3 microns and $A = 10^{-12}$ ergs; I = moles/liter.

There is a large influence of the Hamaker constant on small DCA's (i. e. 0-200 Å). In Fig. II-10 DCA's for one micron spherical particles are shown as a function of surface potential at 10^{-2} and 10^{-3} molar ionic strengths and various values of the Hamaker constant.

The size and shape of the suspended particles also influence the DCA. The energy of interaction has been evaluated for flat plates and spherical particles by Verwey and Overbeek⁷⁴. In the present research only spherical particles have been examined theoretically.

The diameters of the interacting spherical particles affect the total interaction energy through both the repulsive and attractive terms. (See Eqs. II-4 and II-5.) The effect of particle size on the DCA's at various ionic strengths is illustrated in Fig. II-11. In general, the DCA increases with increasing particle diameter.

Both the valence and the concentration of the ions in the bulk solution affect the DCA. The ionic strength, used as a primary variable in several of the previous figures, combines the electrolyte concentration and valence into a single variable. It is re-emphasized that the ionic strength is determined from the valence and concentration of the counter-ions.

In Figs. II-12 and II-13 the DCA's are evaluated for different counter-ion valencies. With increasing valence the DCA decreases at constant ionic concentration and surface potential.

The repulsive energy between particles is directly proportional to the dielectric constant of the bulk solution. See Eq. II-4.

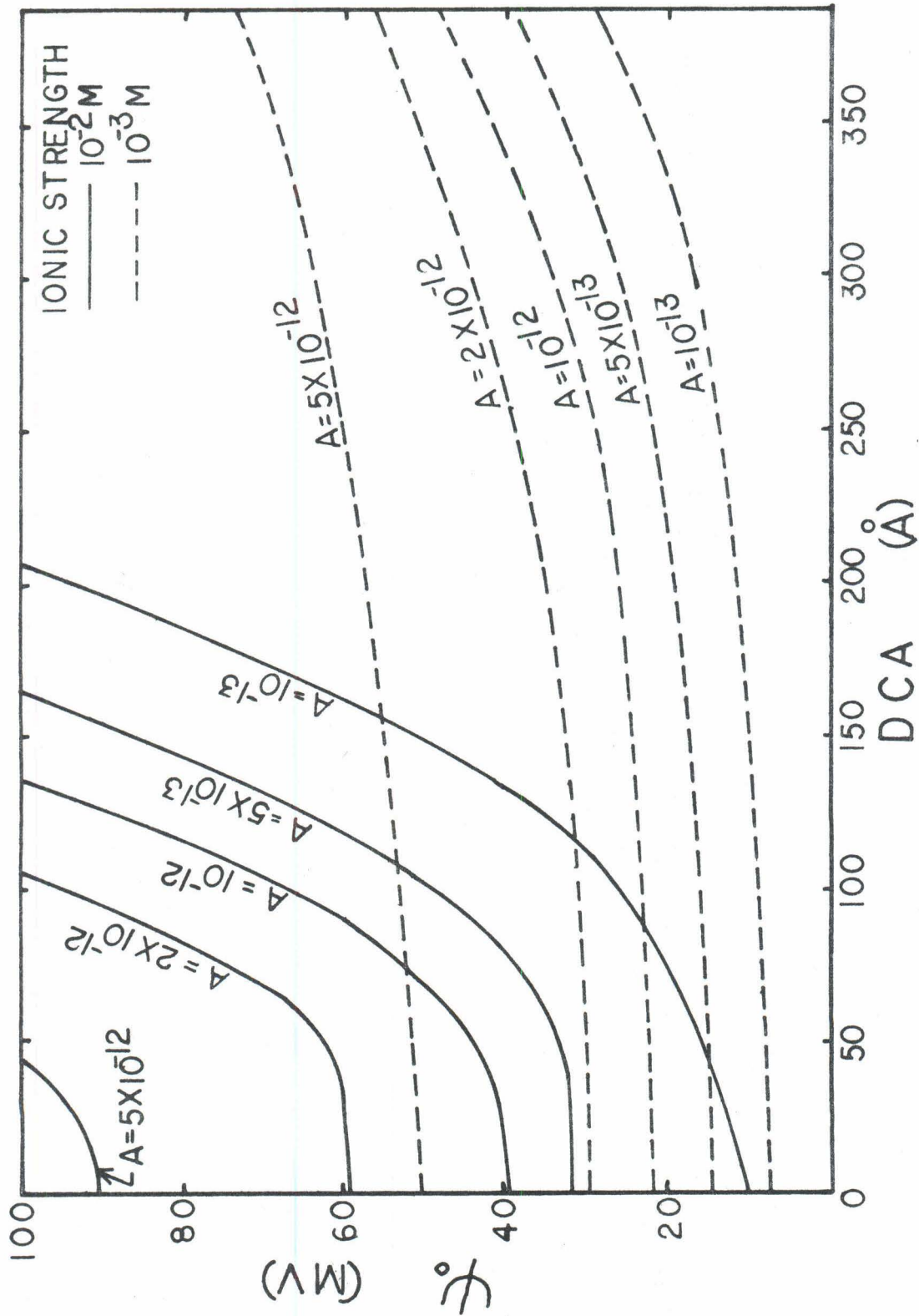


Fig. II-10. Effect of A , the Hamaker constant (ergs), on the DCA variation with ψ_0 . Particle diameter = 1 micron.

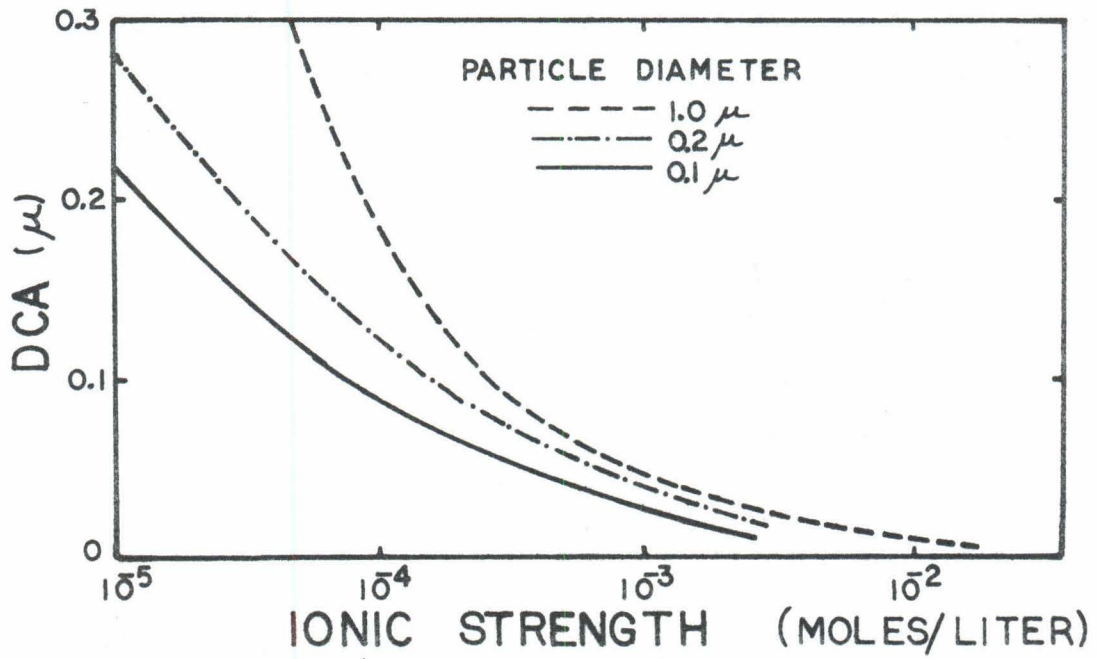


Fig. II-11. Influence of particle size on the DCA variation with ionic strength. $\Psi_0 = 50$ mv and $A = 10^{-12}$ ergs.

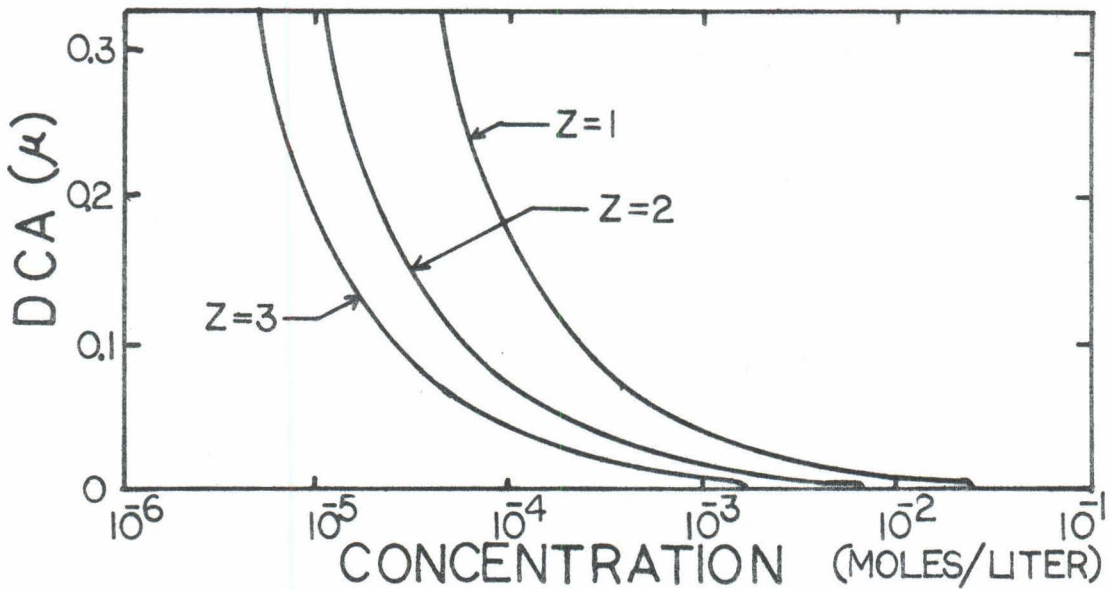


Fig. II-12. Effect of counterion valence (Z) on the DCA. Particle diameter = 1 micron, $A = 10^{-12}$ ergs and $\psi_0 = 50$ mv.

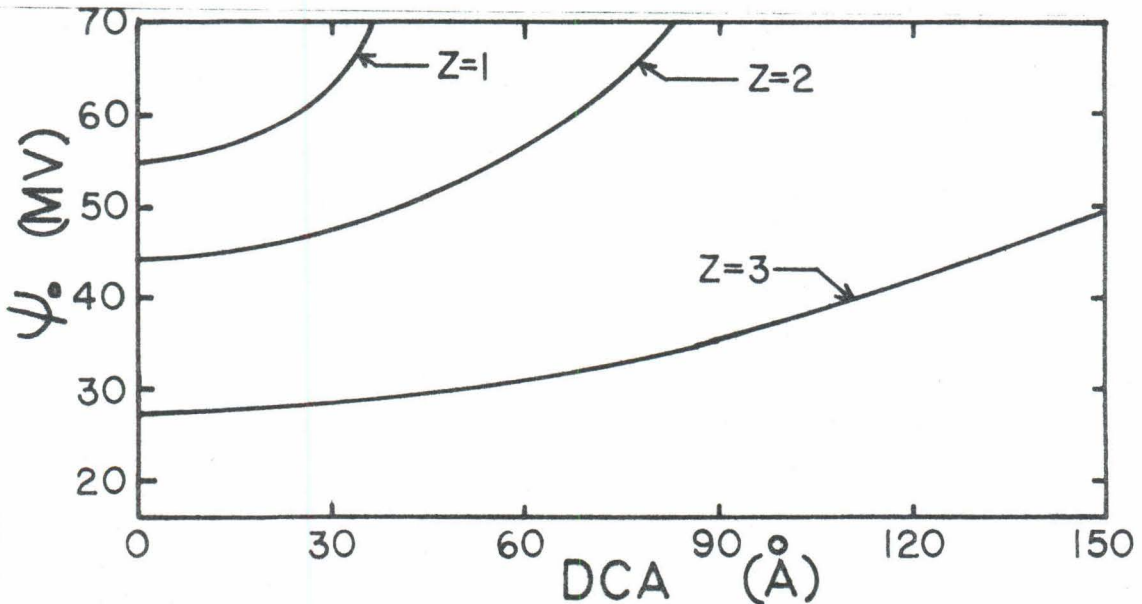


Fig. II-13. Variation of DCA- ψ_0 relationship with counterion valence (Z) at a constant counterion concentration of 3×10^{-3} moles/liter. Particle diameter = 1 micron.

However, DCA's were not evaluated in any other solvent than water since aqueous suspensions are the primary interest of this research.

The temperature affects both the dielectric constant and the thickness of the double layer. See footnote page 16. The DCA's at 0°C, 20°C and 40°C are tabulated in Table II-2 for various surface potential values at two ionic strengths. It is seen that the influence of temperature on the DCA is small over the forty-degree range.

In summary, the parameters most important in determining the DCA, the necessary length of polymer loops for flocculation by the bridging mechanism, are the surface potential, Hamaker constant, particle size and ionic strength. The DCA variation with DCA energy barrier height and solution temperature is small.

D. Adsorbed Polymer Configuration

The configuration of the adsorbed polymer molecules is a controlling factor in determining the destabilization mechanism of flocculation. See Fig. II-2. The adsorption of polymer from dilute solutions onto solid surfaces and the configuration of the adsorbed polymer chains at the solid-solution interface are controlled by the chemical and physical properties of the adsorbent surface and the solvent, and the molecular weight, charge and flexibility of the adsorbate.

Three general approaches have been used to determine the geometric configuration of adsorbed macromolecules: interpretation of empirical adsorption data, direct measurement of the adsorbed layer thickness, and statistical mechanical treatments based on

Table II-2. DCA values at temperatures of 0°, 20° and 40°C. System parameters: 1 micron diameter spherical particles, Hamaker constant = 10^{-12} ergs, DCA interaction energy = 5 kT.

(a) Ionic Strength = 10^{-2} moles/liter

Surface Potential (mv)	DCA (Å)		
	0°C	20°C	40°C
40	0	0	0
45	54	51	45
50	68	67	65
60	87	87	87
70	101	102	102
85	117	119	120

(b) Ionic Strength = 10^{-3} moles/liter

Surface Potential (mv)	DCA (Å)		
	0°C	20°C	40°C
25	183	175	161
30	251	250	247
40	334	338	339
50	391	397	402

random walk and/or Markoff Processes. Detailed reviews of polymer adsorption and configuration theories are presented by Patat et al⁴⁸, Steinberg⁶⁶, and Kipling³⁵.

1. Configurations Based on Empirical Adsorption Data

The configuration of adsorbed polymers at the solid-solution interface is related to the molecular weight dependence of the maximum amount of polymer adsorbed. Generally maximum polymer adsorption, A_s , onto nonporous surfaces is related to M , the molecular weight of the polymer, by the relationship

$$A_s = k M^\beta \quad \text{II-10}$$

where k and β are numerical constants. Using the models presented by Perkel and Ullman⁵⁰ the configuration of adsorbed molecules can be related to the values of β by the following simple models:

- (i) $\beta = 0$ All segments are attached to the surface or loops exist in which the number of segments is independent of molecular weight. That is, the number of segments in the loops is a constant fraction of the total number of segments adsorbed.
- (ii) $\beta = 1$ Only one segment of each polymer molecule is attached to the surface
- (iii) $\beta = 1/3$ Polymer molecules are adsorbed in spherical configurations with radii equal to or proportional to the radius of gyration of the molecule in solution. It is assumed that the radius is proportional to the

radius of gyration of the molecule in solution. It is assumed that the radius is proportional to the one-third power of the molecular weight.

- (iv) $0 < \beta < 1$ Adsorbed configuration consists of loops and directly attached trains with the number of segments in the loops proportional to molecular weight.
- (v) Combination of two or more of the above models when the configuration varies with degree of surface coverage. At low degrees of surface coverage polymer molecules lie flat on the surface ($\beta = 0$) while at high degrees of surface coverage loops are formed because unoccupied sites are not available ($0 < \beta < 1$). The maximum adsorption is then related to the molecular weight by

$$A_s = K_1 + K_2 M^\beta. \quad \text{II-11}$$

Two-dimensional illustrations of some of these models are presented in Fig. II-14.

There are several examples of negative β values reported in the literature⁴⁸. It is generally accepted, however, that true β values cannot be negative and that the measured adsorption decrease with increasing molecular weight is due either to lack of equilibrium or to the existence of pores in the surface of the adsorbent. These explanations seem plausible since (i) high molecular weight molecules diffuse slowly and require greater time than low molecular weight

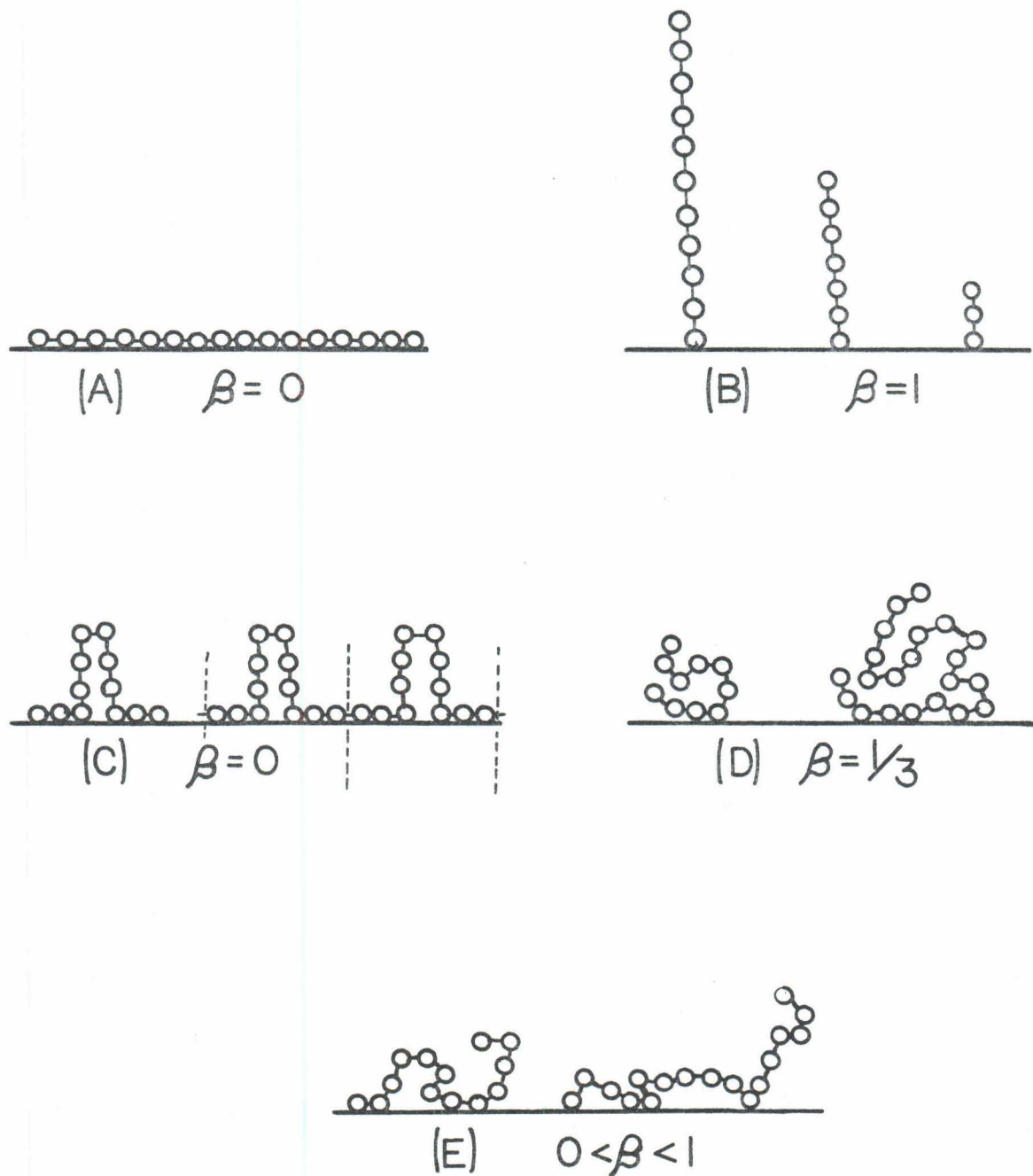


Fig. II-14. Two-dimensional models of adsorbed polymer configurations for various β values.

molecules to reach equilibrium, and (ii) small pores can exclude the large, high molecular weight molecules.

2. Measurement of Adsorbed Layer Thickness. The thickness of adsorbed polymer layers can be estimated by viscosity methods. Experimentally, the flow time of a standard solution through a capillary tube is measured before and after polymer is adsorbed to the walls of the capillary. Increased flow time is related to the effective thickness of the adsorbed polymer layer. An alternative method for determining thicknesses of adsorbed layers on suspended particles is to measure the viscosity of the particle suspension before and after polymer adsorption.

Viscosity methods have the disadvantage of measuring the thickness of the adsorbed layer averaged over the total surface area of the adsorbent. At low degrees of surface coverage the average thickness cannot be related to the real thickness without assuming something about the configuration.

The thickness of the adsorbed layer can be determined directly by measuring the change in the state of polarization of light reflected from a surface (ellipsometry). Smith and Stromberg⁶⁴ have evaluated the constants relating the polarization change to the thickness of the adsorbed layer. This method is limited to certain adsorbates with extremely clean and smooth surfaces.

Fontana and Thomas²³ determined the thickness of adsorbed polymer layers by measuring the change in particle sedimentation velocity due to polymer adsorption. The sedimentation boundary was followed by monitoring the optical density gradient in an ultra-

centrifuge. The disadvantages or limitations of this method are: (i) shapes of particles must be known or assumed for the sedimentation analysis, (ii) polymer configuration is interpreted as an increase in average particle diameter, (iii) particles must be small enough so that adsorbed layers result in measurable volume change, and (iv) method is limited to non-coagulating systems since aggregation increases the sedimentation velocity.

3. Statistical Mechanical Treatments

a. Thermodynamics of Adsorption. The driving force of all adsorption processes is a decrease in free energy. In the presence of an electrostatic double layer the total free energy of adsorption $\Delta\bar{G}$ is

$$\Delta\bar{G} = \Delta G + ZF\Delta\psi \quad \text{II-12}$$

$$\begin{array}{l} \text{total free} \\ \text{energy change} \end{array} = \begin{array}{l} \text{chemical free} \\ \text{energy change} \end{array} + \begin{array}{l} \text{electrical} \\ \text{free energy change} \end{array}$$

where ΔG is the specific adsorption energy due to non-electrostatic forces, Z is the valence of the sorbate, F is the Faraday constant and $\Delta\psi$ is the potential drop between the plane of adsorbed ions and the bulk solution. With double layers based on the Stern model ψ_0 is replaced by ψ_s , the Stern potential. A negative $\Delta\bar{G}$ is required for a spontaneous process.

One or more of the following types of energies may contribute to the change in chemical free energy causing adsorption at the solid-liquid interface:

- (a) hydrogen bond energy
- (b) complex formation energy
- (c) van der Waal's attractive energy
- (d) orientation (dipole-dipole) energy
- (e) induction (charge-dipole) energy
- (f) pi-bonding energy, charge transfer and possibly other polar bonding energies
- (g) desolvation and solvation energy for solid and solute

Stern provides for a specific chemical adsorption energy and the finite size of the ions in his double layer model presented in 1924⁶⁷. ϕ , the specific Stern adsorption energy discussed in Sect. II-C-2, is equal to $(-\Delta G)$.

b. Adsorbed Configuration. Numerous investigators (DiMarzio¹⁷, Hoeve²⁹, McCrackin³⁸, Motomura and Matuura^{41, 40}, Roe^{54, 55}, Rubin⁵⁶, Silberberg^{62, 63}, and Steinberg⁶⁶) have developed theoretical models predicting equilibrium configurations of adsorbed molecules at the solid-solution interface. The general trends predicted by the different models agree quite well, considering the great variety of assumptions used in developing the models.

The general approach followed for the adsorption models is to assign statistical weights to the different adsorption states and then evaluate partition functions which relate the number of segments in each state to the total number of segments. Assumptions are made which permit the adsorption of a single polymer molecule to be considered as a random walk or a Markoff process. Some of the studies^{38, 18} have been carried out by Monte-Carlo computer simulations.

Various models have accounted for the number of segments per molecule (molecular weight), stiffness of polymer, interaction

energy between surface and polymer segments, polymer concentration, and degree of surface coverage. No one model has considered the effects of all the above parameters on the configuration. Some of the results are limited to specific systems consistent with assumed model conditions such as infinite molecular weight, completely flexible polymer backbones, or low degrees of surface coverage.

Configurations are described in terms of number and length of loops, number and length of attached trains, length of dangling ends, average extension from the adsorption surface and fraction of segments bound directly to the surface. The extension from the surface and the fraction of segments attached directly to the surface are of primary importance in the investigation of the flocculation bridging mechanism.

The effects of various parameters on the adsorbed configuration determined by statistical mechanical studies are reviewed by presenting the results of several investigators. Particular attention is given to evaluation of the parameters for polyelectrolyte systems since none of the statistical models are specifically for polyelectrolyte adsorption. In view of disagreements with respect to some specific results obtained by the different approaches emphasis is placed on general dependencies or trends.

The most important configuration parameter is $\Delta\bar{G}$, the total adsorption energy per segment: large adsorption energies, i. e., large negative $\Delta\bar{G}$ values, cause polymer molecules to adsorb in flat configurations with no loops; small adsorption energies result

in configurations having large loops and long tails, and very small adsorption energies result in no adsorption.

The $\Delta\bar{G}$ range for polyelectrolyte adsorption can be determined by examination of Eq. II-12. The electrochemical contribution to $\Delta\bar{G}$ is about 2 kT for the adsorption of a monovalently charged ion or polymer segment to an oppositely charged surface at a potential of 50 mv. Organic molecules may have chemical free energies of adsorption between 1 and 10 kT. Assuming that the chemical adsorption energy of organic molecules and polymer segments are comparable, the total adsorption energy for a polyion segment adsorbing to an oppositely charged surface (25 to 100 mv surface potential) is between 2 and 10 kT.

Ionized polyelectrolytes are less flexible than non-ionic polymers or unionized polyelectrolytes because of the Coulombic repulsion between adjacent ionized segments. The formation of looped configurations is favored by a high degree of flexibility. Other than the work of Silberberg⁶³ and Roe⁵⁵ few investigations have been made on the effects of flexibility on adsorbed polymer configurations. Application of Silberberg's and Roe's results is complicated by the difficulty of defining the degree of flexibility on a quantitative scale.

In Figs. II-15 (Motomura and Matuura⁴¹) and II-16 (Silberberg⁶³) the dependence of the average number of segments per loop (N_L) on the adsorption energy per segment is illustrated for a high molecular weight polymer. The length of a loop is simply the number of segments per loop times the length of a

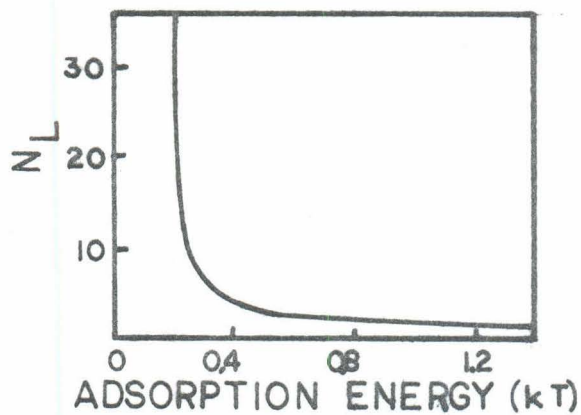


Fig. II-15. Dependence of the average number of segments per loop (N_L) on the adsorption energy per segment. Adapted from Motomura and Matuura⁴¹.

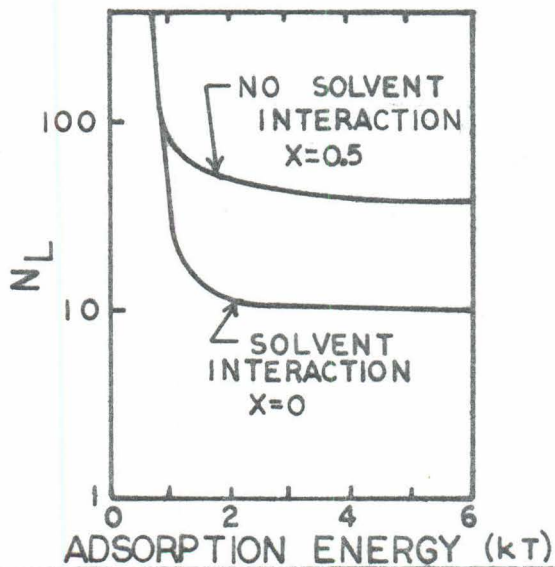


Fig. II-16. Variation of the average number of segments per loop (N_L) with adsorption energy per segment. Adapted from Silberberg⁵³.

segment. N_L is important in analysis of the bridging model because it is proportional to the average thickness of the adsorbed layer.

Fig. II-16 illustrates values of N_L for different degrees of interaction between the polymer molecules and the solvent. The

$\chi = 0.5$ curve is for a system in which the polymer molecules do not interact with the solvent (theta solvent). Ionized polyelectrolytes, surrounded by an electric double layer, interact with the solvent and are perhaps best described by the strong interaction curve, i.e. $\chi = 0$. Polyions having rod-like solution configurations, the result of strong polymer-solvent interactions, adsorb in flatter configurations at solid surfaces than do polymers having coiled solution configurations.

It is interesting to note that Motomura and Matuura (Fig. II-15) find that the number of segments per loop is less than five for adsorption energies greater than 0.4 kT. Silberberg's results, Fig. II-16, indicate that loops contain only ten segments when adsorption energies are greater than 1.5 kT. While there are differences between the results of the two investigations, both indicate that loops contain no more than ten to twenty segments for adsorption energies greater than 2 kT.

A clarification of the exact meaning of the term "segment" is in order since it may take on a different meaning in the statistical mechanical models than that in the previous descriptions of polymers, distances, and adsorption energies. The usual definition is that each segment is equal to one polymer repeating unit. In

some of the statistical mechanical models a segment is assumed to be an element of a polymer chain which is completely independent of the adjacent elements. This definition necessitates the adoption of the Kuhn statistical segment⁷⁰ for polyelectrolytes which have interactions between adjacent repeating units. A Kuhn statistical segment usually contains many polymer repeating units. In the following analyses it will be noted when the term "segment" takes on the meaning of a Kuhn statistical segment.

The distribution of segments with distance from the surface is more important than the average number of segments per loop since it is probable that bridges would be formed by the larger-than-average loops. In Fig. II-17 DiMarzio and McCrackin¹⁸ illustrate the distribution of segments with the distance from the surface for various adsorption energies. Polymers with weakly adsorbed segments are held loosely with the majority of segments being at distances of approximately ten segment lengths from the surface. For adsorption energies on the order of kT , less than one percent of the segments are distances of four segment lengths from the surface.

Fig. II-18, from McCrackin³⁸, shows the average distance to the segment farthest away from the surface as a function of adsorption energy for several degrees of polymerization. It is difficult to extend McCrackin's results to chains containing more segments since his data was obtained by Monte-Carlo computer simulations. The distance to the segment farthest from the surface is especially interesting since the farthest segment is the segment

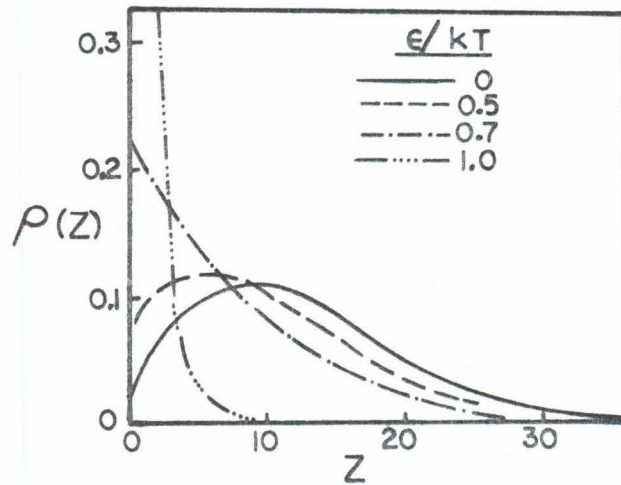


Fig. II-17. Distribution of density of polymer segments $\rho(Z)$ with distance from surface (Z) for various adsorption energies (ϵ). From DiMarzio and McCrackin¹⁸.

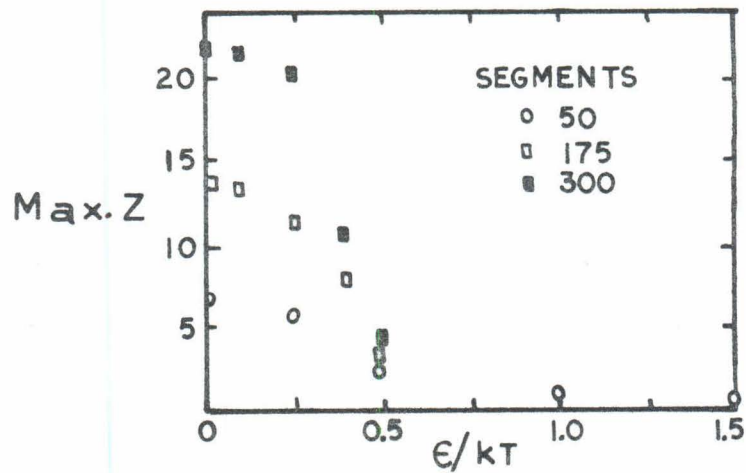


Fig. II-18. The average distance (Max. Z) to the segment farthest from the surface. The distance is given vs adsorption energy (ϵ) for three different degrees of polymerization. Adapted from McCrackin³⁸.

most likely to form bridges with other particles. The rapid flattening of the adsorbed layer with increasing adsorption energy is again seen in McCrackin's results.

Fig. II-19 (Roe⁵⁵) illustrates the dependence of the average number of segments per loop on the adsorption energy for polymer chains having different degrees of flexibility and containing various numbers of segments, i.e., various molecular weights. Polyelectrolytes are best described by the curves for stiff chains. Fig. II-19 indicates that with large adsorption energies neither molecular weight or flexibility effect the loop size since there is a completely flat configuration. Flexibility affects the value of the critical energy above which flat configurations exist while the molecular weight effects the loop size for adsorption energies less than the critical value.

In some models of flocculation by the polymer bridging mechanism it has been proposed that the dangling ends or free tails of the adsorbed molecules form the bridges between particles. In Fig. II-20 (Roe⁵⁵) the average length of the desorbed sequences at polymer chain ends is plotted as a function of the interaction energy for both flexible and stiff molecules. The dangling ends of the flexible molecules adsorb more easily than do the ends of stiff molecules.

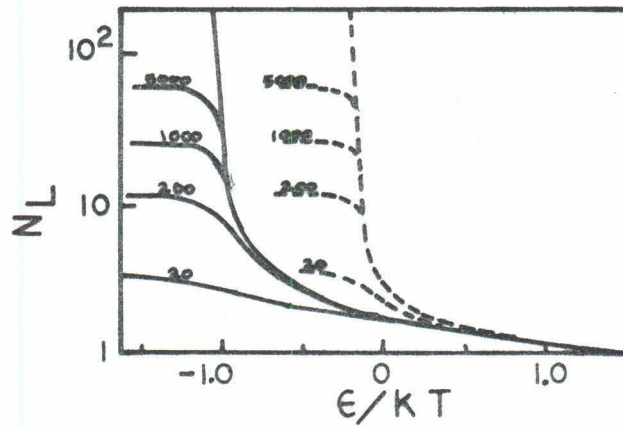


Fig. II-19. The average number of segments per loop (N_L) plotted against adsorption energy for flexible (solid lines) and stiff polymer chains (broken lines). The numbers on the lines indicate degrees of polymerization. From Roe⁵⁵.

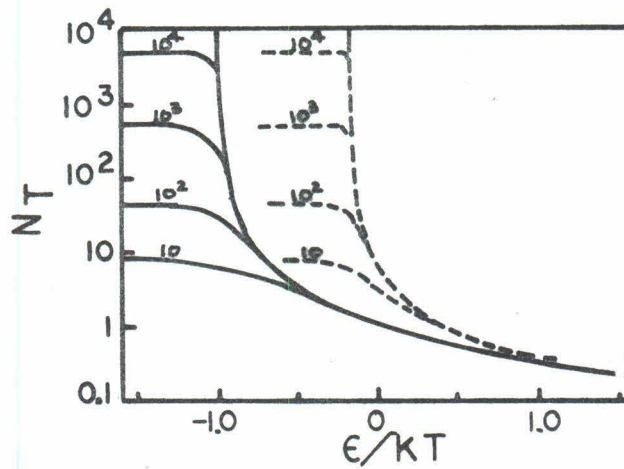


Fig. II-20. The same as Fig. II-19, except that here the number of segments (N_T) of the desorbed sequence at the polymer ends is plotted. From Roe⁵⁵.

From Fig. II-20 it can be concluded that polyelectrolytes adsorb to oppositely charged surfaces without dangling ends since the adsorption energies are large. Bridge formation by free ends does not occur in systems of polyelectrolytes and oppositely charged particles.

The average number of segments per loop and the distance to the farthest segment of each molecule yield no information about the fraction of the total number of segments attached directly to the surface. The segments attached directly to the surface are important in the electrostatic flocculation model because they effect the Stern potential.

In Figs. II-21, II-22, and II-23, from Motomura and Matuura⁴¹, Roe⁵⁵, and Higuchi²⁸, respectively, the dependence of the fraction of segments attached directly to the surface on the adsorption energy is illustrated for molecules with different degrees of flexibility and different molecular weights. The different models indicate that the bound fraction of segments increases with increasing adsorption energy.

Fig. II-22 indicates that stiff molecules adsorb by a "go-or-no-go" process. This is reasonable for stiff molecules since it is probable that segments adjacent to an adsorbed segment will also adsorb. If stiff molecules do adsorb, the majority of segments attach directly to the surface.

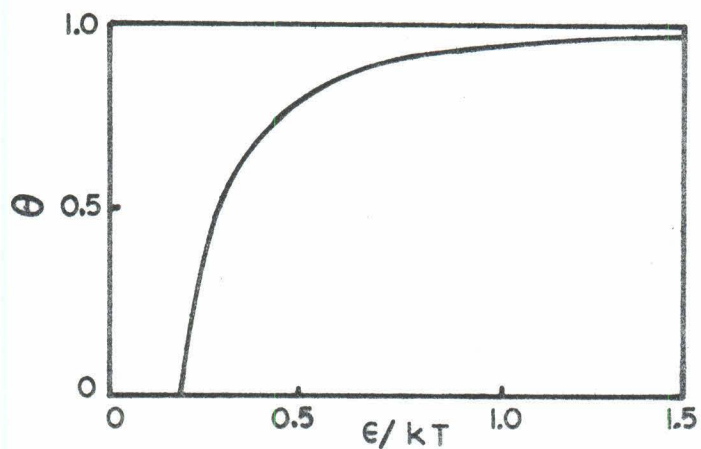


Fig. II-21. Plot of θ , the fraction of the total number of segments which are attached directly to the surface, against adsorption energy in the limit molecular weight $\rightarrow \infty$. From Motomura and Matuura⁴¹.

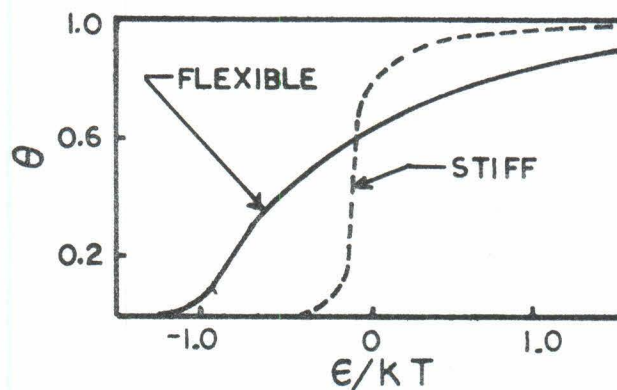


Fig. II-22. The fraction of attached segments (θ) against adsorption energy for flexible (solid line) and stiff polymer chains (broken line). Adapted from Roe⁵⁵.

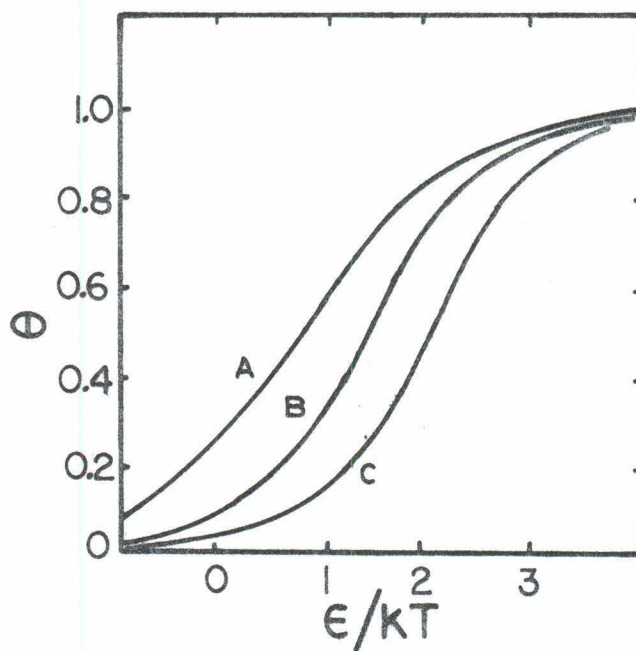


Fig. II-23. A plot of Θ , the attached fraction of segments, against the adsorption energy (E). A, B and C correspond to degrees of polymerization of 10^2 , 10^3 , and 10^4 , respectively. Adapted from Higuchi²⁸.

In Fig. II-23 the effect of molecular weight on the fraction of bound segments is illustrated. Molecular weight affects the bound fraction only when adsorption energy values are intermediate. Molecules which have strong adsorption energies (e.g., polyelectrolytes and oppositely charged surfaces) attach almost every segment to the surface regardless of molecular weight.

In summary, the adsorbed configuration of polymers on solid surfaces is primarily determined by the segment-surface adsorption energy. The adsorption energy of polyions adsorbing onto oppositely charged surfaces is probably greater than $2 kT$ per segment. Polymers with adsorption energies of $2 kT$ or greater adsorb in relatively flat configurations with: (i) essentially no loops extending ten or more segment lengths from the surface, (ii) more than 95 percent of the segments attached directly to the surface, and (iii) no free tails longer than a few segments in length.

The statistical mechanical models also predict that in systems with strong adsorption energies the adsorbed configurations are independent of molecular weight.

E. The Improbability of a Bridging Mechanism in Polyelectrolyte Flocculation of Particles of Opposite Charge.

Assuming that the segment length is equal to the length of a polymer repeating unit, a segment of a vinyl polymer has a length of 2.54 \AA . The majority of polyelectrolytes used as flocculants probably have segment lengths between 2 and 5 \AA . From the results of the statistical mechanical configuration investigations

reviewed it is concluded that the maximum length of polyelectrolyte loops attached to oppositely charged surfaces is less than 120 Å. A loop with a length of 120 Å can extend away from the surface a maximum of 60 Å. Therefore, for a polymer loop to form a bridge between two particles it is necessary for the surfaces of the particles to approach within 60 Å of each other.

The minimum separation distances between particles have been evaluated in terms of a distance of closest approach, or DCA. Three regions are illustrated in Fig. II-24, which is based on the relationships developed in Fig. II-9. The solid line defines the regions of particle stability and instability assuming a stability repulsion barrier height of 5 kT. Spherical particles with surface potentials above the solid line are stable.

A dashed line is also illustrated in Fig. II-24 which relates the surface potential to the ionic strength for systems having the 5 kT DCA equal to 60 Å. The position of this dashed line is evaluated from the curves illustrated in Fig. II-9 by reading the surface potential and ionic strength values at DCA = 60 Å. The region between the two lines in Fig. II-24 represents the systems which have particles separated by less than 60 Å. Since the maximum length of a polyelectrolyte bridge is 60 Å, bridging can only occur for systems in this enclosed region. For this reason this area is referred to as the "bridging region".

Particles in natural waters usually have surface potentials greater than 50 mv. At low ionic strengths, polyelectrolyte bridging can only occur when the surface potential is reduced to about

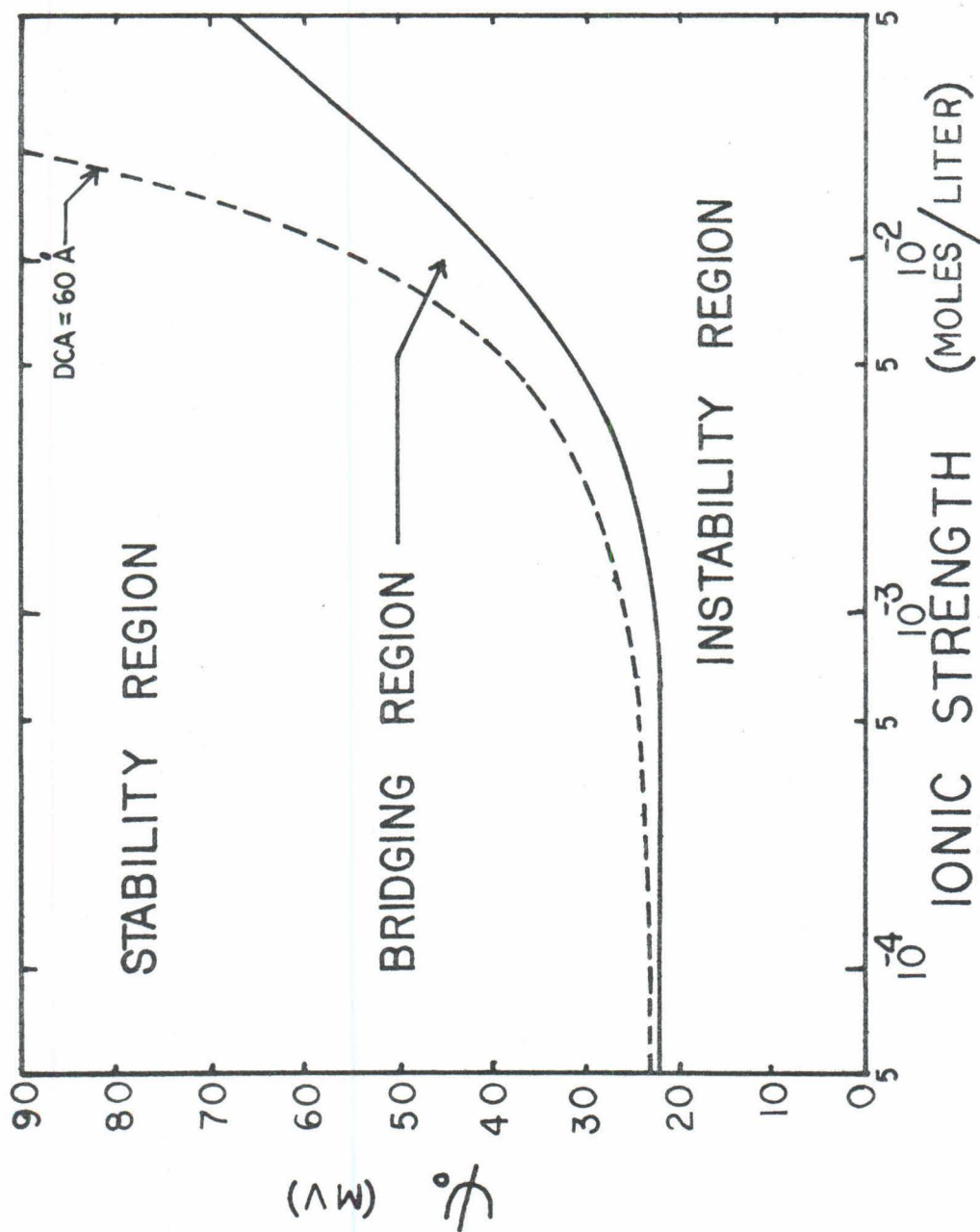


Fig. II-24. Regions of particle stability, particle instability and polymer bridging. Maximum polymer extension = 60 Å, Hamaker constant = 10^{-12} ergs, particle diameter = 1 micron and DCA based on interaction energy of 5 kT.

24 mv. Since the polyelectrolyte segments attached directly to the surface lower the surface potential (Stern potential), it is possible for the system to enter the bridging region by adsorption of polyelectrolyte molecules. Remaining in the bridging region, however, is difficult since adsorption of only a small amount of additional polyelectrolyte causes the system to become unstable. Flocculation is then the result of surface potential reduction and not polymer bridge formation. At high ionic strengths the possibility of bridging increases since the bridging region is wider.

The experimental systems chosen for this investigation were limited to ionic strengths below 10^{-2} moles/liter. The Stern potential values of the experimental systems which are presented in Tables V-3 and V-4 are all located above the bridging region of Fig. II-9. In these systems the probability of flocculation occurring by polymer bridging is very small.

Chapter III

AN ELECTROSTATIC PATCH MODEL OF POLYMER FLOCCULATION

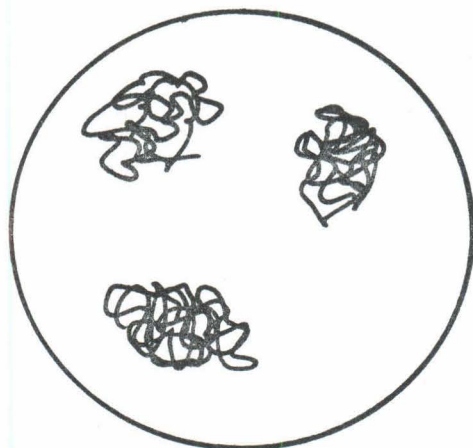
A. Description

1. Polymer Configuration. Polyelectrolyte molecules in solution have ellipsoidal or loose random coiled configurations even though there is repulsion between adjacent ionized segments. The probability that a polyelectrolyte molecule is completely extended is infinitely small even in solutions of zero ionic strength.

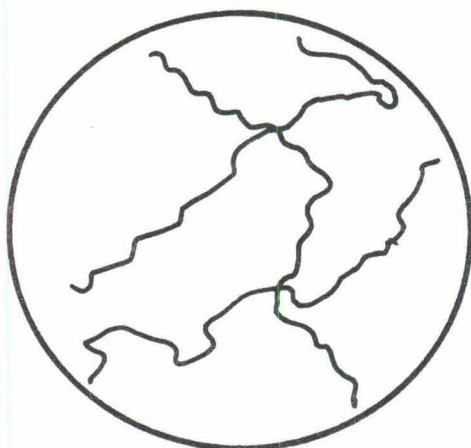
When the adsorption forces are relatively large as in the case of the system investigated here, polyelectrolyte adsorption to surfaces of opposite charge, adsorption causes the polymer configuration to change from a three-dimensional coil to a two-dimensional or flattened coil on the surface. This flattening causes polyelectrolyte molecules to form patches on the adsorption surface and not long, stretched-out rods. See Fig. III-1.

2. Electrical Double Layers. There is not necessarily one-to-one association between the ionized groups of the polyelectrolyte and the charge sites on the adsorption surface since the charge densities of most particulate matter found in nature are in the range of one negative charge per 100 \AA^2 to 1000 \AA^2 . Typical polyelectrolytes used as coagulants are able to take on adsorbed configurations requiring only 20 \AA^2 to 60 \AA^2 per ionized segment.

Ionized groups attached to a vinyl polymer backbone are limited to separation distances of less than 10 \AA since the vinyl groups are separated by 2.54 \AA . The result of the difference in



POLYMER PATCHES



STRETCHED-OUT RODS

Fig. III-1. Adsorbed polymer configurations.

charge densities and the steric hinderance is that a patch of cationic polyelectrolyte adsorbed on a negatively charged particle has a net positive charge. The magnitude of the net charge density depends on the parameters of the system.

Although not all the polymer segments are able to attach directly to a charged surface group the probability of large loop formation remains small since polymer segments can adsorb to unionized surfaces by hydrogen bonding and van der Waal's attraction.

In the proposed patch model particle aggregation is attributed to electrostatic attractions between positively charged polymer patches and free negatively charged surfaces of different particles. The magnitude of the interaction force between two charges varies inversely with the distance separating the charges. In systems of sphere-like particles this dependency on the separation distance causes the total interaction force between two particles to be primarily determined by the charges in the region where the separation distances are smallest. In aqueous solutions the polymer patches and the free surfaces both have double layers, which complicates the computation of the interaction forces.

For aggregation to occur the total net charge of the particle and its adsorbed polyelectrolyte need not be zero since the net interaction force is weighted heavily by certain localized charges. Electrophoretic mobility data of Gregory²⁴, Dixon¹⁹, and Birkner⁵ show in fact that particle mobility need not be zero for flocculation to occur.

The primary difference between this model and previous

electrostatic flocculation models is the existence of charged patches the size of which depends on polymer molecular weight and solution composition.

In Fig. III-2 aqueous solution models of free surfaces and surfaces with adsorbed cationic polymer, together with diagrams of the resulting electrical double layers, are illustrated. Both the free surface and the adsorbed polyelectrolyte patches have strongly attached stern layers. Neglecting the transition zones between polymer patches and free surfaces the illustrated double layers are the only two which can exist. That is, surfaces are free or surfaces are covered by adsorbed polymer molecules. All free surfaces have double layers of the type in Fig. III-2 (a), and all surfaces with adsorbed polymer have double layers of the type in Fig. III-2 (b). Increasing the amount of polyelectrolyte adsorbed only causes an increase in the relative amount of surface area covered by the polymer-type double layer.

The Stern layer of the polymer patch reduces the net charge associated with adsorbed polyelectrolyte molecules. This reduced charge can be thought of as a reduction in the dissociation of the polyelectrolyte molecule. Quantitative electrostatic stoichiometry does not exist between the polyelectrolyte charges and the surface charges because of the Stern layers of the free surface and that covered with adsorbed polyelectrolyte. For example, when a number of charged polymer segments equal in number to the total number of charges on the particle are adsorbed to the particle, the particle still can have a net negative charge.

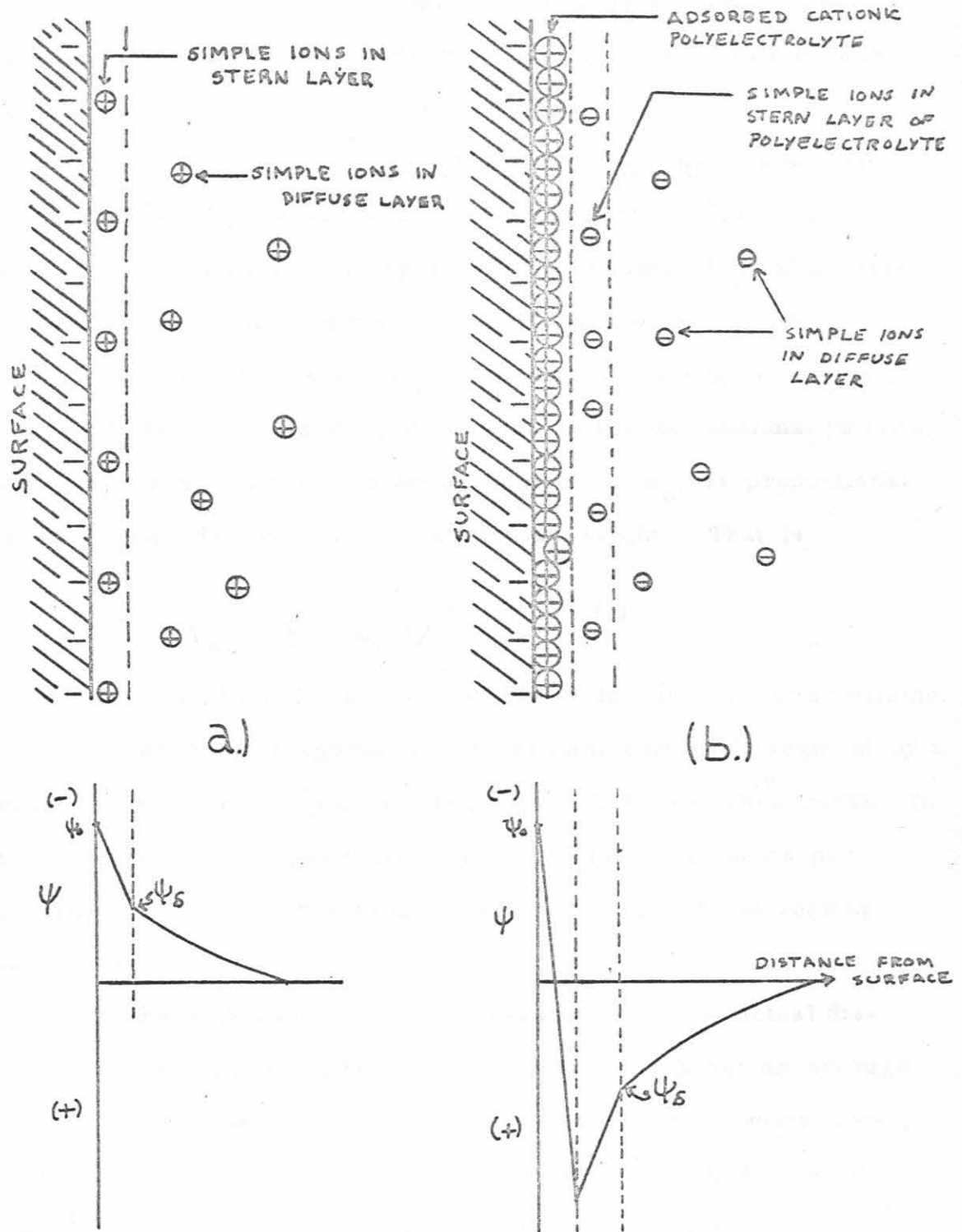


Fig. III-2. Schematic models of double layers and the corresponding potential diagram. (a) Free surfaces, (b) surface with adsorbed cationic polyelectrolyte. Only net charges are illustrated.

The density of the polymer Stern layer may vary with polymer molecular weight, adsorbed polymer configuration, and polymer and solution composition.

3. Effect of Molecular Weight on Patch Size. The size or area of a polymer patch is a function of molecular weight. According to Tanford⁷⁰ the hydrodynamic volume, V_h , of a polyelectrolyte molecule is directly proportional to the molecular weight under constant solution conditions. If, during adsorption, three-dimensional coils simply collapse to two-dimensional patches, the area occupied by each polymer molecule, A_o , is proportional to the two-thirds power of the molecular weight. That is

$$A_o \propto L^2 \propto V_h^{2/3} \propto M^{2/3} \quad \text{III-1}$$

where L is a characteristic dimension of the hydrodynamic volume.

An alternative approach is to assume that each segment of a polymer molecule occupies a fixed area. This approach results in A_o being directly proportional to the number of segments per molecule. With either approach, A_o increases with increasing molecular weight.

In the proposed model it is assumed that the actual distances between patches are normally distributed about an average value. This assumption is based on the fact that between like-charged patches repulsion exists which causes some degree of symmetry in the distribution of patches on the surface.

Fig. III-3 illustrates the adsorption of high and low molecular weight polyelectrolyte molecules to two approaching particles at

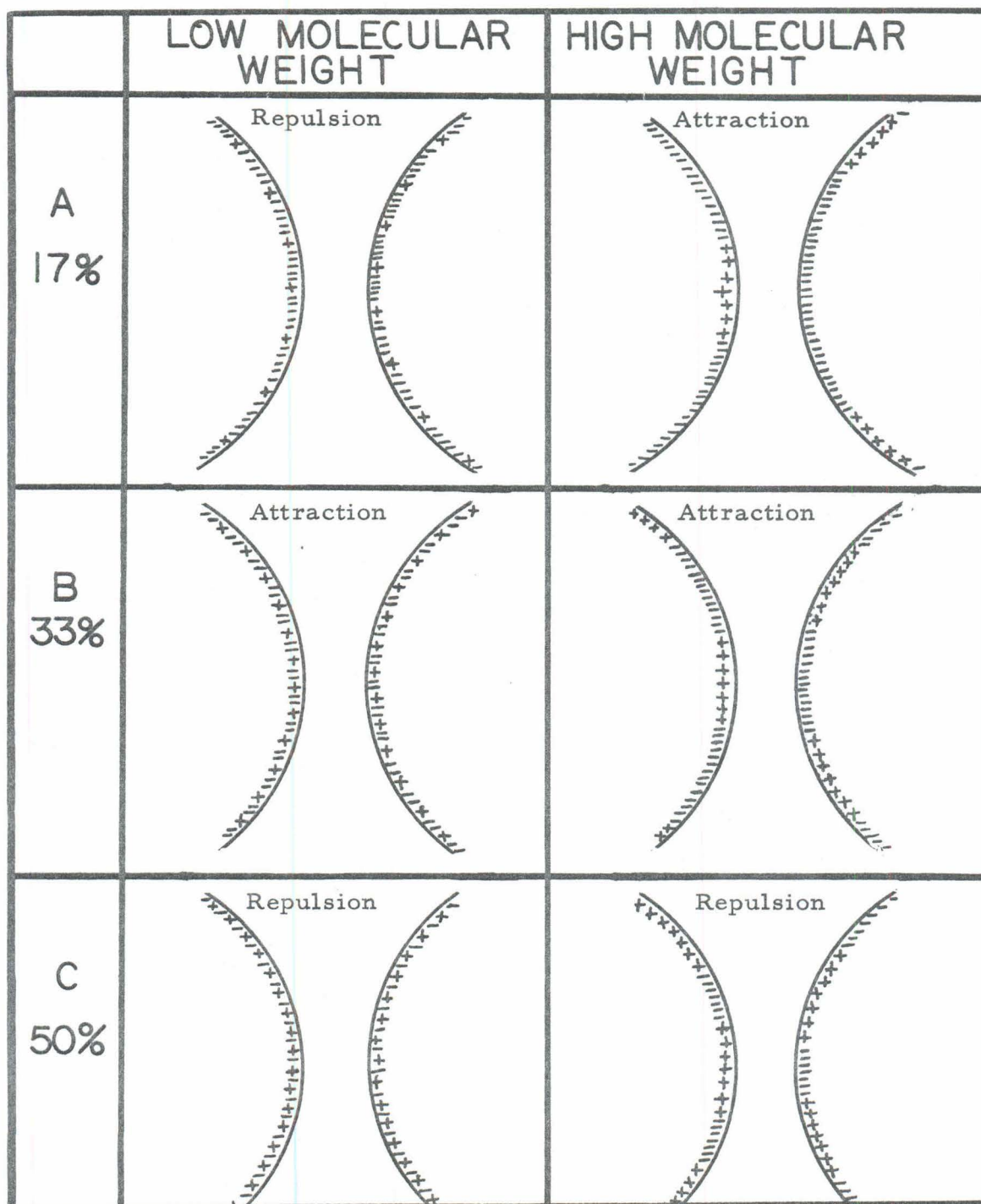


Fig. III-3. Effects of molecular weight and degree of surface coverage on adsorbed polymer patch distributions. Degrees of surface coverage: A - 17%, B - 33% and C - 50%.

three different degrees of surface coverage or amounts of polymer adsorption. At any particular degree of surface coverage the total number of polymer segments or the weight of adsorbed polymer is independent of molecular weight. The area occupied by a polymer patch and the distance separating patches varies with molecular weight. In Fig. III-3 a low molecular weight polyelectrolyte is schematically represented by a single plus sign and a polyelectrolyte with molecular weight twenty times greater is represented by a sequence of seven plus signs (i. e., $20^{2/3} \approx 7$).

When 17 percent of the surface is covered by polyelectrolyte molecules there is net repulsion between the particles in the low molecular weight system while there is net attraction between the particles in the high molecular weight system. This net force difference results from the fact that in the high molecular weight system all the heavily weighted interaction forces are attractive since they are caused by charges of opposite signs; this is not the case in the low molecular weight system. With this electrostatic patch model the polymer dose required for aggregation decreases with increasing molecular weight.

By increasing the degree of surface coverage to 33 percent (part B of Fig. III-3) more positively charged surface is generated and the net forces between particles in both systems are attractive. Additional polymer adsorption causes an excess of positively charged areas which result in net repulsion between particles and restabilization of the suspension. See Fig. III-3 (C).

In Fig. III-3 a specific orientation between approaching

particles is assumed. Since not all particles approach with this particular orientation it is further assumed that the rate of successful collisions can be expressed as the product of the total collision rate and the fraction of orientations having net attractive interactions. The number of different orientations resulting in net attractions depends on the degree of surface coverage and the molecular weight.

4. Effect of Solution Composition on Patch Model. Increasing ionic strength compresses electrical double layers and reduces the distances over which charges can interact. In general, charges separated by more than two double layer thicknesses contribute little to the total interaction force. Increasing the ionic strength reduces the absolute area of interacting surfaces, thereby causing the surfaces separated by the shorter distances to contribute more to the total force. The degree of surface coverage required for flocculation therefore decreases with increasing ionic strength.

Ionic strength also affects the charge density of the adsorbed polyelectrolyte patches by controlling the volume of the polyion in solution. Under conditions of high ionic strength, when the polyelectrolyte solution configuration is compact, adsorption results in patches with relatively high charge densities.

In addition to the effects described above, the solution composition can also affect polymer flocculation of suspensions by:

- a) controlling the surface potential;
- b) lowering the Stern potential of the free surfaces;
- c) interfering with polymer adsorption by occupying adsorption sites;
- d) lowering the Stern potential of the adsorbed polymer surface.

The resultant effect of varying solution composition on the degree of surface coverage required for flocculation depends on which of the above phenomena are dominant under the particular solution conditions imposed.

B. Mathematical Modeling of the Electrostatic Patch Mechanism

The total interaction force between two particles with adsorbed polymer patches was calculated using an IBM 360/75 computer and a program written in Fortran. The effects of polymer molecular weight and solution ionic strength on the degree of surface coverage required for flocculation were investigated. The total interaction between two particles is determined by summing the interactions between each charged site on one particle with every charged site on the other particle.

1. Computer Program. Two approaching particles are approximated by two spheres (I&J) of radius R whose centers are separated by a distance of $2R+S$. The surface of each sphere is subdivided into small sections or grids whose areas are defined by values of $\Delta\theta$ and $\Delta\phi$, the longitude and co-latitude in a spherical coordinate system. Identification of the grids is accomplished by considering the surface a two-dimensional matrix. Those grids with adsorbed cationic polyelectrolyte are assigned positive charges while the grids representing free surface are assigned negative charges. The magnitudes of the charges are a function of the charge densities of the surfaces.

In this investigation the grids were defined by angular displacements of one-quarter degree. In a system of one micron

diameter particles this displacement results in grids of approximately 475 \AA^2 .

For the electrostatic patch model it is assumed that the only interactions are Coulombic attraction and repulsion. $X(a, b:c, d)$, the distance between grid (a, b) on the I sphere and grid (c, d) on the J sphere, is calculated and then the Coulombic interaction is evaluated. That is

$$f(a, b:c, d) = \frac{S(a, b) S(c, d)}{X(a, b:c, d)^2} \quad \text{III-2}$$

where $f(a, b:c, d)$ is a force term proportional to the interaction force between grid (a, b) on the I sphere and grid (c, d) on the J sphere; $S(a, b)$ and $S(c, d)$ are the algebraic values of the charges in the respective grids. Additional details of the program, including the geometric relationship for $X(a, b:c, d)$, are presented in Appendix 2.

A total interaction parameter, F , is defined as the sum of all $f(a, b:c, d)$. F is given by

$$F = \sum_I \sum_J f(a, b:c, d) \quad \text{III-3}$$

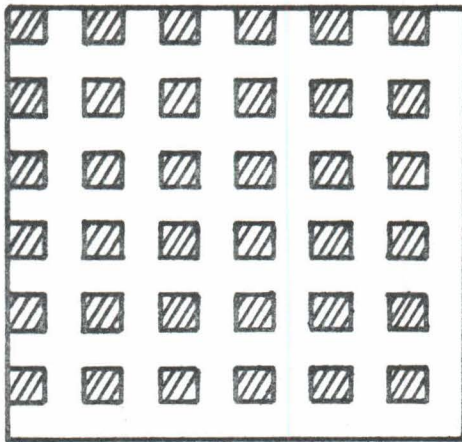
where the summations are over all grids of the I and J spheres. Negative F values indicate net attraction between particles and positive F values indicate net repulsion. Net attraction can occur even though the total charge on each particle is negative.

Additional refinement of the interaction force analysis was not attempted because of certain inherent limitations:

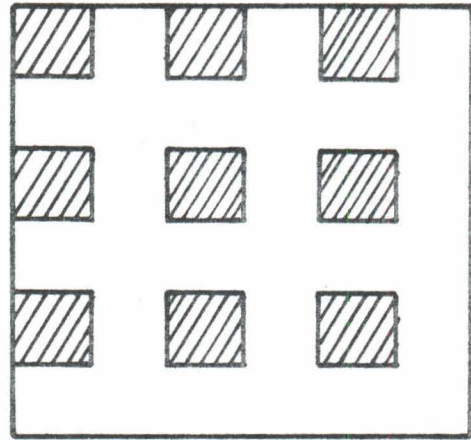
- (i) Interactions occur between both the diffuse double layers and the compact Stern layers;
- (ii) The effect of the transition zones between adjacent positive and negative double layers on particle interaction is unknown;
- (iii) The dielectric constant, which influences the magnitude of the interaction force, probably varies with the separation distance between the surfaces.

2. Effects of Molecular Weight and Ionic Strength. The effect of molecular weight was investigated by varying the sequence of positively and negatively charged grids. In Fig. III-4 the effect of molecular weight on patch size is illustrated for four systems each with 25 percent of its surface covered by adsorbed polymer. The indicated molecular weights are based on a monomer molecular weight of 214 g/mole and a surface area requirement of 40 \AA^2 per polymer segment. The smallest polymer molecule which can be investigated using the one-quarter degree grids has a molecular weight of 2,500.

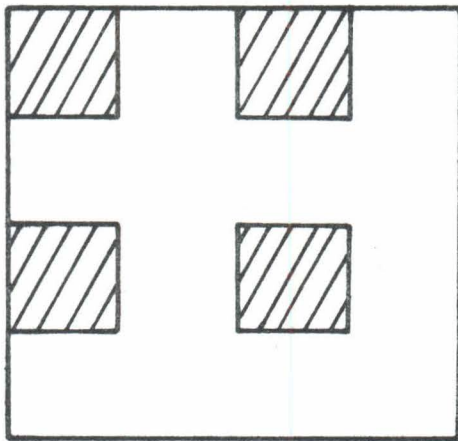
The degree of surface coverage is varied by either increasing or decreasing the number of free surface grids between the polymer patches. It is assumed that the minimum degree of surface coverage resulting in flocculation occurs when F equals zero. With any particular molecular weight polymer the degrees of surface coverage which could be simulated were limited by the particular finite grid size chosen. For example, in a system with 4×10^4 molecular weight polymer (occupies 16 grids) the extents of symmetrical surface coverage which could be modeled were 16, 25, 33, and 44 percent. The usual procedure to determine the surface



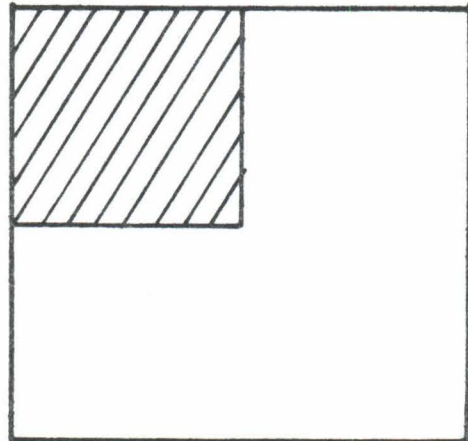
M = 2,500



M = 10,000



M = 22,500



M = 90,000

Fig. III-4. Polymer patch distributions at 25% surface coverage for polymers of various molecular weights.

coverage at zero F is to evaluate F at increasing degrees of surface coverage until F changes sign and then linearly interpolating between F values.

The calculations are made for spheres having maximum attractive orientation. Maximum attraction between two spheres occurs when the point of closest approach of one is the center of a positively charged polymer patch and the point of closest approach on the other is the center of a free surface area. Orientations resulting in maximum and minimum attraction are illustrated in Fig. III-5.

Increasing ionic strength results in compression of the electrical double layer and reduction of the effective distances over which electrostatic forces can act. Ionic strength variations are accounted for in the model by neglecting all interactions between grids separated by distances greater than some d_{\max} . This requires that Eq. III-3 be rewritten as

$$F = \sum_I \sum_J \frac{S(a,b) S(c,d)}{\{X(a,b;c,d)\}^2} \quad \text{III-4}$$

for $X(a,b;c,d) \leq d_{\max}$.

As a matter of convenience d_{\max} is assumed equal to twice the double layer thickness, κ^{-1} , which is defined in Sect. II-C1. This approach assumes that all grids separated by distances less than d_{\max} experience full Coulombic interaction and that the grids separated by distances greater than d_{\max} experience no interaction.

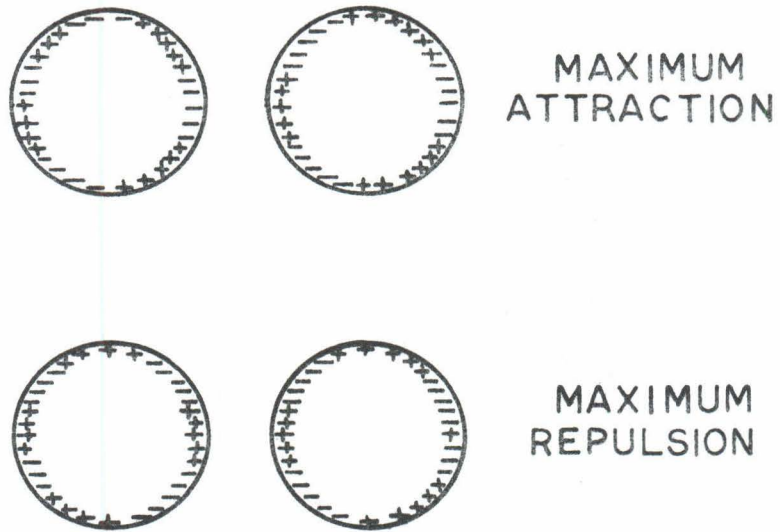


Fig. III-5. Particle-particle orientations resulting in maximum attraction and maximum repulsion for a given polymer patch distribution.

The ionic strength also affects the surface charge density of the polymer patches by controlling patch size. This density variation is accounted for in the mathematical model by varying the values of $S(a, b)$ and $S(c, d)$.

In Fig. III-6 the relationship between the degree surface coverage at zero F and S , the distance between surfaces, is illustrated. For these systems the maximum interaction distances, $2 \kappa^{-1}$, are equal to 60 \AA and 600 \AA for ionic strengths of 10^{-2} and 10^{-4} moles/liter, respectively. Fig. III-6 indicates that as the distance between the surfaces of two spheres is reduced, the surface coverage at zero F passes through a maximum. This maximum is a result of the ionic strength limitation on interaction distance, the assumed particle orientation, and the inverse dependence of interaction force on separation distance.

In the following analyses particle interactions are investigated at separation distances of 30 \AA and 100 \AA for 10^{-2} and 10^{-4} molar ionic strength systems, respectively. These separation distances result in near maximum degrees of surface coverage at zero F .

Fig. III-7 illustrates the effect of molecular weight and ionic strength on the minimum degree of surface coverage required for flocculation. In both the high and low ionic strength systems the charge densities of the adsorbed polyelectrolyte patches and the free particle surfaces have equal and opposite signs. Since the degree of surface coverage is directly proportional to the amount of polymer adsorbed, the following conclusions can be drawn:

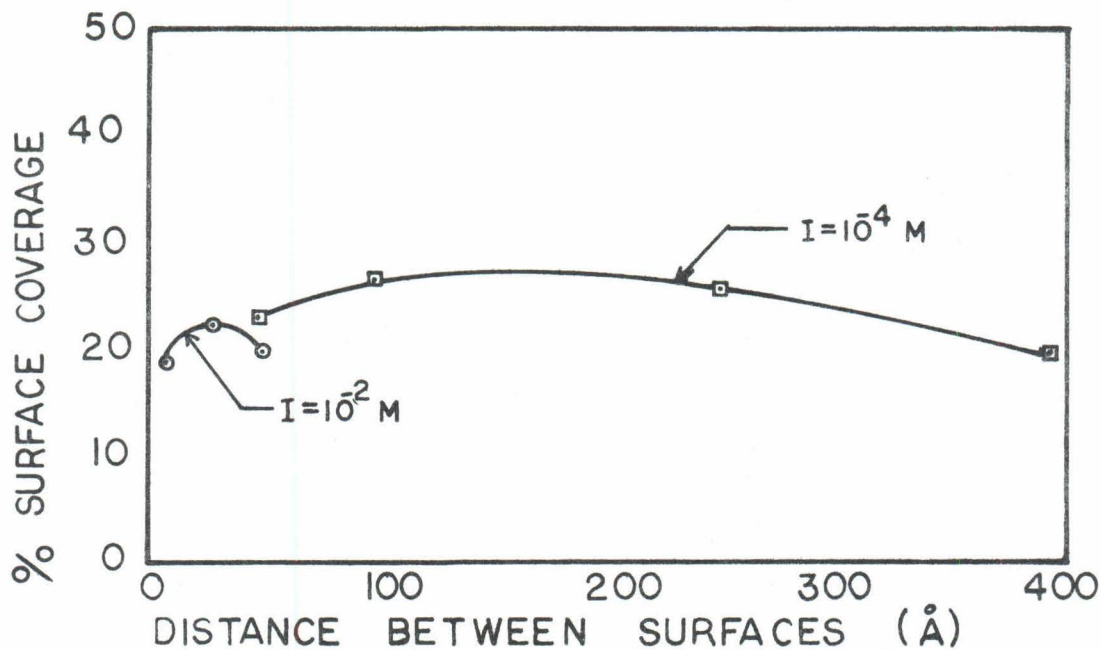


Fig. III-6. Percent surface coverage at zero F versus S , the separation between the surfaces of one-micron spheres. Polymer molecular weight = 1.6×10^5 .

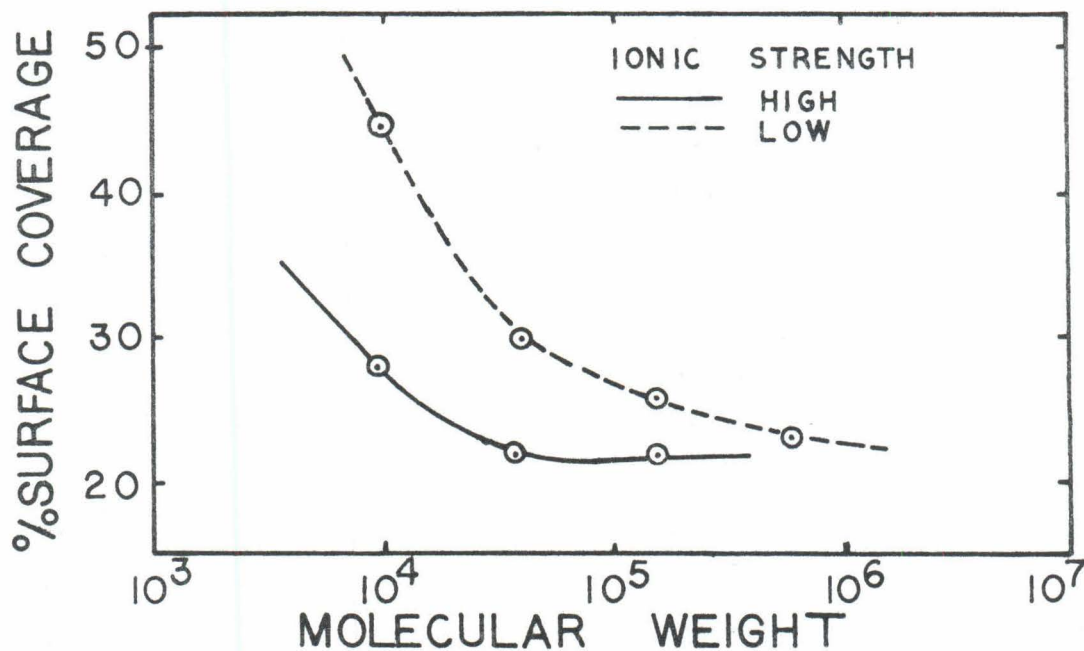


Fig. III-7. The effect of polymer molecular weight on the percent surface coverage required for zero F. Systems: 40 Å²/polymer segment, Mo = 214 and S = 30 Å & 100 Å for 10⁻² molar & 10⁻⁴ molar solutions, respectively.

- (i) The polymer dose required for flocculation increases with decreasing ionic strength, except for high molecular weights.
- (ii) At constant ionic strength, the flocculation dose decreases with increasing molecular weight until a minimum dose is reached; at high molecular weights the flocculation dose is independent of molecular weight.

Chapter IV

EXPERIMENTAL MATERIALS AND METHODS

A. Polymer Synthesis

The 1,2-dimethyl-5-vinylpyridinium bromide polymers were synthesized by the reactions shown in Fig. IV-1. Tritium tagged methyl bromide was used to produce the labeled polymers used for the adsorption studies.

1. Radioactive Methyl Bromide. The tagged methyl bromide was prepared by the method of Riegel and Prout⁵³. It was necessary to use the vacuum manifold shown in Fig. IV-2 for the synthesis because of the low boiling point of methyl bromide. Two portions of methanol, 0.201 grams of ordinary and 0.071 grams of tritium-labeled*, were placed in the manifold and solidified with liquid nitrogen. The labeled methanol was contained in a "break-offsky" tube which was opened after the system was evacuated. A 50 cc. reaction flask containing 1.66 grams of phosphorus tri-bromide and a teflon-coated magnetic stirring bar was connected to the manifold and the system evacuated. The methanol was distilled into the reaction flask by cooling the reaction flask with liquid nitrogen and permitting the methanol storage flask to reach room temperature. When the transfer was complete, the reactor was sealed by closing the reactor stopcock and the liquid nitrogen bath removed. The reactor was kept at room temperature ($24 \pm 2^\circ\text{C}$)

* The radioactive methanol containing 100 millicuries of tritium at specific activity of 44 millicuries per millimole was obtained from New England Nuclear Corporation.

POLY(1,2-DIMETHYL-5-VINYLPYRIDINIUM BROMIDE)

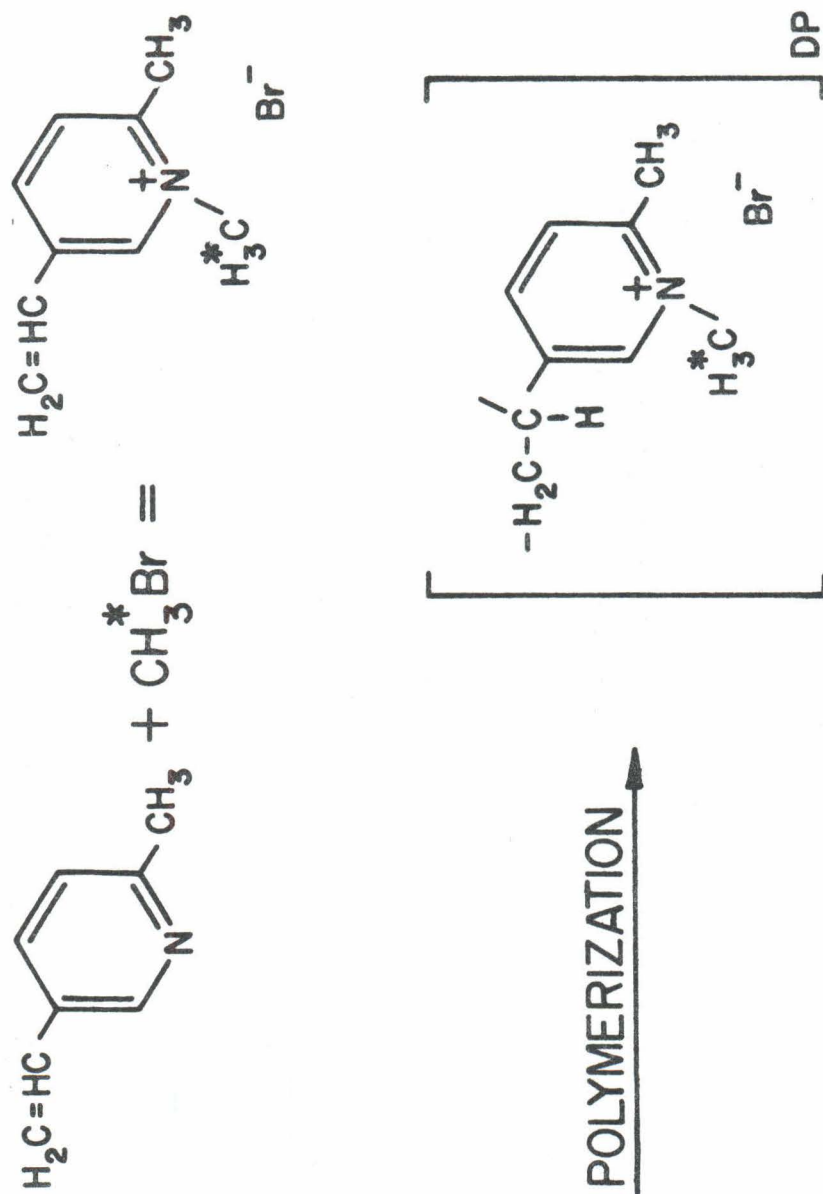


Fig. IV-1. Synthesis reaction of poly (DMVPB).

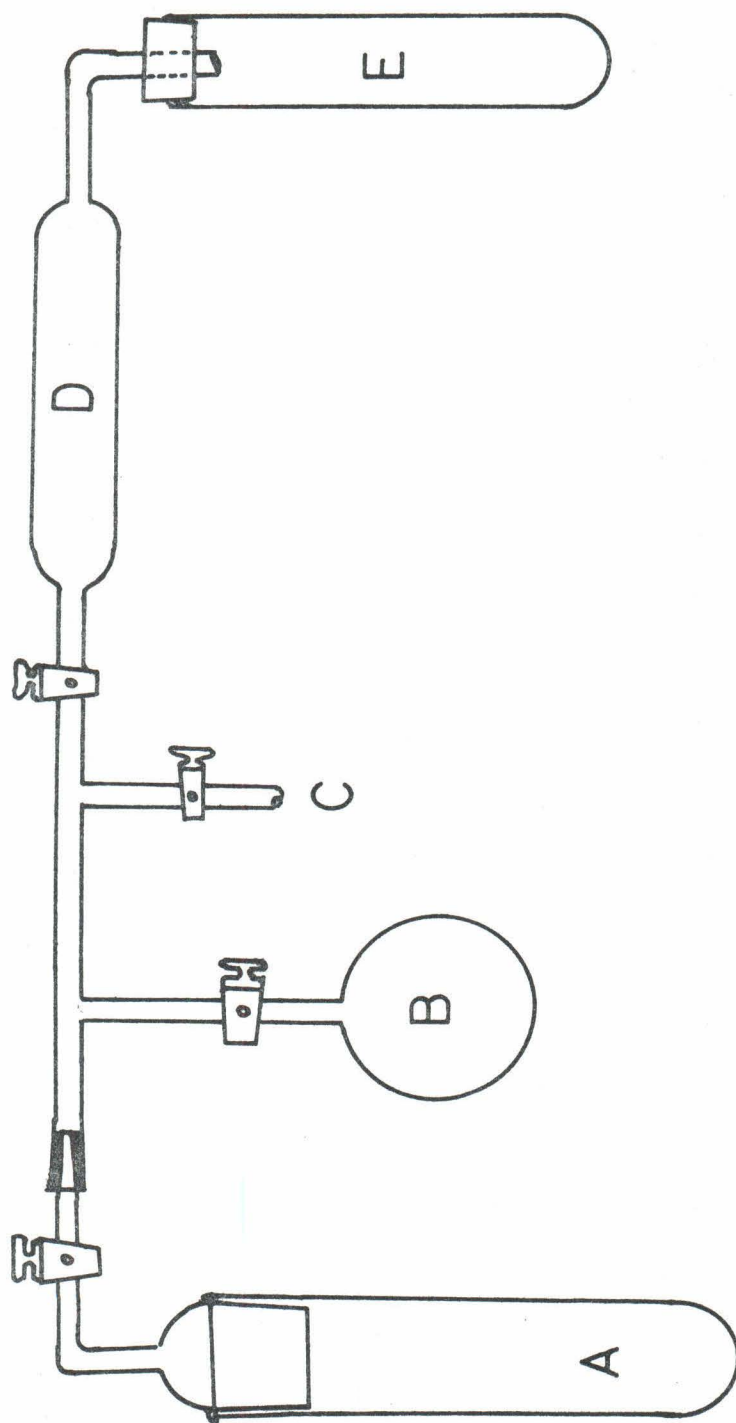


Fig. IV-2. Vacuum manifold for preparation of tritium-tagged methyl bromide. A - vessel to hold "breakofsky" tube, B - reaction flask, c - line to trap and vacuum pump, D - drying tube, E - storage tube.

for 15 hours; a hand held magnet was used to mix the reactants. The product was transferred through a drying tube containing sodium hydroxide pellets into a storage bulb by cooling the storage bulb with liquid nitrogen. The 0.654 gram yield of methyl bromide was 78 percent of the maximum theoretical yield.

2. Monomer Synthesis. The 1,2-dimethyl-5-vinylpyridinium bromide monomer was prepared by the reaction shown in Fig. IV-1. The radioactive monomer preparation was identical except that the tagged methyl bromide was used. The 2-methyl-5-vinyl-pyridine* was distilled at 70°C and 13 mm Hg pressure immediately before use to remove the polymerization inhibitor tertiary butyl catechol. The methyl bromide was distilled by simple condensation using an acetone-dry ice cooling bath. All reactants were cooled in an ice water bath before mixing to reduce the methyl bromide losses.

A methyl bromide-acetone solution (2.3 ml acetone/gram methyl bromide) was mixed with a 2-methyl-5-vinyl pyridine-acetone solution (2.0 ml acetone/gram 2-methyl-5-vinyl pyridine) in a closed flask at 0°C. The reactants were heated to 30°C in a water bath and mixed with a teflon coated magnet for twelve hours. The reaction flask was then stored at 2°C for an additional twelve hours. The monomer (pure white) was then filtered, washed first with acetone and then with ether, and

* A product of Phillips Petroleum.

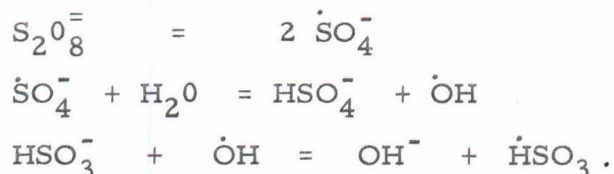
finally dried in a vacuum desiccator. Yields were usually between 70 and 80 percent of the theoretical maximum.

The dry monomer was stable for several months when stored in sealed bottles at 4°C. Incompletely dried monomer became tacky within a few days indicating that some polymerization was occurring. To avoid using partly polymerized or deteriorated monomer, all polymerizations were initiated within a few hours after monomer synthesis. UV analysis indicated that aqueous monomer solutions, 0.2 to 1 percent, did not polymerize for periods of at least one year when stored at 4°C.

3. Polymerization.

a. Reactions. The polyelectrolytes were prepared by free radical polymerizations of the quaternized monomer in aqueous solution. Several polymer texts describe free radical polymerization ^{22, 39}. The advantage of free radical or addition polymerization is that the final molecular weight is controlled by the initiator and monomer concentrations. This enables the preparation of a series of homologous polymers having a broad range of molecular weights.

The bisulfite free radical which initiates polymerization is produced by the following reactions between persulfate and bisulfite ions in aqueous solution:



The polymerization involves three processes:

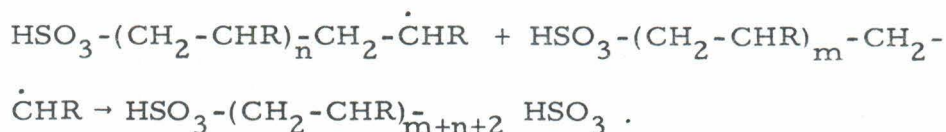
(1.) Initiation



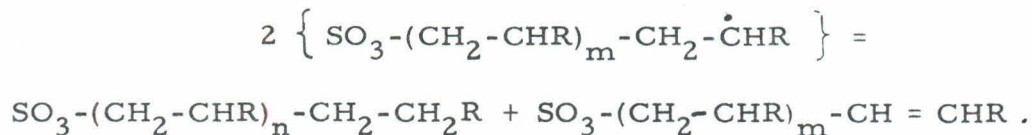
(2.) Propagation



(3.) Termination (combination)



Another possible termination reaction (disproportionation) produces polymers having a bisulfite group at one end only:



No attempt was made to determine whether one or both ends of the polymers involved in this research contained sulfite groups.

b. Procedure. Shyluk's method for the preparation of a similar polymer, poly(1,2-dimethyl-5-vinylpyridinium methyl sulfate⁵⁹), was modified to enable the preparation of small amounts of polymers (one gram) having a wide range of molecular weights. Weighed amounts of monomer were placed in calibrated serum vials which could be diluted to a predetermined volume (2 to 10 ml.). The monomer was then dissolved in a small amount of distilled water. Care was taken to keep the volume of the dissolved monomer to less than one-third the final volume of the vial. Equal amounts of freshly prepared potassium persulfate and sodium

bisulfite solutions, each at four times the desired initiator concentration were mixed. Immediately a volume of the initiator mixture equal to half the vial volume was pipetted into the vial. Distilled water was then added to dilute the monomer-initiator mixture to the calibrated volume.

The air in the vial was removed by evacuation and repressurization to 10 psig with nitrogen. The cycling was accomplished by inserting a hypodermic needle through the serum bottle stopper. A three-way stopcock connected to the hypodermic needle, a vacuum pump and a nitrogen tank was used for the cycling. The polymerizations were carried out for forty-eight hours in a constant temperature bath at 25°C.

Fractionation of the reaction product was required for those polymerizations having initiator concentrations less than 0.01 M because not all the monomer reacted. The reaction product was diluted to a 1 percent aqueous solution and acetone was added until the polymer precipitated. Precipitation usually occurred when the volume of the acetone added was two to three times the volume of the 1 percent aqueous polymer solution. The precipitate was then centrifuged, rinsed with acetone, dried in a vacuum desiccator and dissolved in distilled water to a 1 percent solution. Fractionation has the added advantage of removing the initiator salts from the polymer. The 1 percent polymer solutions prepared in this manner are stable for periods of at least one year when stored at 4°C.

c. Concentrations of Initiator and Monomer. The molecular weight of the polymer is controlled by the relative initiator and monomer concentrations. According to Tanford⁷⁰ the

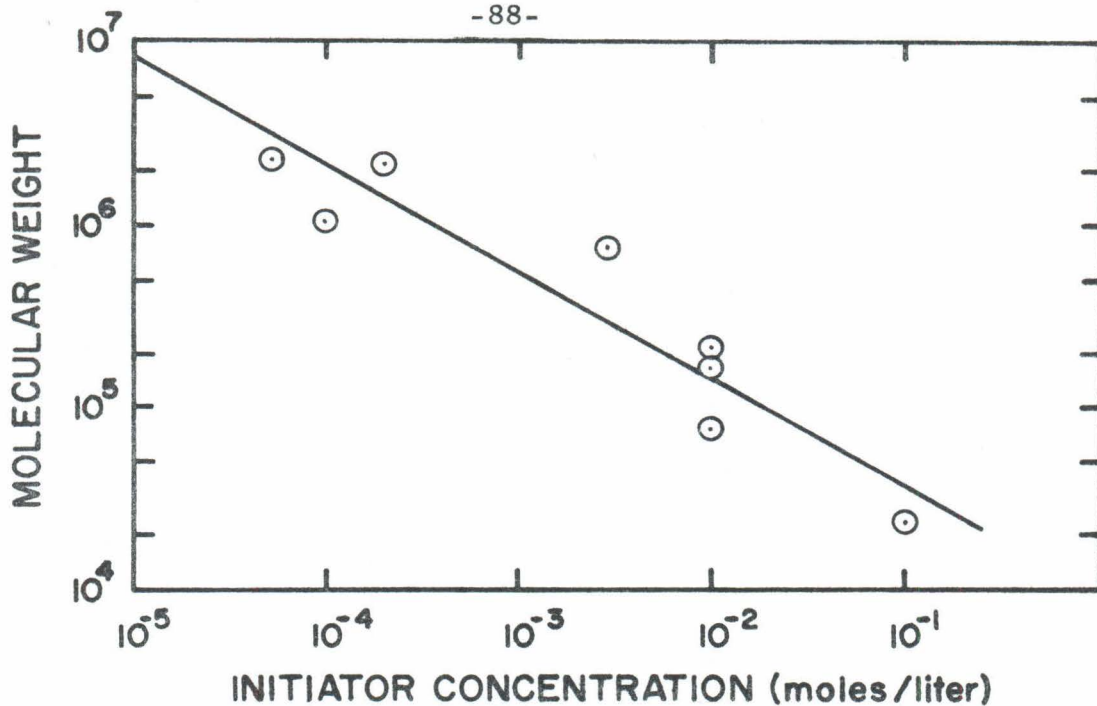


Fig. IV-3. The effect of initiator concentration on molecular weight. Monomer concentration = 1.17 molar.

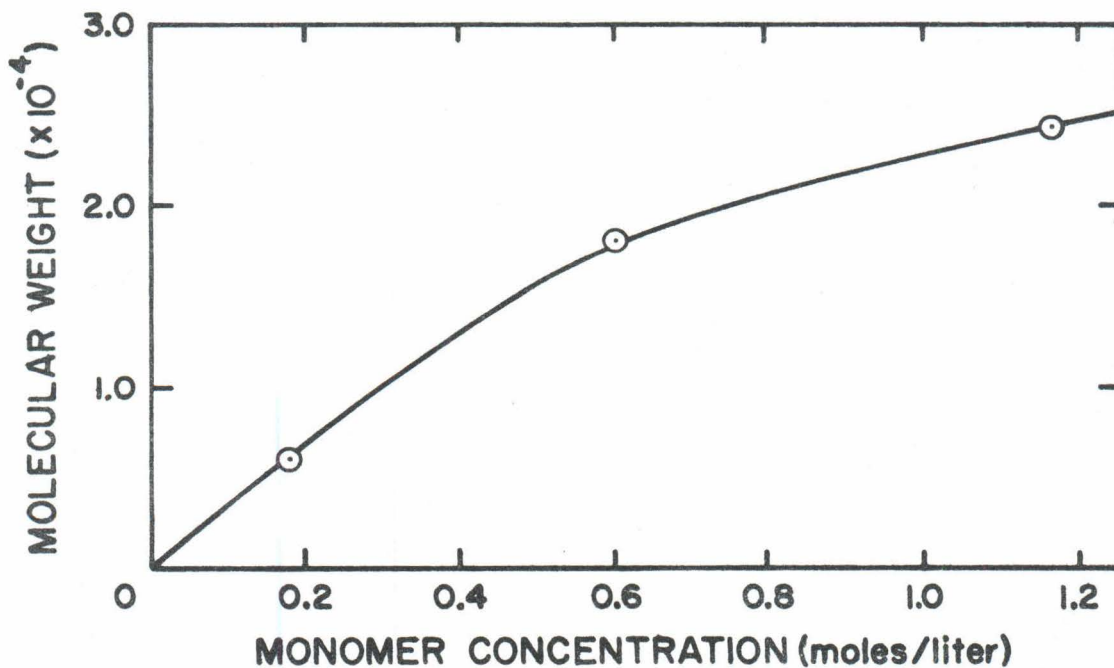


Fig. IV-4. Effect of monomer concentration on molecular weight.

average degree of polymerization for free radical polymerizations can be expressed as $X = k (m) (A)^{-\frac{1}{2}}$ for large molecular weights where k is a constant, m is the monomer concentration, and A is the initiator concentration. Figs. IV-3 and IV-4 show the experimental dependence of the molecular weight on the initiator and monomer concentrations. The empirical relationships derived from the data shown in these graphs and the theoretical relationship agree quite well considering that for the theoretical relationship it is assumed that the monomer concentration remains constant during polymerization and that the rate of free radical production is first order.

The lack of molecular weight reproducibility for polymerizations carried out under identical conditions is due to trace impurities in the monomer which affect the rate of termination reactions.

B. Polymer Characterization

1. Molecular Weight. The molecular weights were determined in 0.3 molar sodium chloride by light scattering. A Brice-Phoenix light scattering photometer model 2000 with a cylindrical cell (Brice-Phoenix catalog no. C101) was used to obtain the experimental data.

All solutions were filtered through Millipore filters directly into the light scattering cell to remove dust particles. Millipore filters of two different pore sizes were used for the high and low molecular weight solutions because of the large differences in the size of the molecules. A 1.0 micron filter was used for polymers

having intrinsic viscosities greater than 0.5 deciliters per gram and a 0.22 micron filter was used for those of lower viscosities.

A 546 millimicron monochromatic light source was used and scattering was measured at nine angles ranging from 45° to 135° . Usually data was taken at four different polymer concentrations in the range 0.05 to 0.5 percent by weight; 50 ml was adopted as the standard volume for the cylindrical cell.

The refractive indexes of the polymer solutions were measured with a Brice-Phoenix Differential Refractometer model B-S. This instrument was calibrated with potassium chloride solutions.

The molecular weights and the radii of gyration were calculated from the scattering data by the method of Zimm⁷⁷. A Zimm network, see Fig. IV-5, enables the intensity of the scattered light to be extrapolated to zero polymer concentration and to zero scattering angle. These extrapolations are necessary because: (i) polymer-polymer interactions occur, except at low concentrations where too little light is scattered to be detected; (ii) scattering theory relates the molecular weight to the intensity of scattering at zero angle (forward direction). It is impossible to measure scattering at zero angle because the photodetector cannot differentiate between the scattered light and the incident light which is several orders of magnitude more intense.

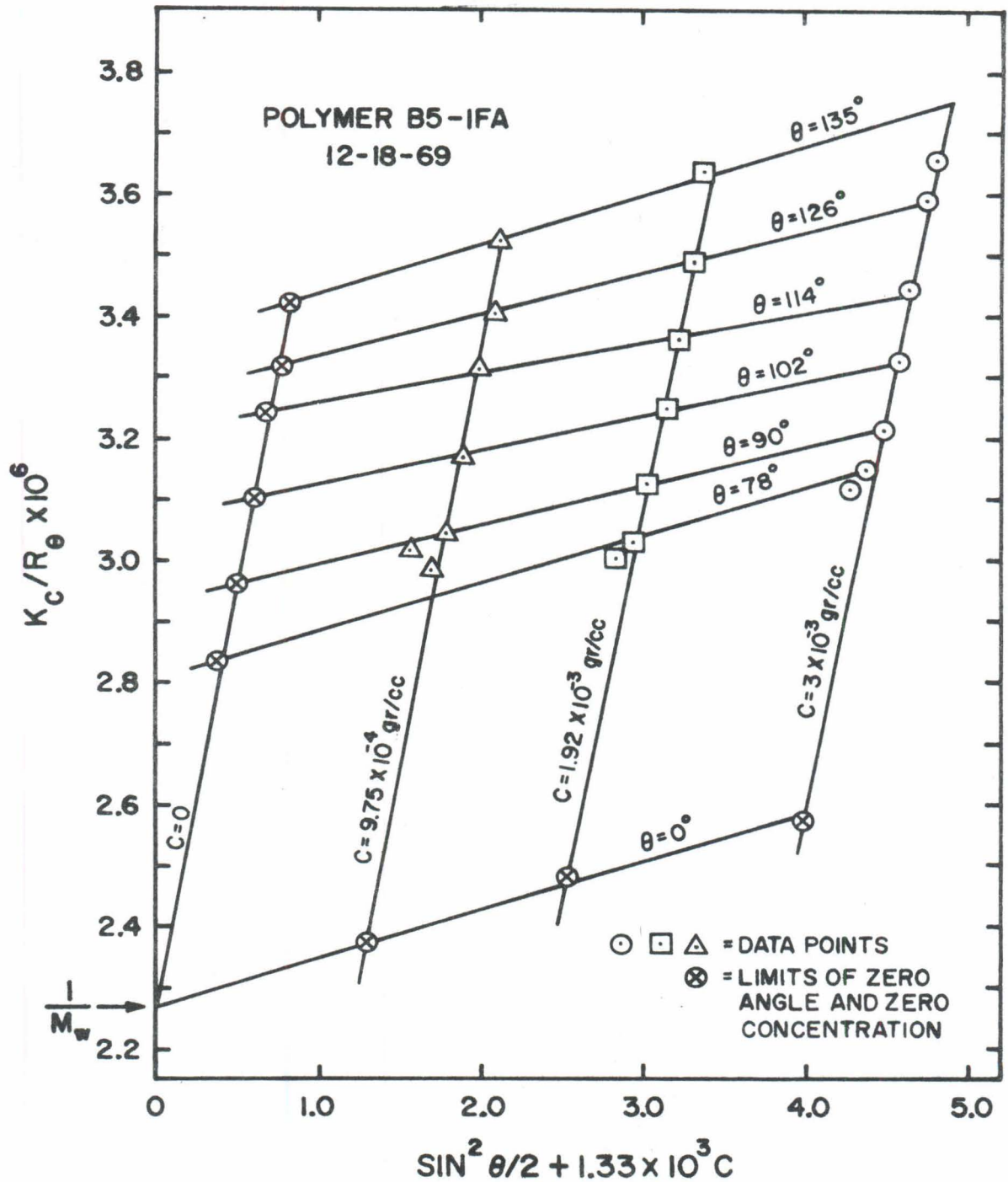


Fig. IV-5. Typical Zimm plot of light scattering data.

The symbols in Fig. IV-5 have the following meanings:

R_{θ} - Rayleigh ratio at angle θ

c - polymer concentration, grams/cc

k - optical constant = $2\pi^2 n_0^2 \left(\frac{dn}{dc}\right)^2 / (N \lambda^4)$

where n_0 and n are the refractive indexes of the solvent and polymer solution respectively, dn/dc is the change of the refractive index with concentration, N is Avogadro's number, and λ is the wavelength of light in the scattering medium.

The constant 1.33×10^3 in the abscissa is an arbitrary plotting constant chosen to provide a convenient spread of the data. The change of the polymer refractive index with concentration was determined with the differential refractometer. The Rayleigh ratio was calculated from the photometer readings according to the relationships given in the Brice-Phoenix operation manual.

On a Zimm plot the molecular weight (M) is the reciprocal of the intercept of the zero concentration line, the zero angle line and the ordinate. The intersection of these three lines at a single point indicates good experimental data. The radius of gyration is calculated from the slope of the zero concentration line by the following formula:

$$R_g^2 = \left(\frac{3 \lambda^2 M}{16 \pi^2} \right) \quad (\text{slope of } c = 0 \text{ line}). \quad \text{IV-1}$$

2. Viscosity. Kinematic viscosities were determined using ASTM procedure D 44-65. A straight-necked Oswald viscometer was used because it was possible to remove polymer solution from

it with a pipette. A standard sample volume of five ml and a standard temperature of $25^{\circ} \pm 0.01^{\circ}\text{C}$ were adopted. Polymer was diluted by removing two ml of polymer solution from the viscometer and replacing it with two ml of solvent at the same ionic strength.

Specific gravities to the fourth decimal were determined with a Christian Becker specific gravity balance. Since the balance was used at room temperature, temperature correction factors were employed.

In polymer characterization several different viscosities are defined⁷⁰:

- absolute η
- kinematic η/ρ where ρ is solution density
- specific $\eta_{SP} = (\eta_{POLY\ SOLN} - \eta_{SOLVENT}) / (\eta_{SOLVENT})$
- reduced η_{SP}/c

Except at low polymer concentrations, interactions between polymer molecules cause the reduced viscosity to vary with concentration. A characteristic viscosity of an isolated molecule is obtained by extrapolating the reduced viscosity to zero polymer concentration. This characteristic viscosity $[\eta]$ is called the intrinsic viscosity in classical terminology and limiting viscosity number in the revised system. The extrapolation was made by assuming that the commonly used Huggins equation is applicable. That is,

$$\eta_{SP}/c = [\eta] + k [\eta]^2 c \quad \text{IV - 2}$$

where k , the Huggins constant, is dependent on the shape of the molecule and the solvent of the system.

Experimentally the intrinsic viscosity is determined by measuring the reduced viscosity at several different polymer concentrations and graphically extrapolating the reduced viscosities to zero polymer concentration. Fig. IV-6 illustrates the viscosity data for a non-radioactive poly(DMVPB) sample having a molecular weight of 1.6 million. The intercepts at zero polymer concentration are the intrinsic viscosities. The variation of viscosity with salt concentration can also be seen in Fig. IV-6.

3. Ultraviolet Absorbance. The monomer and the polymer each have characteristic absorbance spectra illustrated in Fig. IV-7. The following relationships were used for calculating the monomer (m) and polymer (P) concentrations (mg/l):

$$m = (53.8 \Delta_{310}^{274} - 0.27 \Delta_{246}^{274}) / L$$
$$P = (22.9 \Delta_{310}^{274} - 29.8 \Delta_{246}^{274}) / L$$

where Δ_{j}^{i} is the difference in absorbance between $i \text{ m}\mu$ and $j \text{ m}\mu$, and L is the cell path length in centimeters. Using a 10 cm cell the lower concentration limit is about 0.1 mg/l.

C. Particle Characteristics.

Two types of particles were used in the flocculation experiments: polystyrene latex and crystalline silica. The polystyrene latex was used because of its uniformity and well-defined surface area. The crystalline silica was used because it is chemically similar to some of the particles encountered in natural water systems. Electronmicrographs of the particles are shown in Figs. IV-8 and IV-9. Characteristics of the particles are given in Table IV-1.

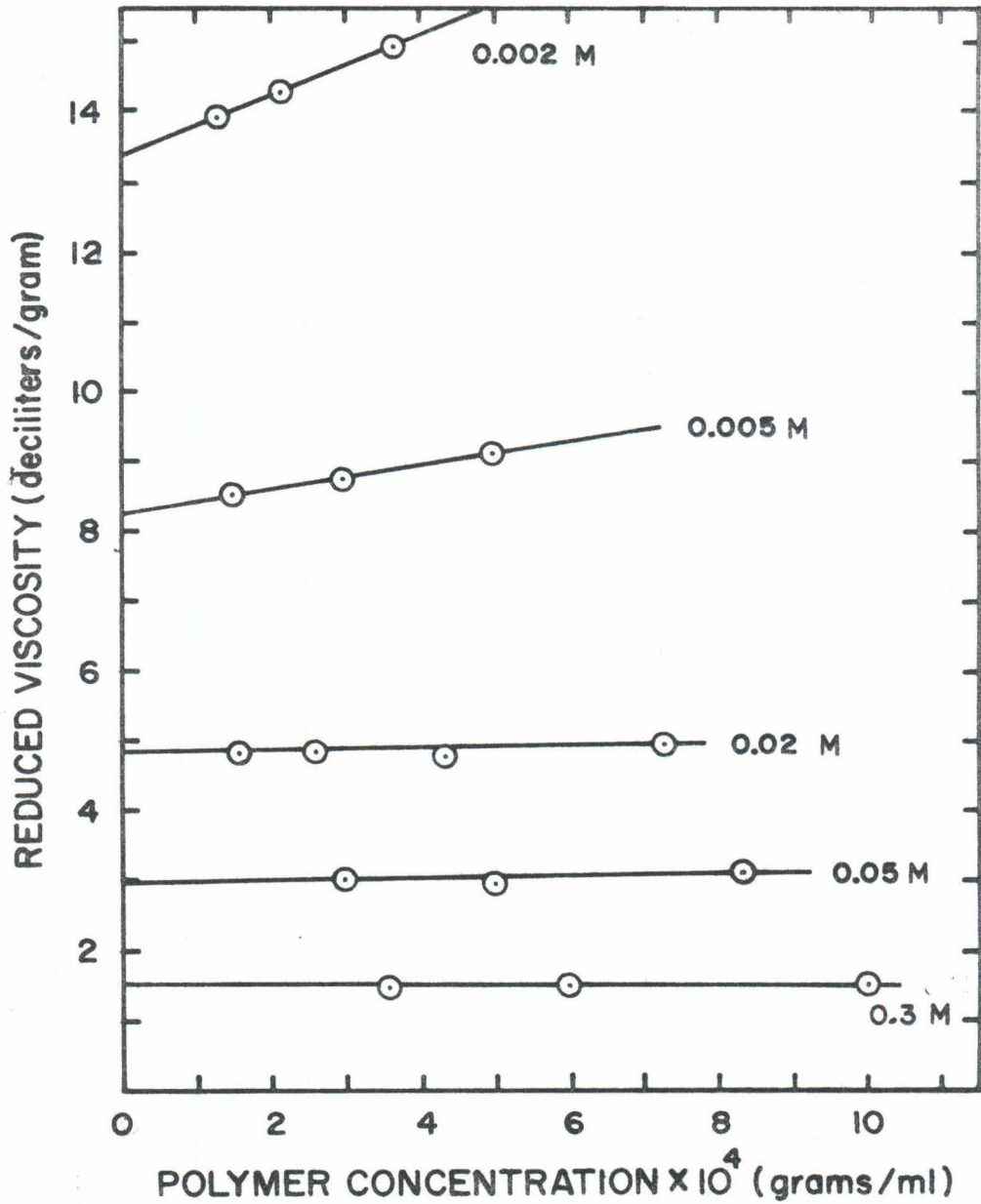


Fig. IV-6. Typical viscosity data for poly (DMVPB) obtained by dilution at various constant NaCl concentrations.

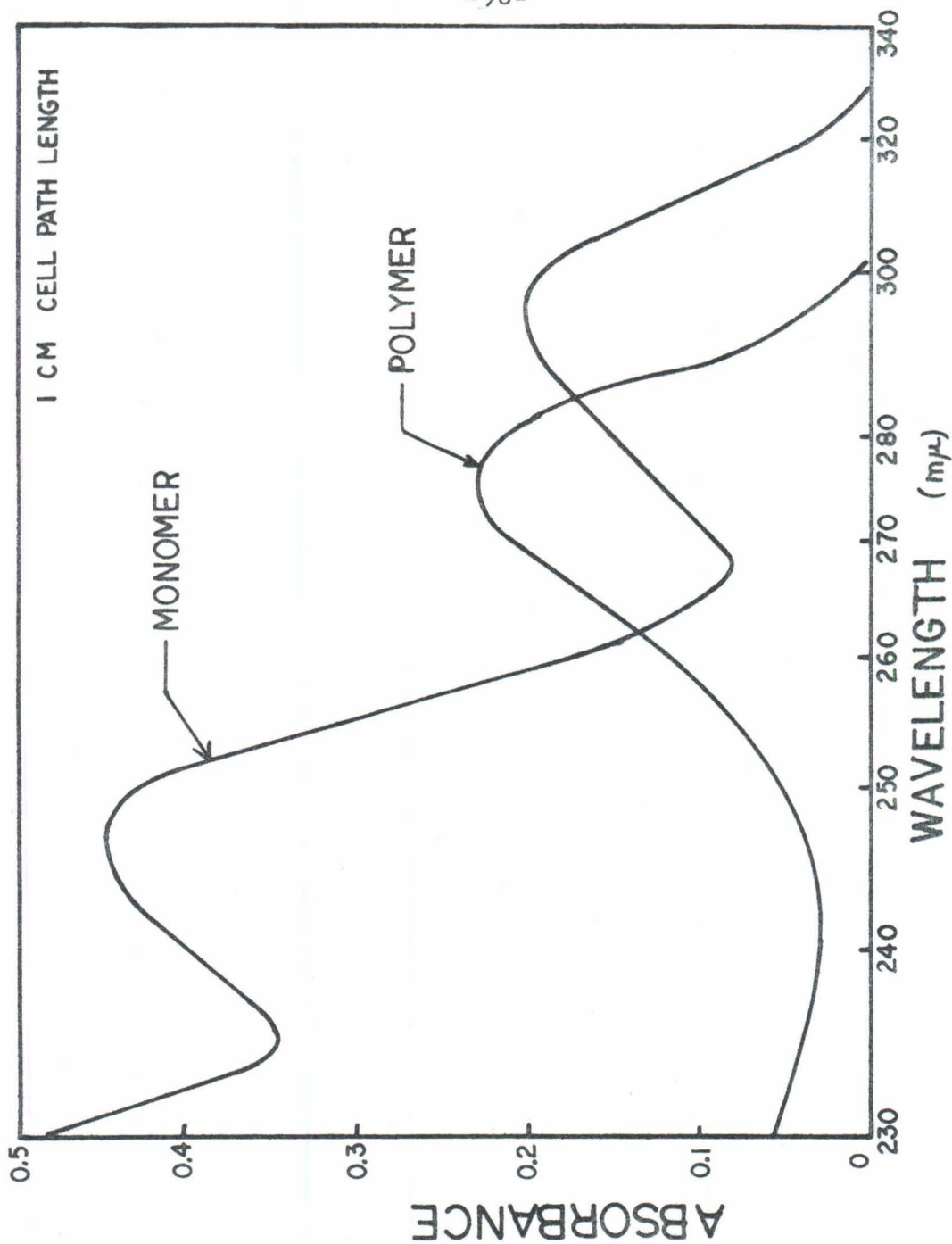


Fig. IV-7. Ultraviolet absorbance of aqueous polymer and monomer solutions at 10 µg/l.

Table IV-1.

Particle Characteristics

Particle Type	PSL	Min-U-Sil
Shape	Spherical	Irregular
Density	1.05 gr/cm ³	2.65 gr/cm ³
Mean Diameter (geometric)	1.305 μ	1.1 μ
Size Distribution	Std. Deviation 0.016 μ	98% < 5 μ 60% < 1.5 μ
Surface Area	4.37 m ² /gr	2.1 m ² /gr* 6.9 m ² /gr**
Surface charges per Particle	5.9x10 ⁶	--

* Air permeability

** BET nitrogen adsorption

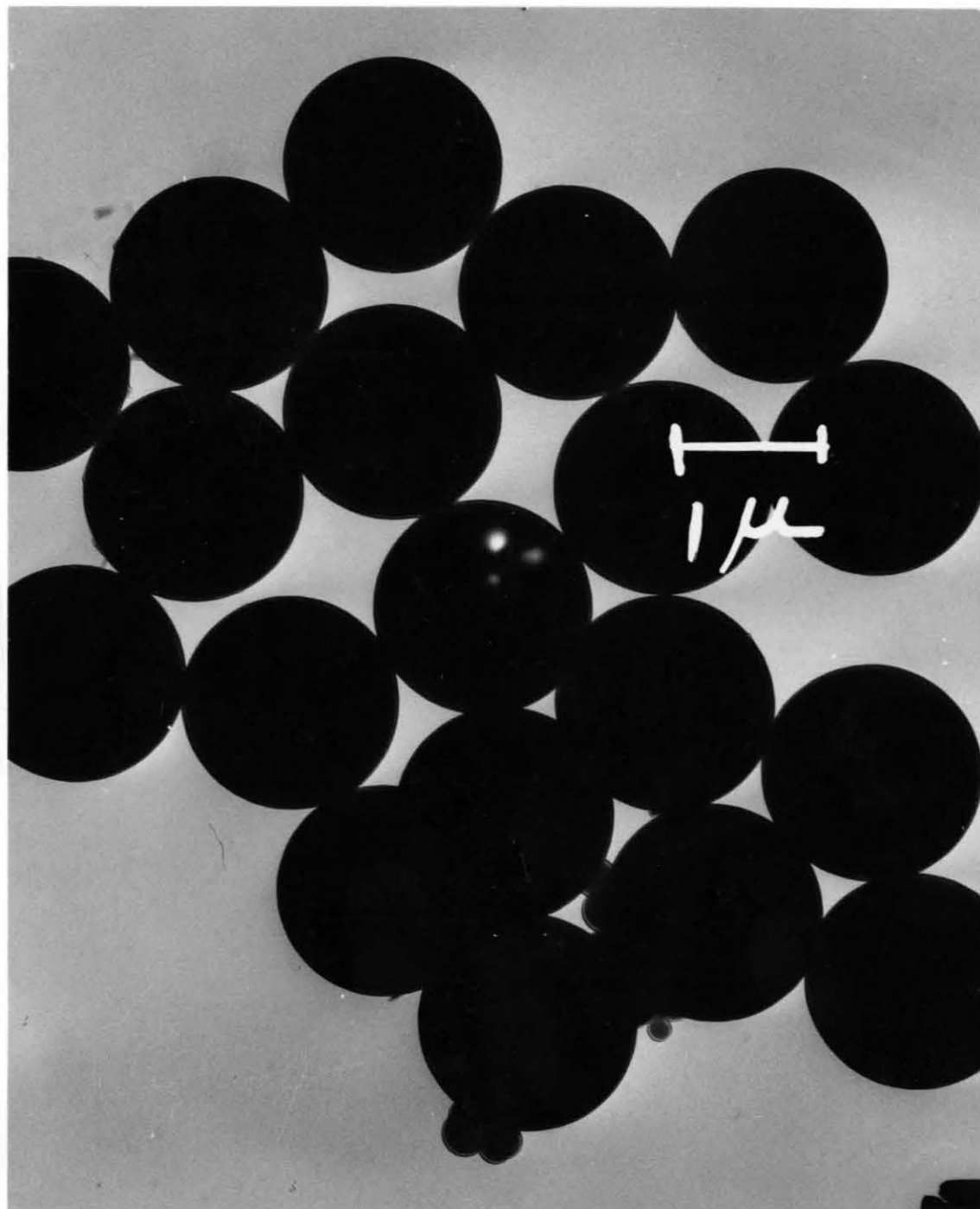


Fig. IV-8. Electron micrograph of 1.3 micron polystyrene latex particles.

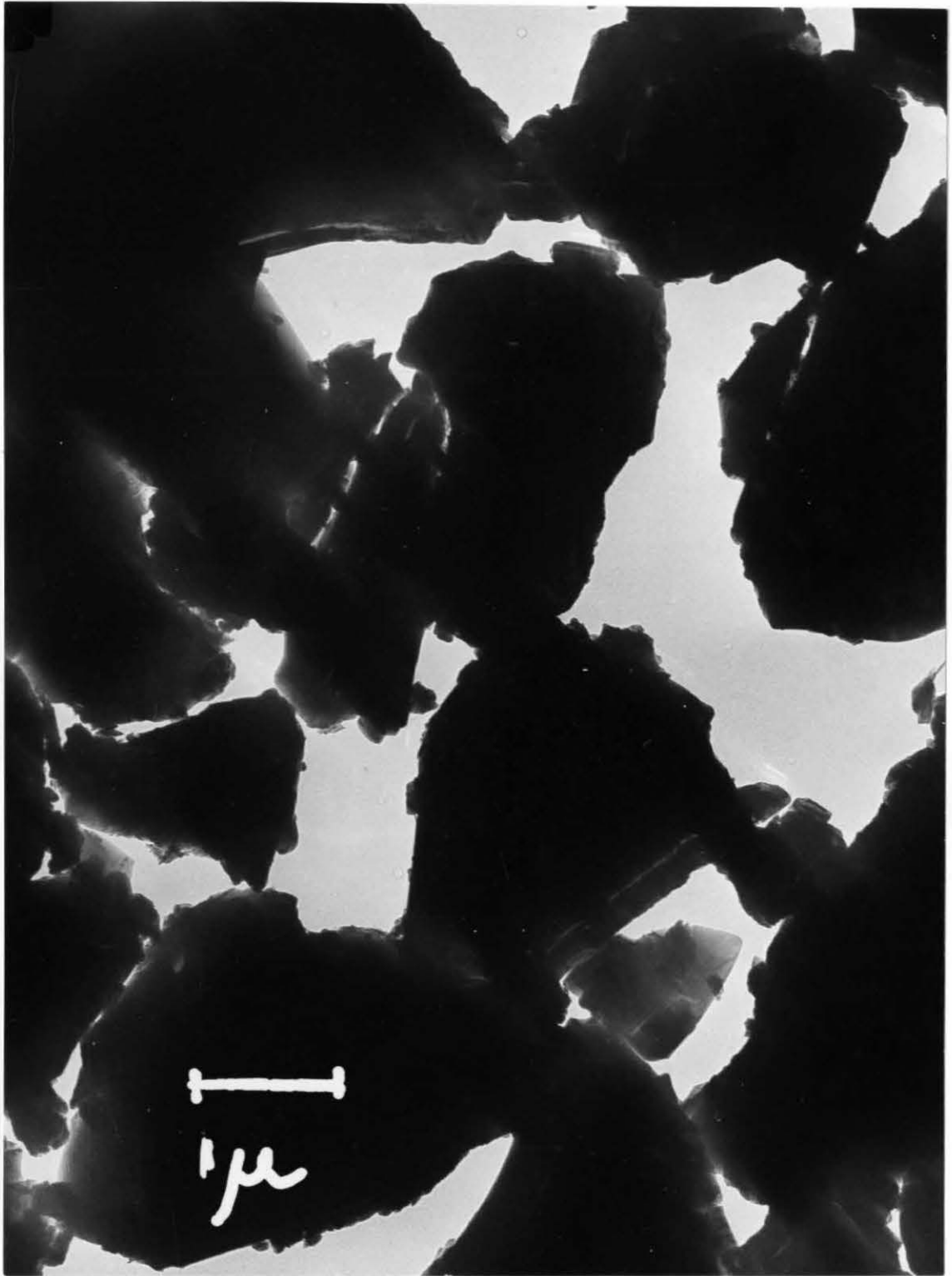


Fig. IV-9. Electron micrograph of Min-U-Sil 5 particles.

The polystyrene latex particles*(PSL) are prepared by emulsion polymerization and stabilized with an organic sulfonate salt which imparts negative surface charge. The density of the negative charges on the particle surface is one of the most important parameters in flocculation and adsorption studies.

The surface charge of the PSL was determined by complexing the sulfonate ions with methylene blue. Nine milligrams of PSL was added to 20 ml of a 7.5×10^{-6} molar methylene blue solution. After mixing for one hour with a magnetic stirrer, the mixture was centrifuged at 120,000 G for thirty minutes. The concentration of the uncomplexed methylene blue remaining in the supernatant was determined colorimetrically at $625 \text{ m}\mu$. A blank with no PSL lost no methylene blue when treated by the above procedure.

Assuming that each sulfonate group complexes one methylene blue molecule and that all complexed methylene blue is removed with the PSL particles, the sulfonate density was found to be 8.61×10^{-6} moles per gram PSL. This corresponds to one sulfonate group per 90 \AA^2 . This surface charge density is within the range found by Ottewill and Shaw⁴⁵ for similar particles.

The crystalline silica particles used in this research were Min-U-Sil 5 particles**. X-ray diffraction analysis indicated that Min-U-Sil has the same structure as alpha quartz.

The specific surface area, determined by BET nitrogen adsorption¹², is $6.90 \text{ m}^2/\text{gr}$. This value is in agreement with

* Product of Dow Chemical Company

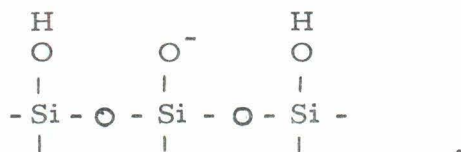
** a product of Pennsylvania Glass Sand Corporation, Pittsburg.

that of O'Melia and Stumm who determined Min-U-Sil 5 surface area by methyl red adsorption⁴³. The specific surface area reported by the manufacturer is only 2.06 m²/gr⁴⁹. The reason for this discrepancy is that the manufacturer determined surface area by the air permeability method which yields a geometric surface area. Permeability methods do not measure surface area due to surface roughness or surface pores.

There is evidence indicating that when silica particles are ground to sizes below 5 to 10 microns, an amorphous layer forms at the surface³². The existence of an amorphous surface layer is in agreement with the surface area data.

The chemical composition, supplied by the manufacturer, indicates that Min-U-Sil is 99.9 percent silicon dioxide with traces of oxides of iron, aluminum, titanium, calcium, and magnesium⁴⁹.

The negative surface charge of the silica particles is due to the ionization of some of the surface hydroxyl groups formed through hydration:



D. Scintillation System

Concentrations of dilute solutions of labeled polymers were determined by liquid scintillation spectrometry. A Beckman Liquid Scintillation System, LS-100 was used. An advantage of the Beckman instrument is that samples are not cooled, which eliminates the need for an anti-freeze agent in the scintillation counting fluid.

Samples were counted in linear-polyethylene vials* which have lower counting backgrounds than glass vials. Vials were disposed of after being used once to avoid contamination.

As a matter of convenience two types of counting fluids were used. A pre-mixed xylene based scintillator (Aquasol) was obtained from New England Nuclear Corporation. Usually 2 ml of sample were mixed with 10 ml of Aquasol; counting efficiencies greater than twenty percent were obtained. The other fluid, described in the LS-100 operational manual, consisted of 5 grams PPO, and 100 grams naphthalene per liter dioxane; 3 ml of sample were mixed with 15 ml of this fluid.

A calibration curve was necessary for each set of adsorption experiments because counting efficiency decreased with increasing sample ionic strength. Calibration curves were prepared by making standard polymer dilutions with water of the same ionic composition as that used in a particular experiment. The scintillation spectrometer response, given as counts per minute (cpm), was proportional to polymer concentration over the investigated range ($10\mu\text{g}/\text{l}$ to $10,000\mu\text{g}/\text{l}$).

Backgrounds of 18 ± 1 cpm and 21 ± 1 cpm were found for the xylene and dioxane fluids, respectively.

Sample counting times were determined by either of the following two modes (whichever occurred first): (i) 40,000 total counts, which corresponds to a standard error of 1 percent, or

* Packard Instruments

(ii) a period of 100 minutes. With a 100 minute period the minimum sensitivity of the polymer determination method was 0.3 ug/l.

Specific activities of the polymers were calculated from the scintillation system counting efficiency and the polymer counting rate (cpm/unit weight polymer). The overall system counting efficiency was determined with standardized tritiated water.

The specific activities of the monomer was 6.5 mC/gr at the time of the polymer syntheses. The specific activities of the resulting polymers ranged between 3.4 and 4.1 mC/gr. The decrease in specific activity occurring during or as a result of polymerization was not investigated.

E. Flocculation-Adsorption Experiments

1. Mixing Procedure. Suspension turbidity or optical density, polymer adsorption, and particle mobility were measured on different portions of a single flocculating suspension. The following procedure was followed for all experiments.

- (i) 100 ml of 75 mg/l Min-U-Sil or 30 mg/l PSL suspension at the desired ionic strength was placed in a beaker.
- (ii) The desired amount of polymer, 0.05 to 2.0 ml of a 10 mg/l solution, was added to 50 ml of solution at the desired ionic strength in a 250 ml beaker.

- (iii) The 100 ml of suspension was added to the 50 ml of polymer solution which was being rapidly stirred (150 RPM) by a multiple laboratory stirrer*. Stirring was reduced to 100 RPM after 15 seconds. The final particle concentrations were 50 mg/l and 20 mg/l for the Min-U-Sil and PSL systems respectively. Additional suspension characteristics are presented in Table IV-2.
- (iv) After 10 minutes of stirring, a 60 ml aliquot was removed for mobility measurements.
- (v) After a total mixing period of 60 minutes stirring was stopped and approximately 30 ml was placed into a centrifuge tube for determination of supernatant polymer concentration.
- (vi) After a 20 minute settling period supernatant turbidity was measured.

In light of evidence indicating that polymer adsorption is irreversible⁴, care was taken to dilute the polymer before adding the suspension so as to avoid exposing a small number of particles to very high polymer concentrations. By diluting the polymer with solution having the desired ionic strength, no change in ionic atmosphere was experienced when the suspension was added to the

* A product of Phipps and Bird, Richmond, Va.

Table IV-2.

Suspension Characteristics

Particles	PSL	Min-U-Sil
Concentration	20 mg/l	50 mg/l
Number Concentration	$1.65 \times 10^7 / \text{cc}$	$2.7 \times 10^7 / \text{cc}^*$
Surface Area	$874 \text{ cm}^2 / \text{l}$	$1,060 \text{ cm}^2 / \text{l}^{**}$ $3,475 \text{ cm}^2 / \text{l}^{***}$
Volume Fraction	1.9×10^{-5}	1.9×10^{-5}

* Based on mean particle diameter

** Air permeability

*** BET nitrogen adsorption

polymer solution. This prevented changes in polymer configuration as a result of ionic strength differences.

A 1.75"x0.75" stainless steel paddle mounted on a 0.25" diameter shaft was used to mix 150 ml in a 250 ml pyrex beaker. Analytical grade salts and distilled water were used in all experiments.

2. Electrophoretic Mobility. Electrophoretic mobilities were determined in a Briggs horizontal flat cell according to the procedure of Black and Smith⁹. Palladium electrodes as described by Neihof⁴² were used rather than liquid junction electrodes to avoid variations in sample ionic strength.

Mobility measurements were taken within thirty minutes after the ten-minute mixing period. Stringent time controls were not necessary since it was found that the mobility remained constant for one hour after the ten-minute mixing period. The Min-U-Sil suspensions were stirred immediately before being placed in the Briggs cell to resuspend any settled particles.

3. Polymer Adsorption. The amount of polymer adsorbed was measured by adding a known amount of polymer to a particle suspension and then determining the residual polymer concentration in the supernatant. It was necessary to centrifuge the PSL suspensions at 3,100 G for thirty minutes to obtain a clear supernatant; the silica particles, being more dense, were centrifuged for only fifteen minutes. Supernatant polymer concentrations were determined by liquid scintillation. The supernatant sample was

pipetted directly from the centrifuge tube into a scintillation vial containing an appropriate volume of fluor.

One of the more difficult experimental problems encountered was the elimination of polymer adsorption to the mixing vessels, paddles and centrifuge tubes. When particle-free polymer solutions in the flocculation concentration range were placed in beakers, 20 to 70 percent of the polymer adsorbed to the walls within thirty minutes. The area of the solution-glass interface for 150 ml of solution in a 250 ml beaker is approximately 120 cm^2 . Since the surface area of 150 ml of a 20 mg/l suspension of PSL is only 131 cm^2 it is impossible to ignore beaker surface area in comparison to the particle surface area.

Paraffin, teflon and silicone coatings were able to reduce but not eliminate polymer adsorption to the walls of the pyrex beakers. Polyvinylchloride, polyethylene and teflon vessels also adsorb polymer. Successful elimination of polymer adsorption was accomplished by using pyrex beakers coated with Siliclad*, a water soluble silicone. It was necessary to re-apply the Siliclad each time the beakers were washed. Paddles were soaked in a Siliclad solution at ten times the recommended concentration for at least thirty minutes.

Siliclad coated glass centrifuge tubes could not be used because the glass sometimes failed at the speeds necessary to settle out the PSL particles. It was found that no additional

* A product of Clay-Adams, Inc., New York, N. Y.

polymer would adsorb to polycarbonate centrifuge tubes soaked with non-radioactive polymer at concentrations one hundred times greater than the flocculation concentrations. If anything, desorption would occur, and, since the desorbing polymer was not radioactive, the supernatant polymer concentration as determined by liquid scintillation would not be altered. As discussed in the results, the amount of polymer adsorbed during a short time (30 minutes) increases with decreasing molecular weight. Therefore, a low molecular weight, non-radioactive polymer was used to saturate the walls of the centrifuge tubes.

4. Optical Density. After a twenty-minute settling period the optical density (or absorbance)* of the flocculated suspension was measured in a cell with a 2 cm path length at 436 m μ with a Beckman DU spectrophotometer. A 30 ml hypodermic syringe without a needle was used to remove the sample from approximately one cm below the surface of the liquid. Care was taken not to include settled particles or particles captured at the surface by surface tension. The syringe was filled and emptied slowly to avoid breaking up flocculated particles.

A comparison of optical density with turbidity, the ratio of light scattered at 90 degrees to the transmitted light, was made. Turbidities were measured with a Brice-Phoenix Scattering Photometer in a 30x30 mm cell. Both measurements were made at 436 m μ . A direct relationship was found between the normalized

* Optical density \equiv absorbance = $\log_{10} \frac{I_0}{I}$, where I_0 is the incident light intensity and I is the transmitted light intensity.

turbidity and optical density values. Therefore as a matter of convenience, optical density was measured.

In the systems investigated the particles are larger than the wavelength used to measure absorbance. For such systems a decrease in absorbance indicates particle aggregation.

F. Adsorption Experiments

The study of adsorption in non-flocculating systems was carried out with glass bottles. Using the walls of the glass bottles as the adsorbing surface eliminated possible errors due to losses on the walls of the container.

Glass stoppered Pyrex bottles were used since Pyrex has a composition similar to that of the Min-U-Sil. The bottles were soaked with concentrated sodium hydroxide and then chromic acid to ensure removal of grease or other surface impurities. The bottles had a volume of 500 ml and a geometric surface area of 341 cm^2 . 400 ml of a salt solution containing 100 to 200 $\mu\text{g}/\text{l}$ tagged polymer was placed into a dry bottle. Polymer adsorption was determined by measuring the decrease in the solution polymer concentration. Samples were pipetted directly into scintillation vials at the appropriate times.

Chapter V

RESULTS OF POLYMER AND PARTICLE
CHARACTERIZATIONS

A. Polymers

1. Molecular Weight. The small amounts of tritium-tagged polyelectrolytes synthesized made it impossible to use the light-scattering method to determine their molecular weights directly. Fig. V-1 illustrates the relationship between the intrinsic viscosity and the molecular weight determined by light-scattering with non-radioactive polyelectrolytes dissolved in 0.3 molar sodium chloride. The Mark-Houwink relationship, calculated from the data in Fig. V-1 is

$$[\eta] = 1.28 \times 10^{-3} M^{0.813} \quad \text{V-1}$$

Eq. V-1 was used to calculate the molecular weights of the labeled polymers from measurements of their intrinsic viscosities. The value of the exponent, 0.813, indicates that even in 0.3 molar sodium chloride, where the electrostatic interaction between adjacent segments is a minimum, the polymer molecules have a rod-like or ellisoidal configuration. The exponent has a value of 0.5 for random-coiled solution configurations⁷⁰.

The characteristics of the labeled polyelectrolytes used in this research are tabulated in Table V-1. The range of molecular weights, 6×10^3 to 5.5×10^6 , varies over three orders of magnitude; the corresponding number of monomer units per polymer molecule is 28 and 25,600, respectively. The contour lengths are based on a

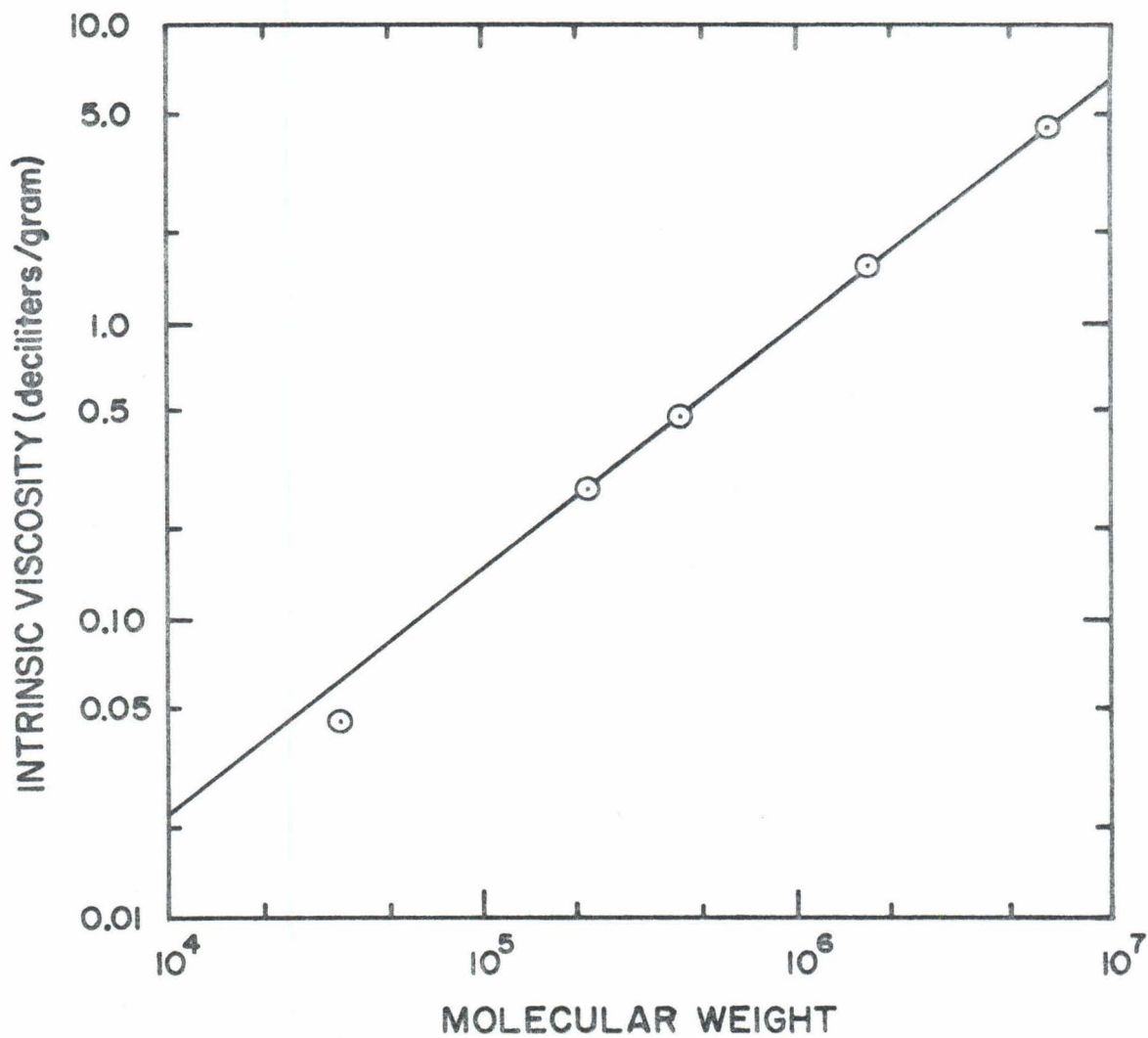


Fig. V-1. Relationship between the intrinsic viscosity and the molecular weight determined by light scattering. Aqueous polymer solutions in 0.3 molar NaCl.

Table V-1.
 Characteristics of Tritium Labeled
 (1, 2 dimethyl-5-vinylpyridinium bromide) Polymers

Number	Intrinsic Viscosity dl/g	Molecular Weight	Degree of Polymerization	Contour Length Microns	R _G max, microns	R _G min, microns
BR 9-1F	0.0145	6.0×10^3	28	0.007	0.0020	0.0016
BR 10-1F	0.117	7.6×10^4	354	0.09	0.026	0.0057
BR 10-2F	0.147	1.0×10^5	467	0.12	0.035	0.0066
BR 8-1F	0.46	4.0×10^5	1.87×10^3	0.47	0.14	0.013
BR 8-3F	0.80	7.8×10^3	3.64×10^3	0.92	0.27	0.0185
BR 8-5F	1.06	1.1×10^6	5.14×10^3	1.30	0.38	0.022
BR 9-2F	1.88	5.5×10^6	2.56×10^4	6.50	1.88	0.049

vinyl segment length of 2.54 Å. The maximum radius of gyration, R_G max., is calculated for a completely stretched-out solution configuration and the minimum radius of gyration is calculated for a completely coiled configuration. The true solution radius of gyration is between these two limits.

2. Branched Polymers. The formation of branches along the polymer backbone is second only to molecular weight in influencing the properties of polymers and polymer solutions. With free radical polymerization, the method used to prepare the polymers for this research, it is possible for side reactions to occur which produce branched structures. Since branching probably would affect flocculation a homologous series of linear polyelectrolytes is desired.

The relationship between the intrinsic viscosity and the molecular weight is affected by the presence of branching. The exponent in the Mark-Houwink equation decreases for branched, high molecular weight polymers. For a system of unbranched polymers a log-log plot of the intrinsic viscosity against the weight average molecular weights should be linear. The linear relationship illustrated in Fig. V-1 indicates that significant branching does not occur.

3. Polymer Configuration in Solution. The solution configuration of polyelectrolyte molecules depends on the nature of the polymer backbone, the degree of ionization, and the ionic composition of the solution. According to Flory²² both DMVPB monomer and polymer are completely dissociated in aqueous

solution. Experimentally, complete dissociation is indicated by the relatively large specific conductivity. At equal molar concentrations, potassium bromide, monomer, and polymer* have specific conductances of 6.3, 4.2, and 1.9 milli-mohs/cm, respectively. The difference between the conductances of the potassium bromide and the monomer is attributed to the larger size of the monomer cation, i. e., (1,2-dimethyl-5-vinylpyridinium)⁺ vs. K⁺.

As the concentration of simple ions in an aqueous solution containing polyelectrolytes decreases, the polyion uncoils because of the increased range of Coulombic repulsive forces between adjacent ionized segments. In Fig. V-2 the variation of intrinsic viscosity with sodium chloride concentration is illustrated for two unlabeled DMVPB polymers and Cat-Floc, a commercially available cationic polymeric coagulant**. Intrinsic viscosity increases more than tenfold when the sodium chloride concentration is reduced from 10⁻¹ to 10⁻⁴ moles/liter.

The solution configuration of polyelectrolyte molecules is also affected by the valence of the solution ions having charge opposite that of the polyion. Using data published by Shyluk⁶¹, the effect of counterion valency on the reduced specific viscosity of a cationic polyelectrolyte is illustrated in Fig. V-3. Within certain limits the viscosity decreases with increasing valence at constant salt concentration. This behavior is consistent with the electrical double layer theory.

* molar concentration based on M_o

**a product of Calgon Corporation

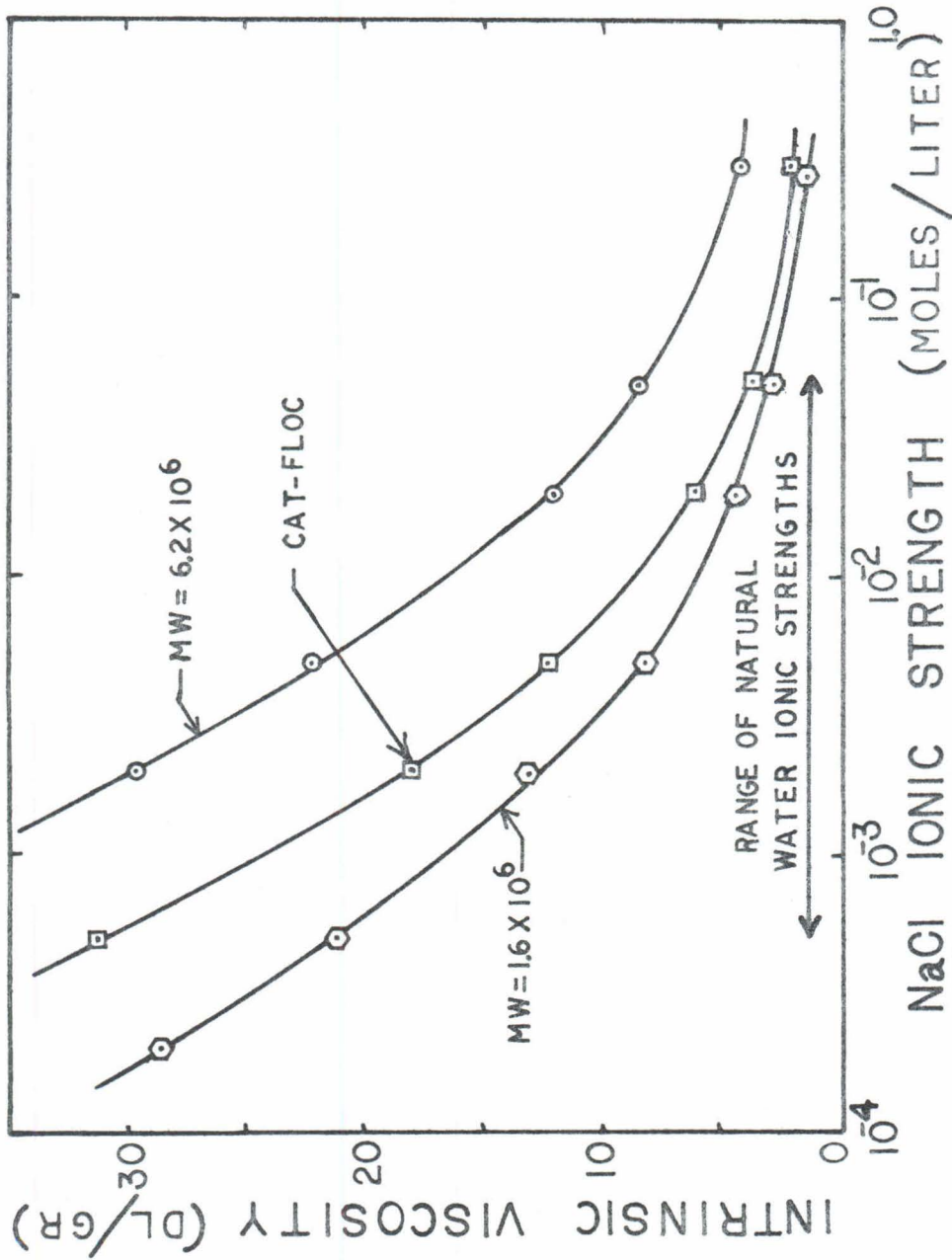


Fig. V-2. Effect of NaCl ionic strength on intrinsic viscosity (deciliters/gram)

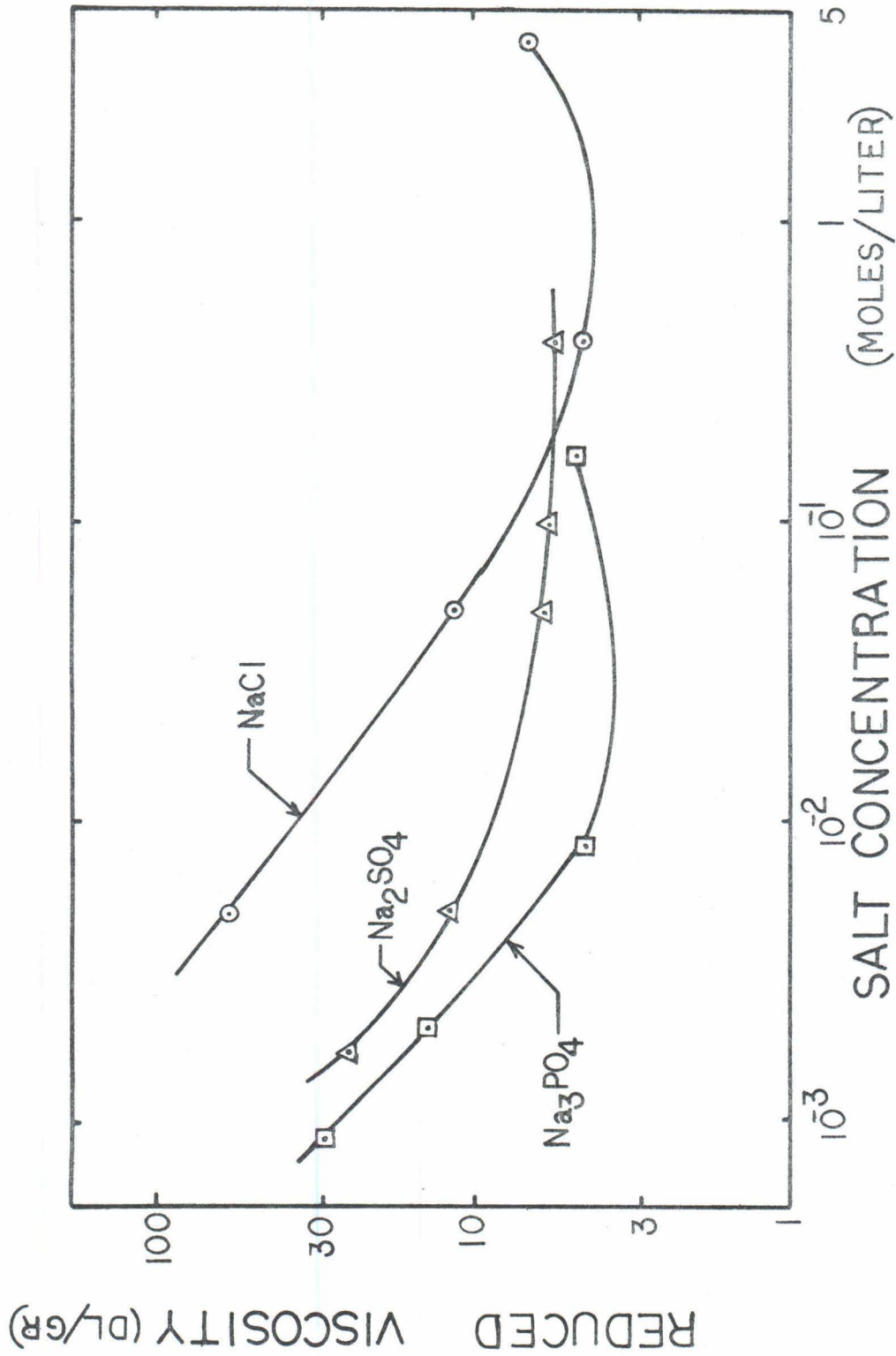


Fig. V-3. Effect of anion valence on viscosity-salt concentration relationships for cationic polyelectrolytes.

Some authors have correlated hydrodynamic volumes determined from viscosity measurements with adsorption data for polymers in organic solvents^{26, 57}.

According to Tanford⁷⁰ the intrinsic viscosity is related to the hydrodynamic volume (V_h) by the following equation:

$$[\eta] = K \frac{N}{M} V_h \quad V-2$$

where N is Avogadro's number, M is the molecular weight, and K is a constant dependent on the shape of the macromolecule. The hydrodynamic volume is defined as the volume of the macromolecule and its solvated ions. Since the shape of a polyelectrolyte molecule is a function of ionic composition, the variation of the hydrodynamic volume with ionic composition cannot be followed by intrinsic viscosity data, i. e., K is not constant.

B. Particles

In order to apply the double layer theory and the DCA concept to the experimental system it is necessary to know the electrical surface properties of the particles. In aqueous solutions surface charges on particles arise primarily by three mechanisms: (i) ionization of surface groups, e. g., ionization of surface carboxyl and amino groups on biological particles; (ii) isomorphous substitution in lattices of solids, e. g., replacement of Si^{IV} by Al^{III} in clays; and (iii) specific ion adsorption, e. g., ionic surfactants at oil-water interface or preferential adsorption of Ag^+ over I^- onto AgI solids. Each mechanism has characteristic properties which cause the

surface to have either constant charge or constant potential.

The two particles used in this research obtain their surface charges by two different mechanisms. Polystyrene latices (PSL) are stabilized by the attachment of sulfonate groups to the surface. Above pH 2, protons are completely dissociated from the sulfonate groups and the surface charge remains constant. The constant surface charge is characteristic of biological particles at constant pH and of mineral particles with surface charge due to isomorphous substitution. Silica, the second kind of particle material used in this research, adsorbs hydroxide ions to the surface atoms. pH is one of the most important variables with respect to the charge density of the silica system because hydrogen and hydroxide ions are potential-determining ions for the surface. H^+ and OH^- are potential-determining ions for many other particles including oxides, hydroxides, and complex oxide compounds such as silicates and phosphates.

As discussed in Chapter II, the Stern correction to the Gouy-Chapman double layer model is used to calculate the Stern potential, ψ_s , which then is used instead of ψ_0 to determine interaction energies between particles.

The Stern relationships for the ionic atmosphere near a flat plate are presented in Appendix I. The relatively large particles used in this research can be approximated as flat plates for the Stern layer calculations since the Stern layer is very small in comparison to the particles. Spherical models, however, are used to calculate the interaction energies of the diffuse layers.

To apply the mathematical Stern relationships presented in Appendix 1 three parameters in addition to the usual double layer parameters are needed: (i) δ , the thickness of the Stern layer, (ii) ϵ' , the dielectric constant in the Stern layer, and (iii) N_1 , the number of Stern adsorption sites per unit surface area. The effects of varying these three parameters on the pertinent double layer properties of the particles used in this research are examined in the following sections because the exact numerical values of these parameters are unknown.

1. PSL. The sulfonate group density on the surface of the PSL particles is 1.1×10^{14} per square centimeter. Above pH 2, all the sulfonate groups are dissociated and the surface charge density is 5.32×10^4 esu cm^{-2} . In a system of constant surface charge the Stern potential is found to be independent of ϵ' and δ by solving the equations in Appendix 1. In Table V-2, where values of Stern potentials are listed for various adsorption site densities at three ionic strengths, it is seen that the Stern potential is also rather insensitive to the adsorption site density. A 100 percent change in N_1 results in only a 10 percent change in the Stern potential.

Although the Stern potential in a constant surface charge system is independent of ϵ' and δ , the surface potential, ψ_0 , is greatly affected by changes in the values of these parameters. The difference between the surface potential and the Stern potential ($\Delta \psi = \psi_0 - \psi_s$) is plotted in Fig. V-4 as a function of ϵ' and δ . van Olphen⁷³ gives 3-10 Å as the range of the Stern layer thicknesses and 3-6 as the range of dielectric constants in the Stern

Table V-2.

Values of PSL Stern potential for various Stern layer adsorption site densities (N_1). Surface charge density = 5.32×10^4 esu/cm².

N_1 (cm ⁻²)	area/ site (Å ²)	Ionic Strength (moles/liter)		
		10 ⁻¹	10 ⁻³	10 ⁻⁵
2×10^{15}	5	74 mv	187 mv	305 mv
1×10^{15}	10	85	200	315
5×10^{14}	20	95	210	325
2×10^{14}	50	102	217	333

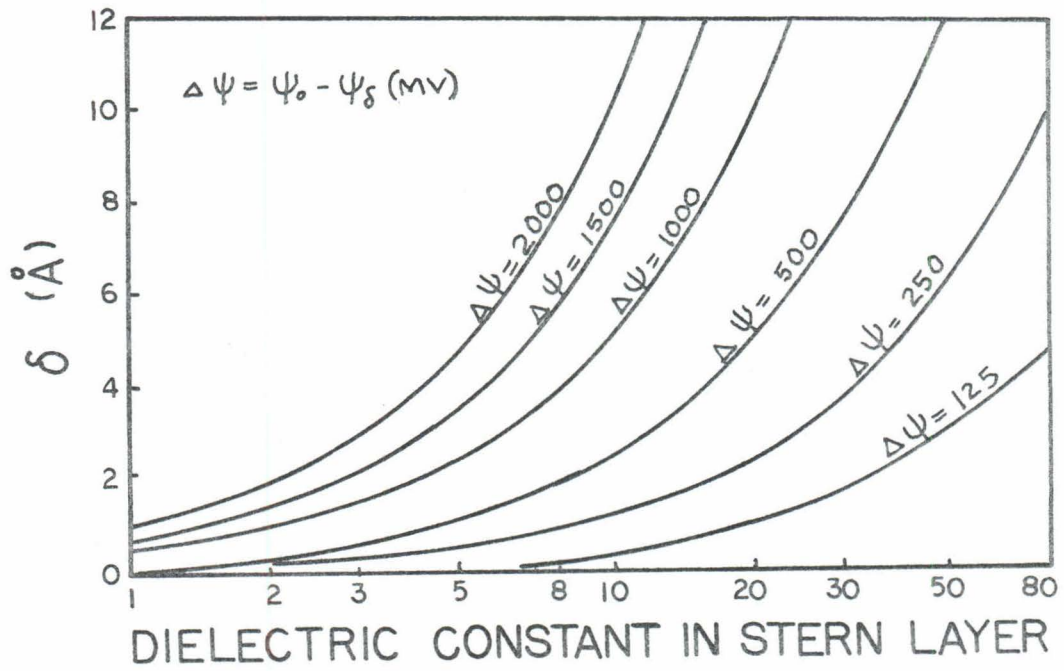


Fig. V-4. The effects of ϵ' and δ on ψ_0 , the surface potential, for a constant charge surface, $\sigma = 5.32 \times 10^4$ esu/cm², $N_1 = 10^{15}$ /cm².

layer. The large variation possible in the surface potential does not, however, affect the particle interaction energies which are dependent on the Stern potential.

The PSL double layer parameters needed for the application of the DCA results are presented in Table V-3. The values are based on a Stern adsorption site density of $10^{15}/\text{cm}^2$.

2. Min-U-Sil. For surfaces whose potential is determined by the activity of potential determining ions, the surface potential is given by

$$\psi_0 = \frac{kT}{e} \log_e \left(\frac{a}{a_0} \right) \quad \text{V-3}$$

where a is the activity of the potential determining ion and a_0 is the activity of the potential determining ion at the point of zero charge for the surface. For quartz, Parks⁴⁷ found the point of zero charge to occur at pH 2.6. Substituting this value into Eq. V-3 the surface potential of the Min-U-Sil particles at any pH is

$$\psi_0 = 59 \text{ mv } [2.6 - \text{pH}]. \quad \text{V-4}$$

Many of the Min-U-Sil experiments were carried out at pH 8.3, which corresponds to a constant surface potential of 338 mv.

Although all three Stern parameters effect the Stern potential in a constant potential system, ψ_s is primarily a function of ϵ' and δ . ψ_s is only slightly dependent on the adsorption site density. In Figs. V-5 and V-6 the Stern potential and the surface charge density is illustrated for various values of ϵ' and δ . As

Table V-3.

Double Layer Characteristics of PSL Particles.
 $\sigma = 5.32 \times 10^4$ esu/cm², $N_1 = 10^{15}$ cm⁻², one charge per 90 Å².

Ionic Strength (moles/liter)	Stern Potential (mv)
10 ⁻¹	85
10 ⁻²	140
10 ⁻³	200
10 ⁻⁴	256
10 ⁻⁵	315

Table V-4.

Double Layer Characteristics of Min-U-Sil
 Particles. Assumed conditions: pH = 8.33,
 $\psi_0 = 338$ mv, $N_1 = 10^{15}$ cm⁻², $\delta = 5$ Å,
 $\epsilon' = 6$, and T = 20°C.

Ionic Strength (moles/liter)	ψ_s (mv)	σ (esu/cm ²)	Elementary charges/cm ²	Å ² per charge
10 ⁻¹	29.8	9.76x10 ³	2.03x10 ¹³	492
10 ⁻²	75	8.30x10 ³	1.73x10 ¹³	587
10 ⁻³	120	6.90x10 ³	1.43x10 ¹³	688
10 ⁻⁴	165	5.48x10 ³	1.14x10 ¹³	877
10 ⁻⁵	200	4.38x10 ³	0.91x10 ¹³	1100

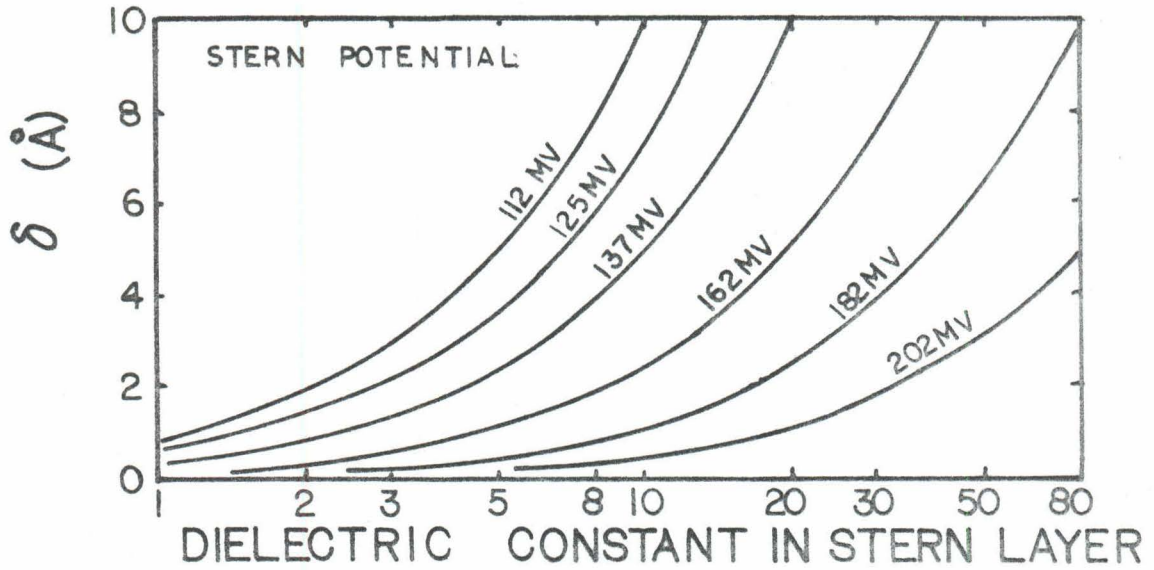


Fig. V-5. Dependence of Stern potential on ϵ' and δ for constant potential surface. $\psi_0 = 338$ mv, ionic strength = 10^{-3} moles/liter and $N_1 = 10^{15}/\text{cm}^2$.

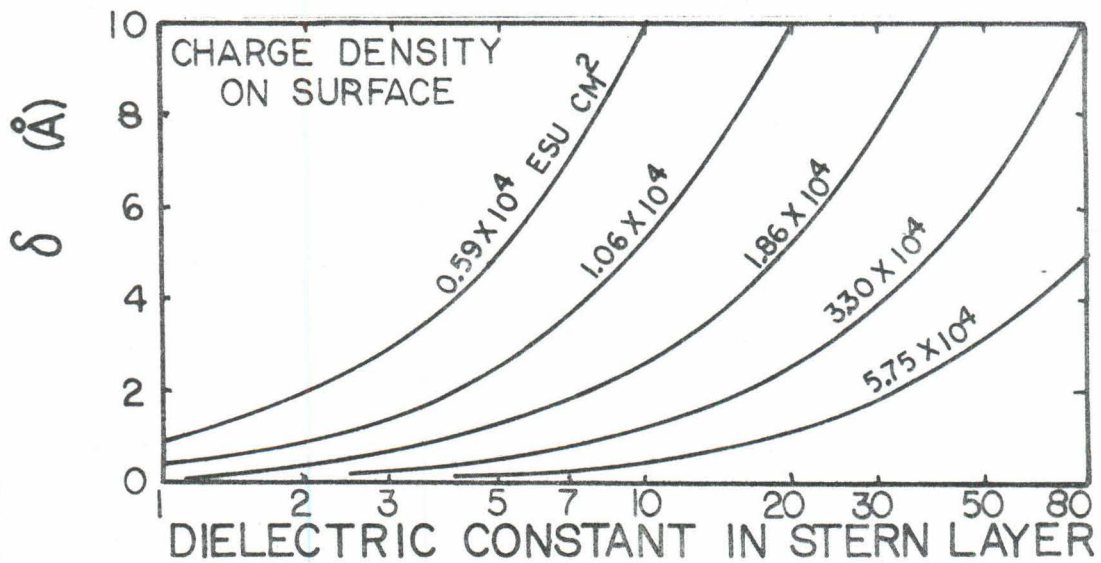


Fig. V-6. Dependence of surface charge density, σ , on ϵ' and δ for constant potential surface. $\psi_0 = 338$ mv, ionic strength = 10^{-3} moles/liter and $N_1 = 10^{15}/\text{cm}^2$.

in the case of the PSL particles the interaction energies between particles are controlled by the value of the Stern potential. In Fig. V-5 it is seen that ψ_s is very dependent on ϵ' and δ .

Values of the double layer properties at various ionic strengths are presented in Table V-4 for the Min-U-Sil system. The assumed conditions are $\epsilon' = 6$, $\delta = 5 \text{ \AA}$, $\psi_0 = 338 \text{ mv}$, and $N_1 = 10^{15} \text{ cm}^{-2}$.

In summation, the Stern potential of surfaces characterized by constant surface charge is determined primarily by the ionic strength of the solution and the surface charge. In contrast, the Stern potential of constant potential surfaces is determined by the concentration of potential determining ions, the ionic strength, the Stern layer thickness, and dielectric constant in the Stern layer.

Chapter VI

KINETICS OF POLYMER ADSORPTION AND PARTICLE AGGREGATION

Polymer aggregation of suspended particles requires that colliding particles have polymer molecules adsorbed to their surfaces. If the rate of polymer adsorption is slow in comparison to the particle-particle collision rate, the aggregation rate will be limited by the polymer adsorption process. It is also possible that the destabilization mechanism (whether a bridging or electrostatic one) is influenced by the relative rates of polymer adsorption and particle-particle collisions. In the following sections the rates of polymer adsorption and particle coagulation are investigated theoretically and experimentally.

A. Theory

It is assumed that both the polymer adsorption rate and the particle aggregation rate are equal to the product of an appropriate efficiency factor (α_1) and the rate of polymer-particle collisions or particle-particle collisions, respectively. In the first part of this analysis collision rates are examined.

1. Collision Rates. In an aqueous suspension containing polymer molecules the particle-particle and polymer-particle collisions are brought about by Brownian movement and by velocity gradient transport. By assuming that all particles and all polymer molecules can be modeled by equivalent spheres and that only laminar velocity gradients exist, von Smoluchowski's kinetic theories can be used to compute the collision rates.

a. Diffusion Transport. von Smoluchowski's theory of rapid coagulation describes the rate of the collisions resulting from the Brownian transport of particles⁶⁵. Mathematically the rapid coagulation theory for the rate of polymer-particle collisions is expressed as

$$(b_{sp})_B = 2 \pi (D_s + D_p) (d_s + d_p) N_s N_p \quad \text{VI-1}$$

where $(b_{sp})_B$ = rate of polymer-suspended particle collisions due to Brownian diffusion, (sec^{-1})

D_s, D_p = diffusion coefficients of suspended particle and polymer, respectively, ($\text{cm}^2 \text{sec}^{-1}$)

d_s, d_p = diameter of suspended particle and polymer, respectively, (cm).

N_s, N_p = number of particles and polymer molecules per cm^3 , respectively.

This same theory is used to evaluate $(b_{ss})_B$, the rate of collisions between equal-sized suspended particles moved by Brownian diffusion:

$$(b_{ss})_B = 4 \pi D_s d_s N_s^2 \quad \text{VI-2}$$

For spherical particles the diffusion coefficients can be evaluated by the Einstein diffusion equation

$$D = \frac{k T}{3 \pi \mu d} \quad \text{VI-3}$$

where k = Boltzmann's constant
 T = absolute temperature
 μ = dynamic viscosity
 d = particle diameter

For an aqueous solution at 20°C, Eq. VI-3 can be rewritten as

$$D = \frac{K}{d} = \frac{4.2 \times 10^{-13} \text{ cm}^2}{d \text{ sec}} \quad \text{VI-4}$$

Substituting Eq. VI-4 into Eqs. VI-1 and VI-2 yields

$$(b_{sp})_B = 2\pi K \frac{(dp+ds)^2}{ds dp} N_s N_p \quad \text{VI-5}$$

$$(b_{ss})_B = 4\pi K N_s^2 \quad \text{VI-6}$$

If $ds = dp$ in Eq. VI-5, b_{ss} equals $8\pi K N_s^2$, which is twice the result obtained by using Eq. VI-6. This is because every collision between equally sized particles is counted twice by Eq. VI-5.

b. Laminar Velocity Gradient Transport. A second kinetic expression due to Smoluchowski describes the rates of collisions between particles transported by laminar velocity gradients⁶⁵. Mathematically,

$$(b_{sp})_L = \frac{G}{6} (ds + dp)^3 N_s N_p \quad \text{VI-7}$$

where $(b_{sp})_L$ = rate of suspended particle-polymer collisions due to laminar shear, (sec^{-1})

G = laminar velocity gradient, (sec^{-1}).

Likewise

$$(b_{ss})_L = \frac{2}{3} G ds^3 N_s^2 \quad \text{VI-8}$$

In the systems investigated the effects of turbulent shear gradients on the total rates of collision are neglected.

The total collision rate can be approximated as the sum of the rates of collisions caused by Brownian diffusion and laminar velocity gradients:

$$(b_{sp}) = N_s N_p \left[\frac{2\pi K(ds + dp)^2}{ds dp} + \frac{G}{6} (ds + dp)^3 \right] \quad \text{VI-9}$$

$$(b_{ss}) = N_s^2 \left[4\pi K + \frac{2}{3} G ds^3 \right]. \quad \text{VI-10}$$

Using Eqs. VI-9 and VI-10, R, the ratio of the particle-particle collision rate to the particle-polymer collision rate can be evaluated:

$$R = \frac{(b_{ss})}{(b_{sp})} = \frac{N_s}{N_p} \frac{[4\pi K + \frac{2}{3} G ds^3]}{\left[\frac{2\pi K (ds + dp)^2}{ds dp} + \frac{G}{6} (ds + dp)^3 \right]}. \quad \text{VI-11}$$

For a given system having constant G, dp, and ds, R can be expressed as the product of a constant (called the collision rate factor, B) and the ratio of the particle and polymer number concentrations. That is

$$R = (N_s/N_p) (B) \quad \text{VI-12}$$

where

$$B = \frac{[4\pi K + \frac{2}{3} G ds^3]}{\left[\frac{2\pi K (ds + dp)^2}{ds dp} + \frac{G}{6} (ds + dp)^3 \right]}. \quad \text{VI-13}$$

In Fig. VI-1, B, the collision ratio factor is evaluated as a function of particle diameter for polymer molecules of several different sizes at $G = 0$ and at $G = 100 \text{ sec}^{-1}$. Fig. VI-1 illustrates that the collision rates of large particles are not influenced by Brownian motion (i. e., $G = 0$ curve) and that the collision rates of particles smaller than 0.2 microns are not influenced by laminar velocity gradients, i. e., by mixing.

In systems experiencing only Brownian motion ($G = 0$) the maximum collision ratio factor occurs when the particles and the polymer molecules have the same diameter. The reason the maximum B value is equal to 0.5 and not unity is most easily explained in terms of R. For a system with $N_s/N_p = 1$, R equals B. The maximum value of R is equal to 0.5 which means that the rate of polymer-particle collisions is twice the rate of particle-particle collisions. This is reasonable since the number of entities involved in polymer-particle collisions is twice the number involved in particle-particle collisions.

In Fig. VI-2 the dependence of B on particle size is illustrated for a 0.01 micron diameter polymer molecule at various G values. Fig. VI-2 shows that in a system of 0.1 micron or smaller particles mixing does not affect the coagulation rate until the particles aggregate to approximately 0.5 microns, i. e., for $G = 10 \text{ sec}^{-1}$.

According to Eq. VI-12 the ratio of the particle-particle collision rate to the polymer-particle collision rate is directly proportional to N_s/N_p . In Table VI-1 values of N_s/N_p are tab-

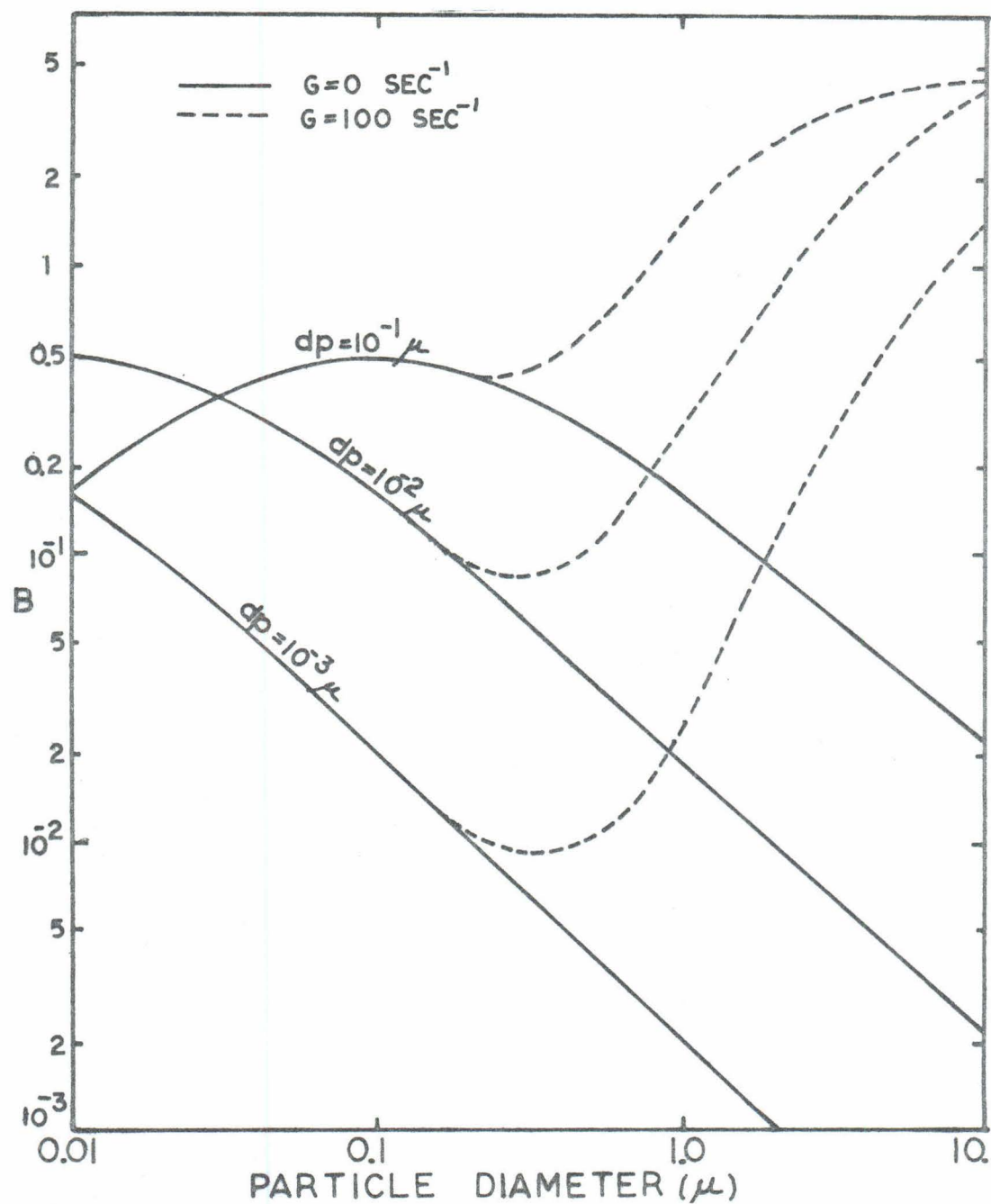


Fig. VI-1. Dependence of B, the collision ratio factor, on particle diameter and on solution polymer size (dp) for $G = 0$ and $G = 100 \text{ sec}^{-1}$.

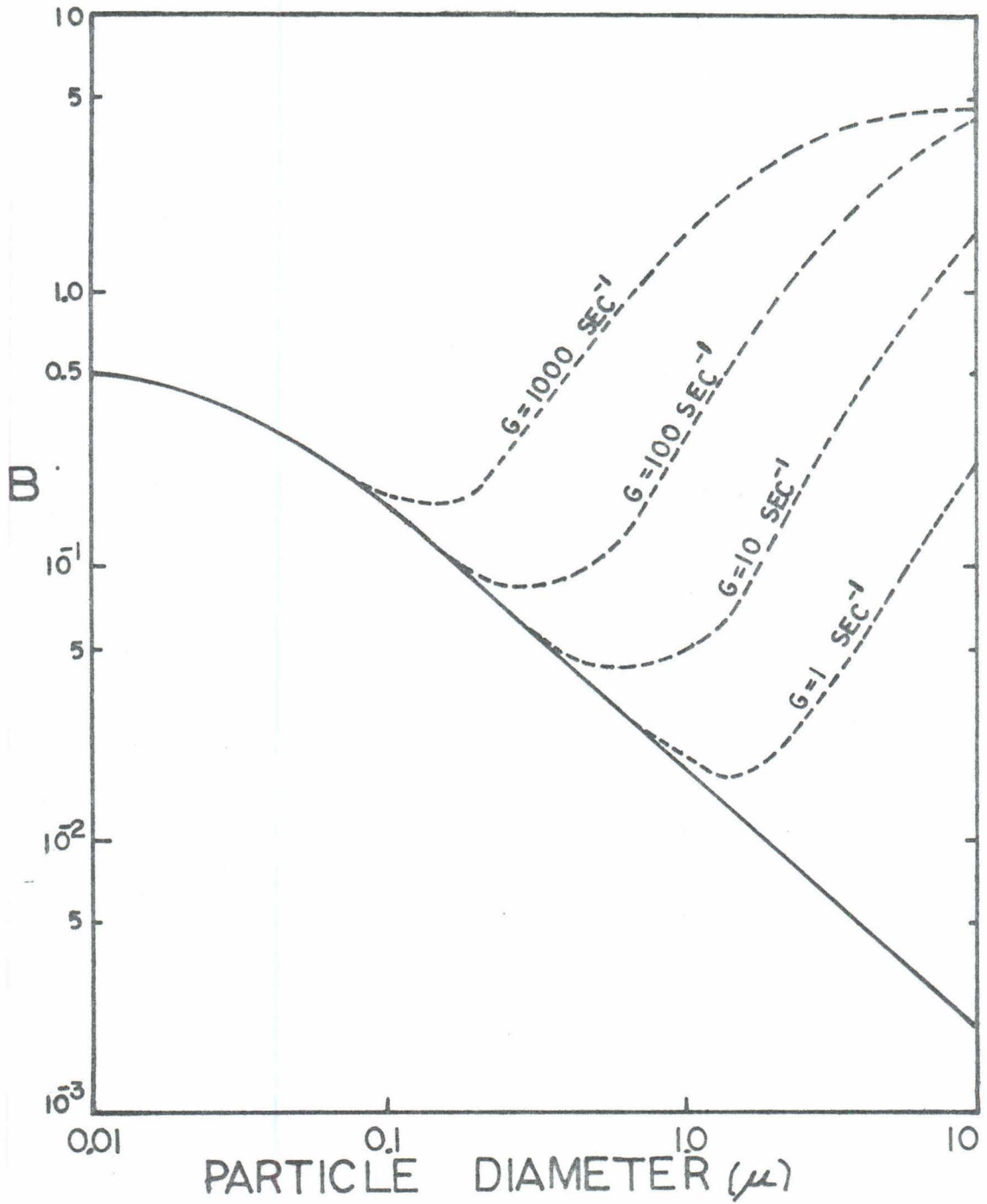


Fig. VI-2. Effect of G (sec^{-1}) on B , the collision ratio factor. $d_p = 0.01$ microns.

Table VI-1.

Particle-Polymer Number Ratios for Various Flocculating Systems

System	N_s	N_p	Molecular Weight	N_s/N_p	Ref.
Cat. ^{1/} -Kaolinite	9.2×10^9	3.6×10^{13}	5×10^4	2.5×10^{-4}	10
Cat. ^{1/} -Silica	1.2×10^8	1.2×10^{13}	5×10^4	1.0×10^{-5}	10
Cat. ^{1/} -PSL	1.2×10^8	6.0×10^{12}	5×10^4	2.1×10^{-5}	10
Cat. ^{1/} -PSL	1.2×10^{11}	6.0×10^{13}	5×10^4	2.0×10^{-3}	10
Cat. ^{2/} -Silica	1.7×10^8	1.9×10^{14}	1×10^3	9.2×10^{-7}	20
Cat. ^{2/} -Silica	1.7×10^8	3.0×10^{12}	3.2×10^4	5.5×10^{-5}	20
Cat. ^{2/} -PSL	2.1×10^8	7.3×10^{12}	3.4×10^4	3.5×10^{-5}	7
Non. ^{3/} -Kaolinite	1.6×10^9	6.0×10^{10}	5×10^6	2.7×10^{-2}	6
Cat. ^{2/} -E. coli	3.7×10^8	6.0×10^{12}	2.1×10^4	6.2×10^{-5}	71
Cat. ^{2/} -Algae ^{4/}	10^7	9×10^{14}	2.1×10^4	1.1×10^{-6}	71
Cat. ^{5/} -PSL	1.6×10^7	2.4×10^9	5.5×10^6	6.9×10^{-3}	*

Abbreviations: Cat. -Cationic; Non. -Nonionic; PSL-Polystyrene latex.

- 1/ poly(diallyldimethyl ammonium chloride)
- 2/ polyethyleneimine
- 3/ polyethylene oxide
- 4/ Chlorella ellipsoidea
- 5/ poly(1, 2 dimethyl-5-vinylpyridinium bromide)
- * This research

ulated for various flocculating polymer-particle systems. N_p is based on the polymer dose at optimum flocculation. In the majority of systems N_s/N_p is between 10^{-2} and 10^{-6} .

2. Collision Efficiency Factors. The collision rate analysis does not yield any information about the rates of polymer adsorption or particle aggregation unless the collision efficiency factors, α_i , are known. For polyelectrolyte molecules colliding with oppositely charged surfaces α_{sp} is close to unity; collisions between particles having the same surface charge are usually not successful and α_{ss} is less than unity. In the case of a collision between a polymer coated particle and an uncoated particle α_{ss} is probably close to unity. Although the numerical values of the collision efficiency factors are not known it can be remarked that $\alpha_{ss}/\alpha_{sp} \leq 1$.

The ratio of the particle aggregation rate to the polymer adsorption rate, R' , is approximated by

$$R' = \left(\frac{\alpha_{ss}}{\alpha_{sp}} \right) R = \left(\frac{\alpha_{ss}}{\alpha_{sp}} \right) \left(\frac{N_s}{N_p} \right) B \quad \text{VI-14}$$

Since $(\alpha_{ss}/\alpha_{sp}) \leq 1$, $N_s/N_p < 10^{-2}$, and $B < 5$, it can be concluded that polyelectrolyte adsorption to oppositely charged surfaces occurs rapidly in comparison to particle aggregation.

This difference in the time scales for the two processes is significant because it allows suspension coagulation by polyelectrolytes to be analyzed as two separate processes: (i) relatively rapid polyelectrolyte adsorption, which is a function of the physical and chemical properties of the macromolecules and the particles; (ii)

particle aggregation which is dependent on the interparticle forces and the rate of particle-particle collisions.

B. Experimental Results

1. Non-aggregating Systems. The polymer adsorption process was investigated in a non-aggregating system by adsorbing polymer to the inside walls of pyrex bottles. The experimental advantages of non-aggregating systems are that the adsorbed polymer configurations are not disturbed by the aggregation or de-aggregation of particles, that available surface areas are not reduced by aggregation, and that polymer losses to surfaces other than that of the adsorbent do not occur.

The effect of salt concentration on the adsorption of high molecular weight polymer onto pyrex glass surfaces is illustrated in Fig. VI-3. The initial adsorption rate and the amount adsorbed at saturation increase with increasing salt concentration. The increase in the initial adsorption rate with increasing ionic strength reflects increased diffusion coefficients resulting from compaction of the polymer molecules in solution. The increase in saturation adsorption with increasing ionic strength is due to decreased interactions between the ionized segments of the adsorbed polymer; decreased interactions permit a closer, more dense packing of the polyion segments.

In Fig. VI-4 the amount of polymer adsorbed as a function of time is illustrated for several molecular weights at two different salt concentrations. The initial polymer concentrations were 200 $\mu\text{g}/\text{l}$ in all systems illustrated. The following conclusions can be

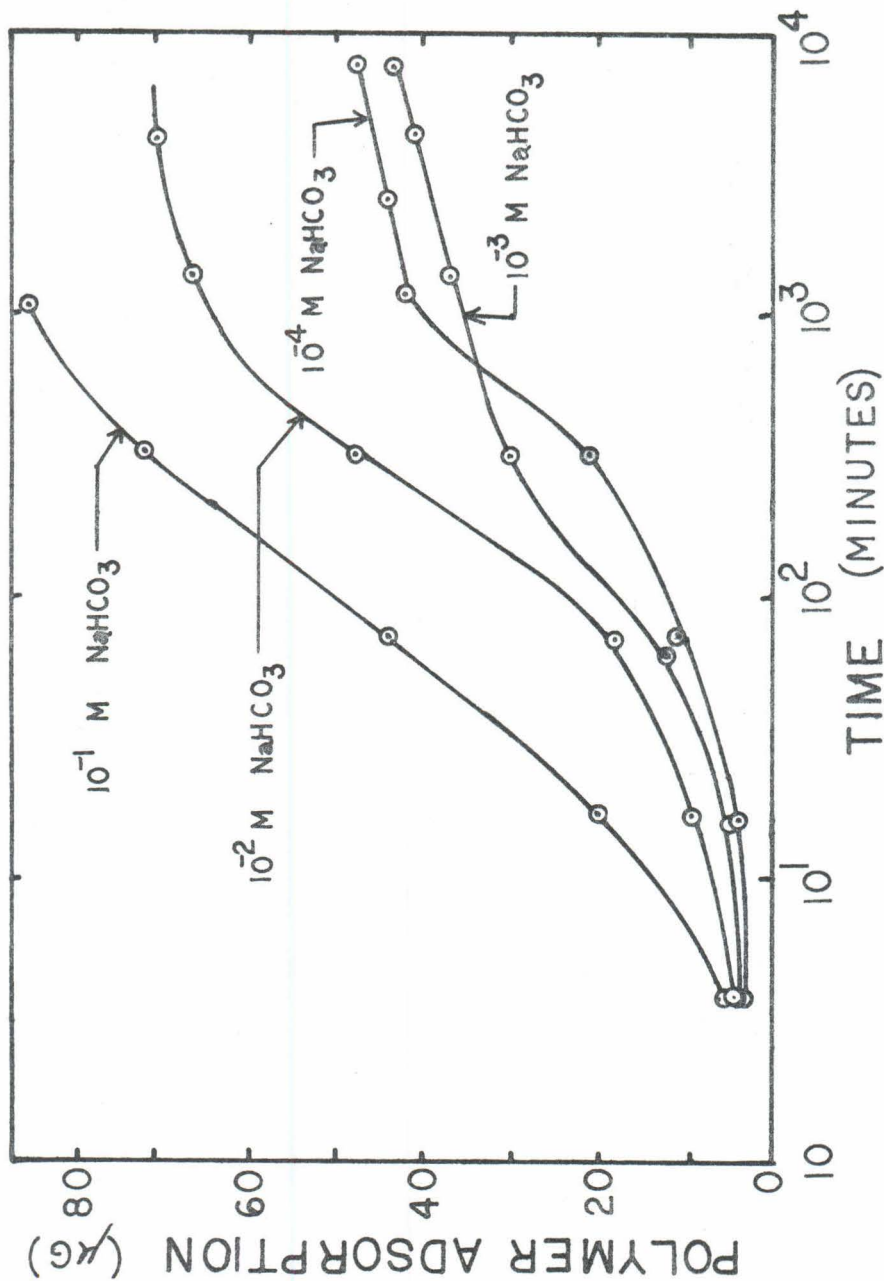


Fig. VI-3. Effect of NaHCO₃ concentration on adsorption of poly (DMVPB) to Pyrex glass surfaces. M = 5.5 x 10⁵, pH = 8.3, surface area = 341 cm², solution volume = 400 ml and initial polymer concentrations = 200 µg/l.

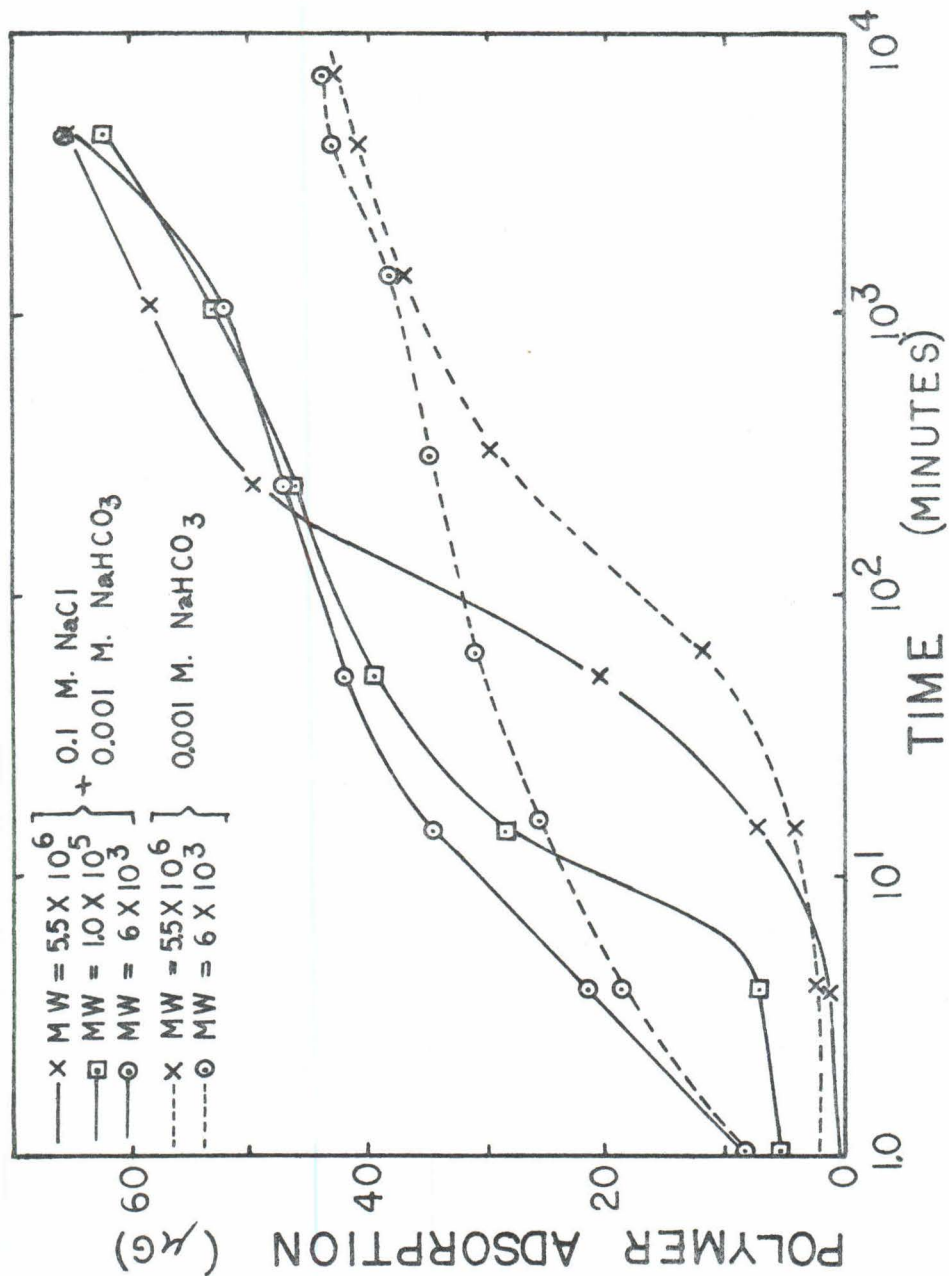
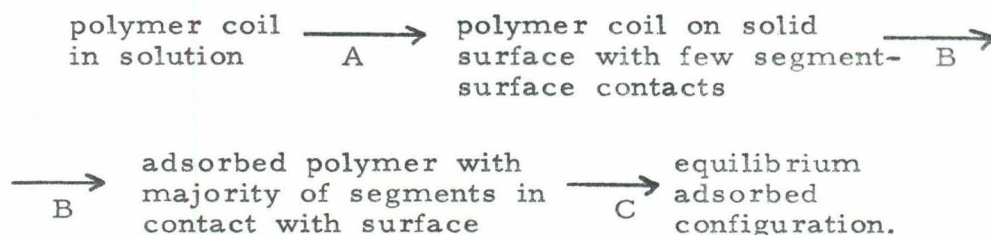


Fig. VI-4. Effect of molecular weight on adsorption of poly(DMVPB) to Pyrex glass surfaces. pH = 8.3, surface area = 341 cm², solution volume = 400 ml and initial polymer concentrations = 200 µg/l.

drawn from the data presented in Figs. VI-3 and VI-4: (i) polymer adsorption continues for long time periods, (ii) the ultimate amount of adsorbed polymer is independent of molecular weight, (iii) the amount of polymer adsorbed at saturation increases with increasing salt concentrations, and (iv) the initial rate of polymer adsorption is dependent on the molecular weight.

On the basis of an adsorption model proposed by Peterson and Kwei⁵¹ the overall adsorption process can be described in terms of the following steps:



The rate of process A is limited by the rate of polymer diffusion and the hydrodynamic transport conditions of the system. In process B the adsorbed molecule undergoes re-orientation from a three-dimensional, coil-like solution configuration having only a few segments attached to a two-dimensional, flat configuration with a majority of segments attached directly to the surface. The rate of process B should be relatively fast in comparison to the rate of process A⁵¹.

In process C the flat, two-dimensional configuration is rearranged to the equilibrium adsorbed configuration. Process C should be relatively slow in comparison to processes A and B. If additional adsorption sites are made available by process C,

then the overall removal rate of polymer from solution is limited by the rate of process C.

The rate of process C may or may not be dependent on molecular weight. An example of a molecular weight dependent rate is the diffusion of adsorbed polymer molecules into the pores of porous adsorbents. Since the diffusion rate decreases with increasing molecular weight, the rate of process C decreases with increasing molecular weight.

For the systems illustrated in Fig. VI-4 the initial adsorption rate is limited by the rate of process A. Two of the experiments were repeated with different initial polymer concentrations and it was found that the adsorption rate increases with increasing solution concentration of polymer. The adsorption rates at times greater than 300 minutes are molecular-weight-independent and are probably limited by the rate of process C.

The fact that the amount of polymer ultimately adsorbed is independent of molecular weight is in agreement with the statistical mechanical models for the case of large adsorption energies between the polymer segments and the surface. The statistical mechanical models also predict that the adsorbed configurations are flat. It is difficult, however, to interpret flocculation models in terms of these conclusions since flocculating systems are not saturated and are not at equilibrium.

2. Aggregating Systems. Variations in polymer adsorption and suspension turbidity with time for a Min-U-Sil system is illustrated in Fig. VI-5. The effect of initial polymer concentra-

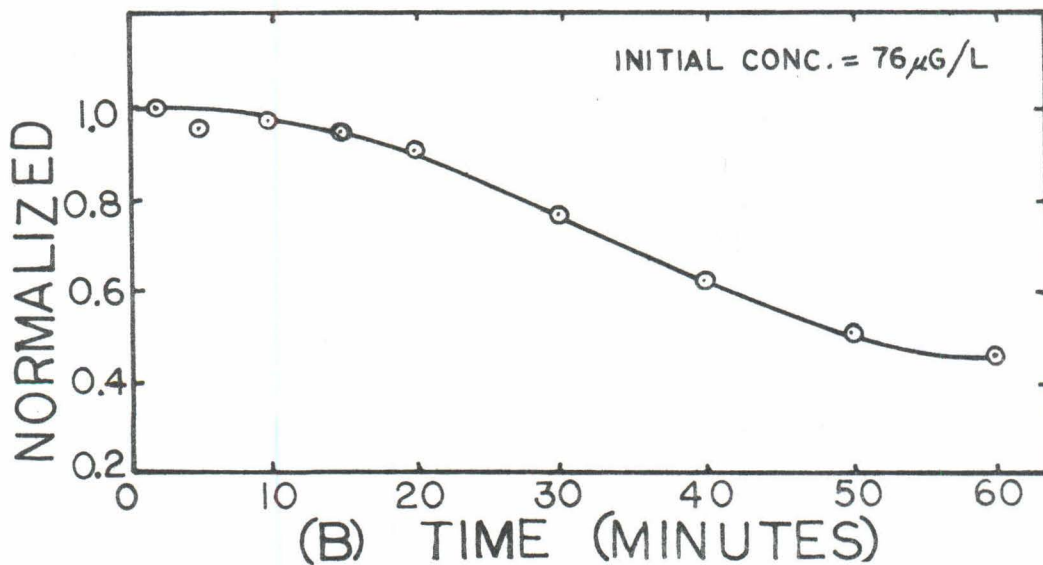
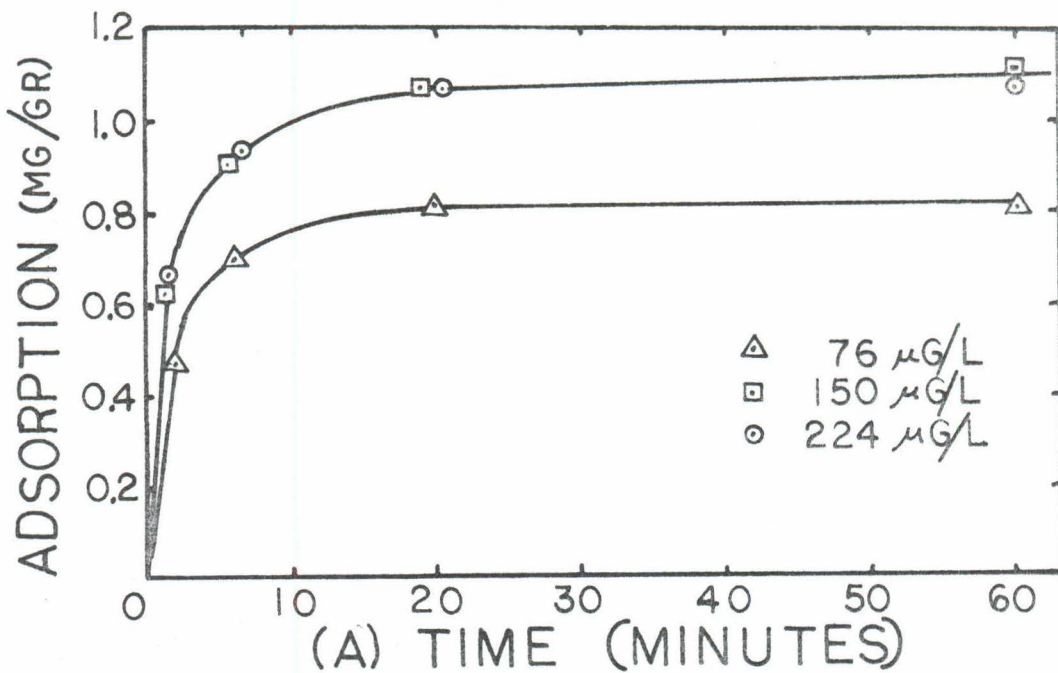


Fig. VI-5. Time variations of: (A) polymer adsorption from solutions of various initial polymer concentrations and (B) supernatant turbidity. 50 mg/l Min-U-Sil suspension in 10^{-3} molar NaHCO_3 . pH = 8.3, $M = 5.5 \times 10^6$ and stirring at 100 rpm.

tion on the adsorption is seen in part (A) of Fig. VI-5. Adsorption is more than 50 percent complete within two minutes and more than 90 percent complete within ten minutes. The amount of polymer adsorbed remained constant between 20 and 180 minutes. After 180 minutes the concentration of the polymer in solution decreased because of losses to the surfaces of the mixing vessel and possibly because of additional adsorption to the silica particles. Lower molecular weight polymers with larger transport rates approach the adsorption plateau more rapidly than the systems illustrated in Fig. VI-5 (A).

Long term adsorption in aggregating systems was not investigated further because of experimental uncertainties associated with such processes as particle attachment to the surfaces of the mixing vessel, polymer degradation by hydrodynamic forces on particles, de-aggregation of particles, and polymer losses to the surfaces of the mixing vessels.

In part (B) of Fig. VI-5, the suspension turbidity normalized with respect to the value at zero time is plotted as a function of time. Turbidity is a complex function of the degree of aggregation of the system. At ten minutes, when polymer adsorption is almost complete, turbidity is almost unchanged.

The size distribution or the total number of particles in a heterogenous system having initial particles larger than one micron cannot be related to the turbidity in any simple way. Aggregation rates cannot be determined from optical data. Birkner and Morgan⁷, using an electronic particle counter to measure particle size distri-

butions as a function of time, determined flocculation rate constants for 1.3 micron PSL destabilized by a cationic polyelectrolyte. In a comparable system (approximately same particle concentration and degree of agitation) these investigators measured a first order aggregation rate constant of $1.6 \times 10^{-4} \text{sec}^{-1}$. In a system having this rate constant, less than 10 percent of the initial particles have aggregated after ten minutes. That is, the total number of particles at ten minutes is more than 90 percent of the initial number of particles. The particle aggregation rate is therefore slow in comparison to the polymer adsorption rate.

Summary

A theoretical analysis based on Smoluchowski's kinetic theories indicates that polymer adsorption is fast in comparison to the rate of particle aggregation in systems consisting of polyelectrolyte molecules and suspended particles of opposite charge. This theoretical analysis is experimentally verified.

In the non-aggregating poly(DMVPB)-pyrex glass system ultimate polyelectrolyte adsorption is dependent on the salt concentration of the solvent and independent of the molecular weight. The initial rate of polymer adsorption is, however, highly dependent on molecular weight.

Chapter VII

FLOCCULATING SYSTEMS: EXPERIMENTAL RESULTS AND DISCUSSION

Fig. VII-1 illustrates the dependence of residual turbidity, electrophoretic mobility and polymer adsorption on the polymer dose. These three parameters were measured for the majority of the systems investigated.

The residual turbidity variation with polymer dose is characterized by the optimum flocculation dose (OFD) which is defined as the smallest flocculation dose which produces the minimum residual turbidity. The OFD is indicated by an arrow on the relative residual turbidity-polymer dose graph of Fig. VII-1.

Operation of an industrial water processing system at the lowest polymer dose resulting in good flocculation is difficult since the raw water characteristics of many industrial systems vary with time. Industrial processes would require a polymer dose greater than the minimum to produce good flocculation at all times. An "operational dose range" is schematically illustrated next to the OFD arrow in Fig. VII-1. Within this dose range, essentially the same final water clarity would be realized.

A number of other flocculation system parameters are of interest. These are: the electrophoretic mobility and the amount of polymer adsorption at the OFD; the polymer dose and the amount of polymer adsorption at zero mobility; and the saturation value or the maximum amount of polymer adsorption. The adsorption data can be described by Langmuir isotherms. Detailed discussion of

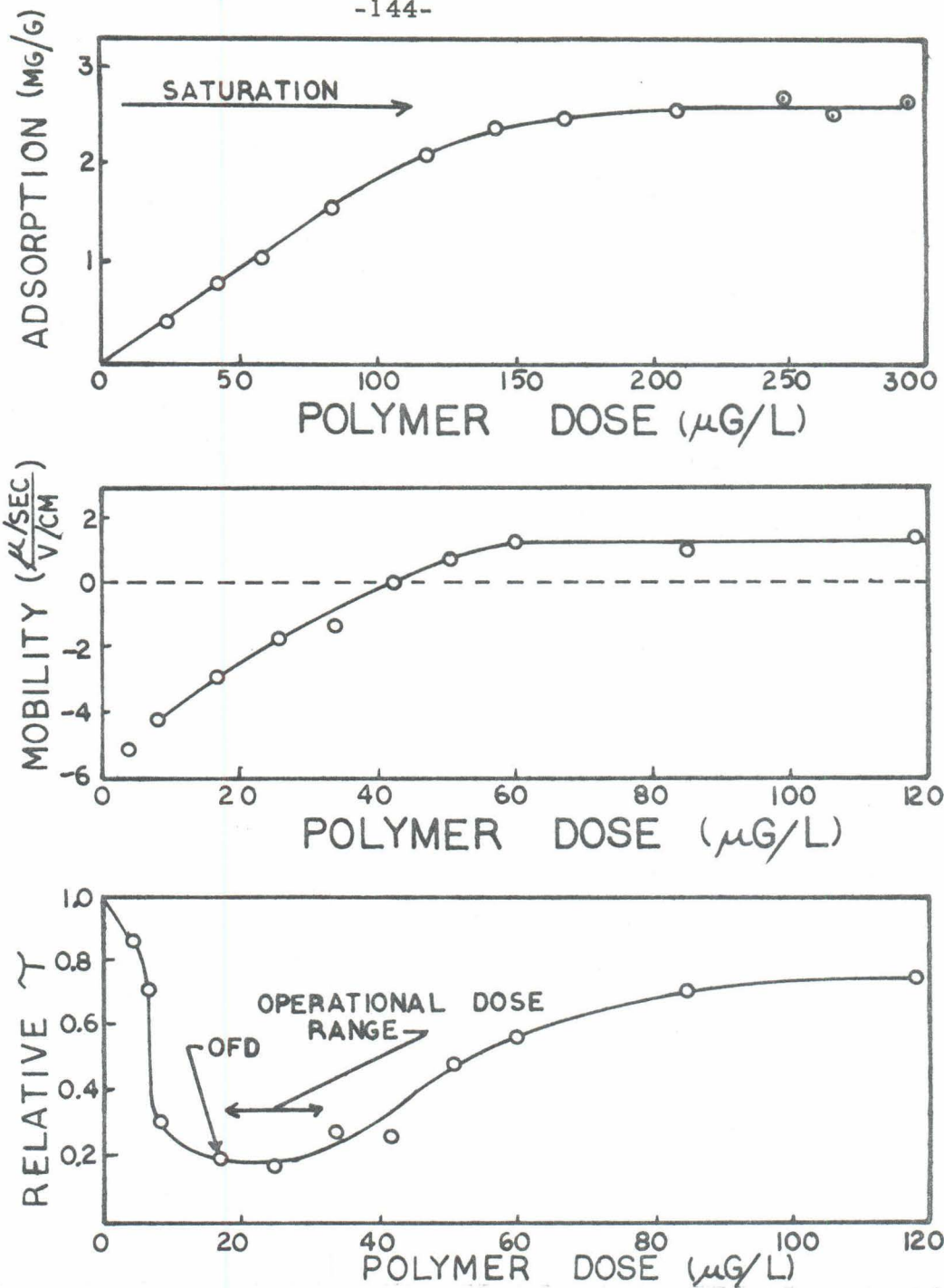


Fig. VII-1. Typical results illustrating the dependencies of residual turbidity, electrophoretic mobility and polymer adsorption on the initial polymer dose.

the adsorption data is presented in section VIII-C.

At large polymer doses it is possible to reverse the particle charge if the number of adsorbed polyion segments is greater than the original number of surface charges. Large charge reversals result in restabilization of the suspension which is indicated by an increase in turbidity at doses greater than the OFD.

A. Residual Turbidity

1. Min-U-Sil Particles. The flocculation experiments were carried out according to the procedures described in Chapter IV.

a. pH Effects. The surface potential of the silica particles is controlled by the pH of the solution since hydrogen ions are potential determining ions (see Eq. V-4). Fig. VII-2 shows an increase in the OFD with increasing pH in agreement with the fact that the surface potential becomes more negative with increasing pH. In the majority of Min-U-Sil systems investigated the pH was held constant at 8.3 (NaHCO_3) or at 6.0 (NaCl , CaCl_2 , Na_2SO_4 , etc., and CO_2 of the atmosphere).

b. Effects of Polymer Molecular Weight and NaHCO_3 Concentration. At low salt concentrations polymer molecular weight greatly affects flocculation. For a 50 mg/l Min-U-Sil suspension in 5×10^{-5} molar NaHCO_3 , the dependence of the residual turbidity on polymer dose is illustrated in Fig. VII-3. The number of polymer segments at any polymer dose is independent of molecular weight if dose is expressed in weight concentrations. Polymer doses required for flocculation decrease with increasing molecular weight.

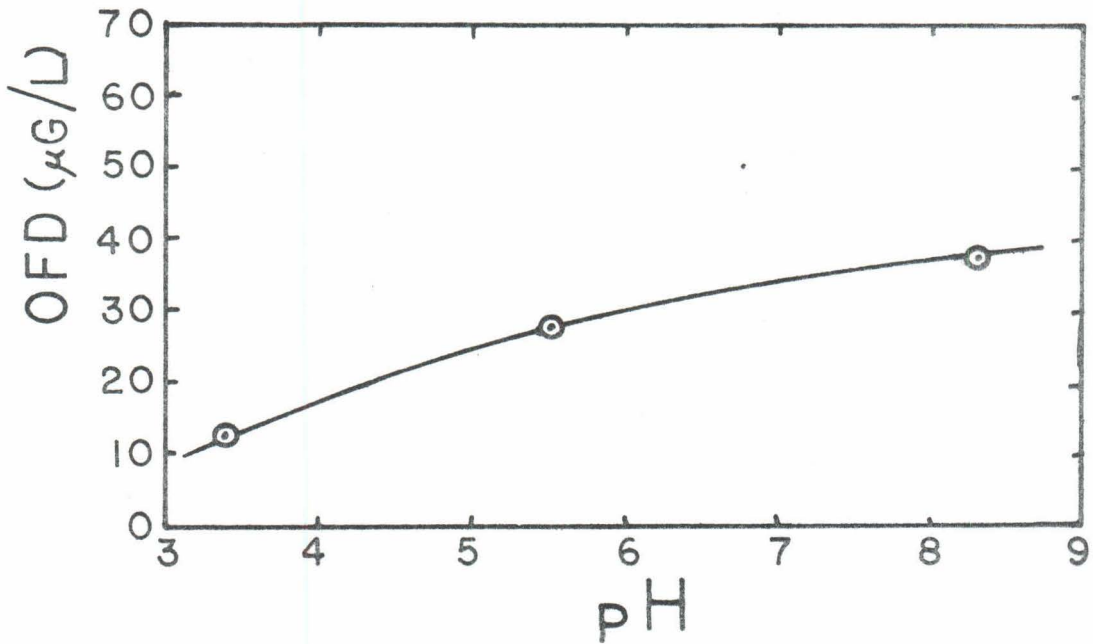


Fig. VII-2. Effect of pH on the OFD's of 50 mg/l Min-U-Sil suspensions in 5×10^{-4} molar ionic strength solutions. $M = 6 \times 10^3$.

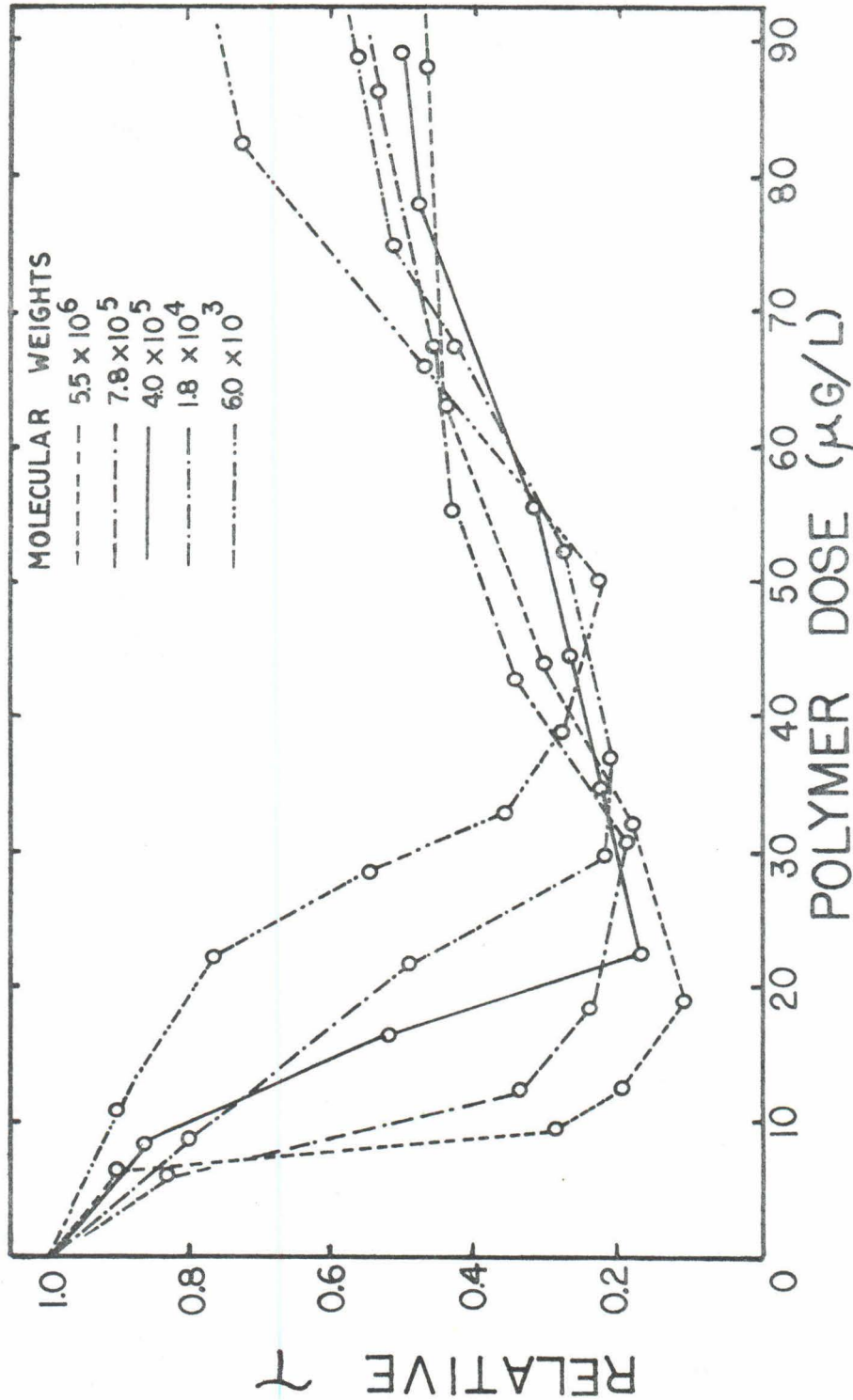


Fig. VII-3. Effect of polymer molecular weight on relative residual turbidity-polymer dose relationship for 50 mg/l Min-U-Sil suspensions in 5×10^{-5} molar NaHCO_3 . pH = 8.3.

The residual turbidity at the OFD decreases with increasing molecular weight.

Fig. VII-4 illustrates the effect of polymer molecular weight on the residual turbidity-polymer dose relationship for a 50 mg/l Min-U-Sil suspension in 10^{-2} molar NaHCO_3 . Data for only three different molecular weights are shown since all data for molecular weights greater than 1.8×10^4 coincide. This coincidence indicates that for Min-U-Sil suspensions in 10^{-2} molar NaHCO_3 the OFD is independent of molecular weight for polymers with molecular weights greater than 1.8×10^4 .

Fig. VII-5 illustrates the dependence of the OFD on polymer molecular weight and NaHCO_3 concentration. At low salt concentrations the OFD decreases with increasing molecular weight; at high salt concentrations the OFD decreases with increasing molecular weight until a "limiting molecular weight" is reached above which the OFD is independent of molecular weight.

Some investigators using cationic polyelectrolytes to flocculate negatively charged suspensions have found the OFD dependent on polymer molecular weight^{37, 24, 20} while others have found the OFD independent of molecular weight^{19, 34}. These apparently conflicting results can be explained by Fig. VII-6 in which the "limiting molecular weight" is plotted as a function of salt concentration. Two regions are defined in Fig. VII-6: Region I, OFD independent of molecular weight and Region II, OFD dependent on molecular weight.

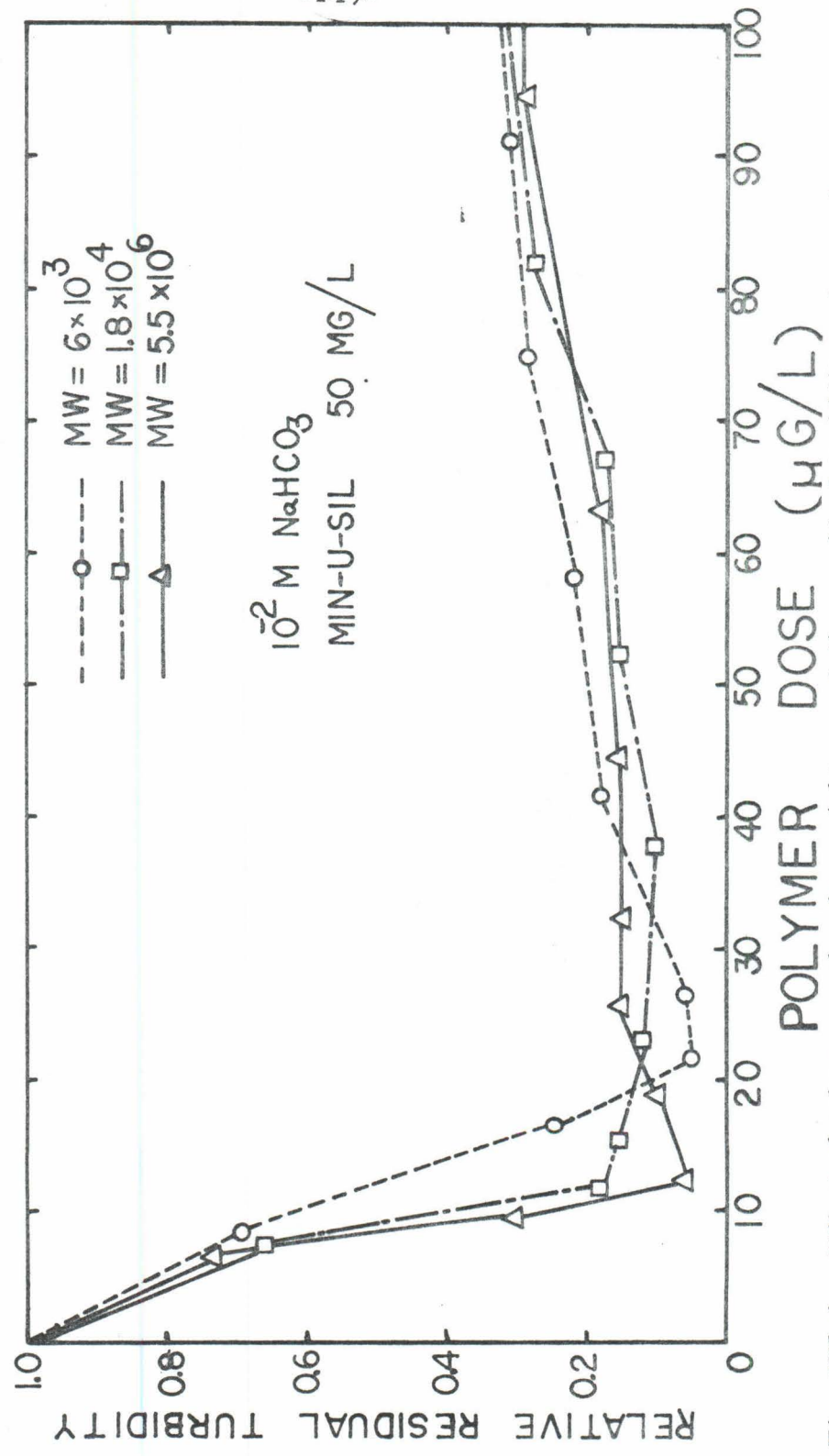


Fig. VII-4. Effect of polymer molecular weight on relative residual turbidity-polymer dose relationship for 50 mg/l Min-U-Sil suspensions in 10⁻² molar NaHCO₃. pH = 8.3.

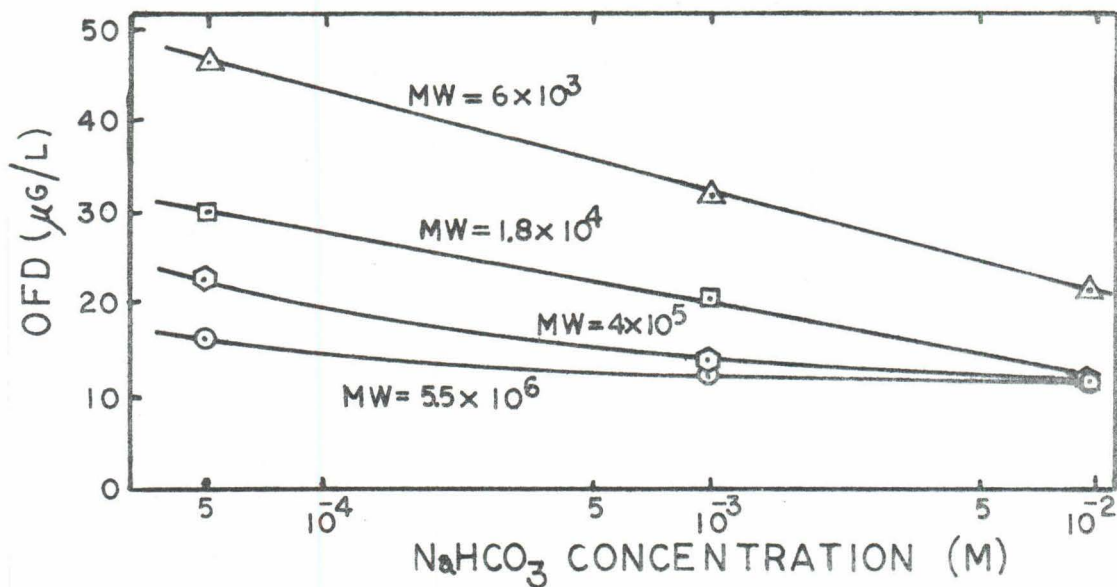


Fig. VII-5. Dependence of OFD on polymer molecular weight and concentration of NaHCO₃. System: pH = 8.3 and Min-U-Sil at 50 mg/l.

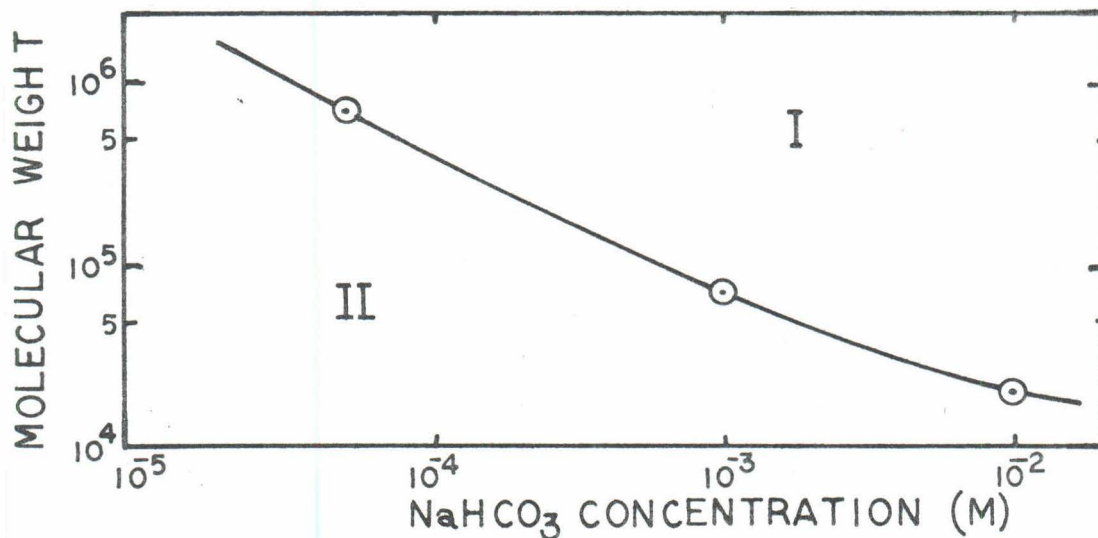


Fig. VII-6. Flocculation regions defined by position of "limiting molecular weights". In Region I the OFD is independent of molecular weight. In Region II the OFD decreases with increasing molecular weight.

The exact position of the line dividing the two regions is a function of the type of suspension, composition of polymer and composition of solution. Those investigators finding the OFD independent of molecular weight generally used solutions with high ionic strengths and/or polymers with high molecular weights (Region I).

c. Solution Composition Effects. The effect of solution ionic composition on the OFD can be seen in the data presented in Table VII-1. The ionic species investigated are mainly those prevalent in natural waters. Trivalent ions were not investigated since they are not common in natural waters having pH's between 5.0 and 9.0.

In the investigated systems, cations affect the colloidal stability of the negatively charged particles (see Fig. II-3) and anions control the solution configuration of the cationic polyelectrolyte molecules (see Fig. V-3).

The small differences between the OFD's of concentration-comparable NaCl and Na₂SO₄ suspensions indicate that polymer solution configuration does not greatly influence the flocculation process. This lack of solution configuration effect on flocculation indicates that the polymer molecules are strongly adsorbed in configurations independent of solution configurations. Strong adsorption energies result in flat adsorption configurations.

The effect of cation valency on the OFD is also seen in the data of Table VII-1. In systems of comparable electrolyte concentrations there are two different trends, depending on molecular

Table VII-1. Effects of solution composition on OFD of Min-U-Sil (50 mg/l). pH = 6.0.

Salt	Ionic Strength (molar)	Cation conc. (molar)	Anion Conc. (molar)	OFD ($\mu\text{g/l}$)	
				Molecular Weight	
				5.5×10^6	6×10^3
NaCl	5×10^{-5}	5×10^{-5}	5×10^{-5}	10	33
	5×10^{-4}	5×10^{-4}	5×10^{-4}	8.2	28
	5×10^{-3}	5×10^{-3}	10^{-2}	6.5	18
Na_2SO_4	7.5×10^{-5}	5×10^{-5}	2.5×10^{-5}	10	32
	7.5×10^{-4}	5×10^{-4}	2.5×10^{-4}	12	23
	7.5×10^{-3}	5×10^{-3}	2.5×10^{-3}	6.0	11
MgSO_4	10^{-4}	2.5×10^{-5}	2.5×10^{-5}	--	27
	10^{-3}	2.5×10^{-4}	2.5×10^{-4}	19	29
	10^{-2}	2.5×10^{-3}	2.5×10^{-3}	12	17
MgCl_2	7.5×10^{-5}	2.5×10^{-5}	5×10^{-5}	--	27
	2.2×10^{-4}	7.5×10^{-5}	1.5×10^{-4}	--	26
	7.5×10^{-4}	2.5×10^{-4}	5×10^{-4}	15	19
	7.5×10^{-3}	2.5×10^{-3}	5×10^{-3}	12	11
CaCl_2	7.5×10^{-5}	2.5×10^{-5}	5×10^{-5}	16	32

weight range. For flocculation by low molecular weight polymers, the OFD's are lower with divalent cations than with monovalent cations. With the 5.5 million molecular weight polymer, OFD's are greater with divalent cations than with monovalent cations.

Three distinct phenomena occur which have different effects on flocculation: (1) divalent cations adsorb in the Stern layer of the free surfaces to reduce the Stern potential, thus reducing the OFD; (2) the electrical double layer is compressed more by divalent cations than by monovalent cations at equal concentrations, thus reducing the OFD to a greater degree; (3) divalent cations adsorbed in the free surface Stern layer interfere with polymer adsorption, thus increasing the OFD.

Polymer adsorption interference by divalent cations decreases with decreasing molecular weight since small polymer molecules can fit in between the adsorbed divalent cations. For example, silica particles in a 10^{-3} molar ionic strength solution have one hydroxide group per 700 \AA^2 (see Table V-4). Assuming that the charge density of the divalent cations in the Stern layer is one-fourth the charge density of the hydroxide groups, there is one divalent ion per $5,600 \text{ \AA}^2$. Assuming an adsorption area of 40 \AA^2 per monomer segment, molecules with degrees of polymerization of 25,600 and 28 require $1,020,000 \text{ \AA}^2$ and $1,120 \text{ \AA}^2$, respectively. While the small, low molecular weight molecules can adsorb in between the divalent ions, each of the large, high molecular weight molecules covers an area occupied by more than 100 divalent cations.

In low molecular weight polymer systems replacement of monovalent cations by divalent cations reduces the OFD's because the electrical double layer is compressed and the Stern potential is reduced; polymer adsorption is unaffected. In high molecular weight systems, where the decrease in polymer adsorption outweighs the effects of double layer compression and Stern layer reduction, the OFD's are increased.

2. Polystyrene Latex (PSL):

a. pH Effects. At pH's greater than three the surface charge of the PSL particles is independent of pH. The sulfonate groups are completely ionized. The electrophoretic mobility is constant for pH's greater than three. In Fig. VII-7 the OFD variation with pH is shown for PSL suspensions flocculated by high molecular weight polyelectrolyte in intermediate ionic strength solutions.

The OFD increase with increasing pH indicates that the stability of the PSL is greater at higher pH's or that the poly (DMVPB) is a more efficient flocculating agent at lower pH's. Watillon and Petit⁷⁶ found that the salt concentration required to coagulate sulfonated PSL particles increases with increasing pH. Their data seems to indicate that PSL stability increases with increasing pH.

In the majority of the PSL systems studied here NaCl was used to adjust the ionic strength and the pH was constant at 6.0.

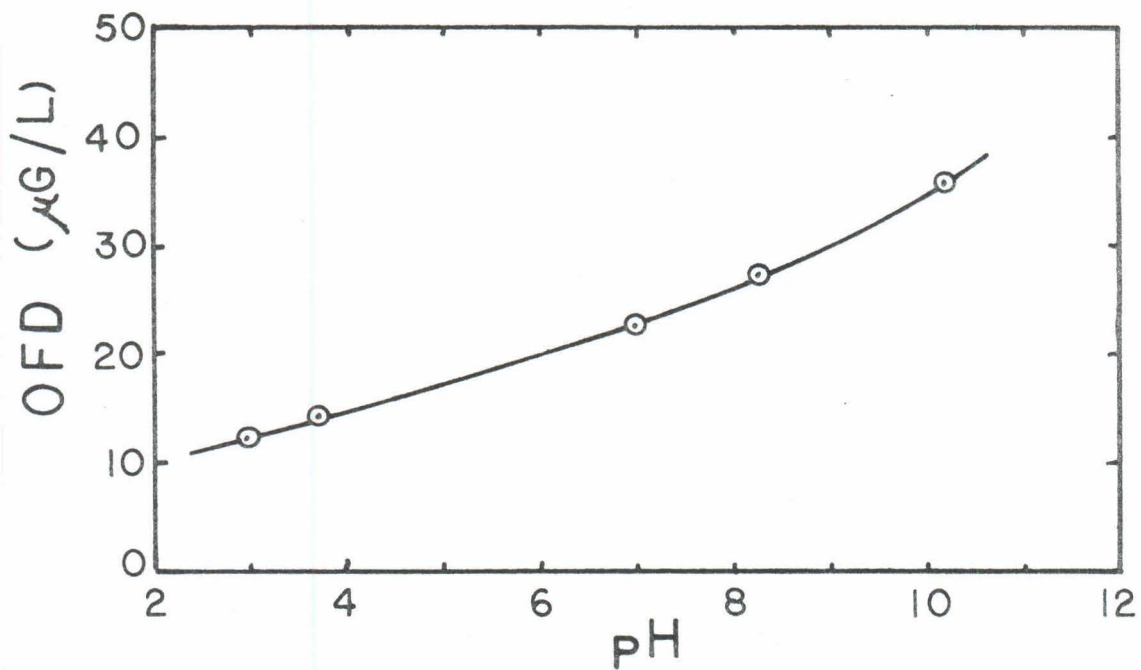


Fig. VII-7. Effect of pH on the OFD's of 20 mg/1 PSL suspensions in 10^{-3} molar ionic strength solutions. $M = 5.5 \times 10^6$.

b. Effects of NaCl Concentration and Polymer Molecular Weight. The OFD exhibits the same general dependencies on NaCl concentration and the polymer molecular weight for the PSL particles as it does for the Min-U-Sil systems. In Figs. VII-8 and VII-9 the effects of NaCl concentration on the residual turbidity-polymer dose relationships are shown for flocculation by polymers having molecular weights of 6×10^3 and 5.5×10^6 , respectively. With increasing salt concentration the OFD and the absolute minimum turbidity both decrease while the width of the destabilization zone increases.

The variations of the OFD's with salt concentration and polymer molecular weight are summarized in Fig. VII-10. At low salt concentration the effect of molecular weight is large, while at high salt concentrations the effect of molecular weight is less.

It is interesting to note that the OFD has the same general dependency on polymer molecular weight and solution ionic strength for the two vastly different PSL and Min-U-Sil particle systems.

B. Electrophoretic Mobility Data

1. Zero Mobility. The majority of the electrophoretic mobility data obtained in this investigation is limited to qualitative interpretation because the position of the shear plane is unknown. It was originally planned to quantitatively analyze the adsorption data at zero mobility by the techniques of Ottewill et al.⁴⁵ For systems in which the particle charge can be reversed it can usually be assumed that at zero mobility the Stern potential is also zero. While this equality assumes nothing about the position of the Stern

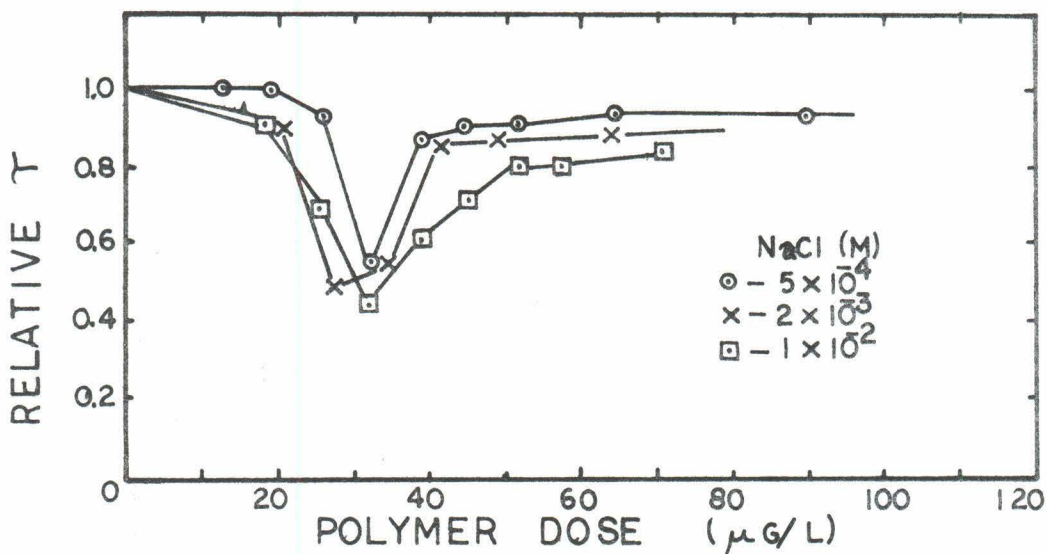


Fig. VII-8. Effect of NaCl concentration on flocculation of 20 mg/l PSL suspensions. pH = 6.0 and $M = 6 \times 10^3$.

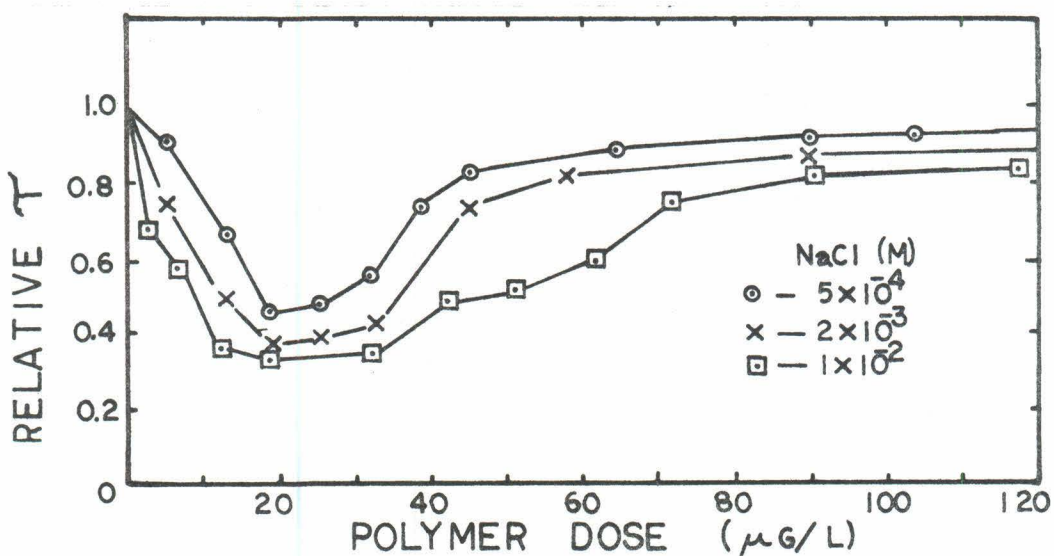


Fig. VII-9. Effect of NaCl concentration on flocculation of 20 mg/l PSL suspensions. pH = 6.0 and $M = 5.5 \times 10^5$.

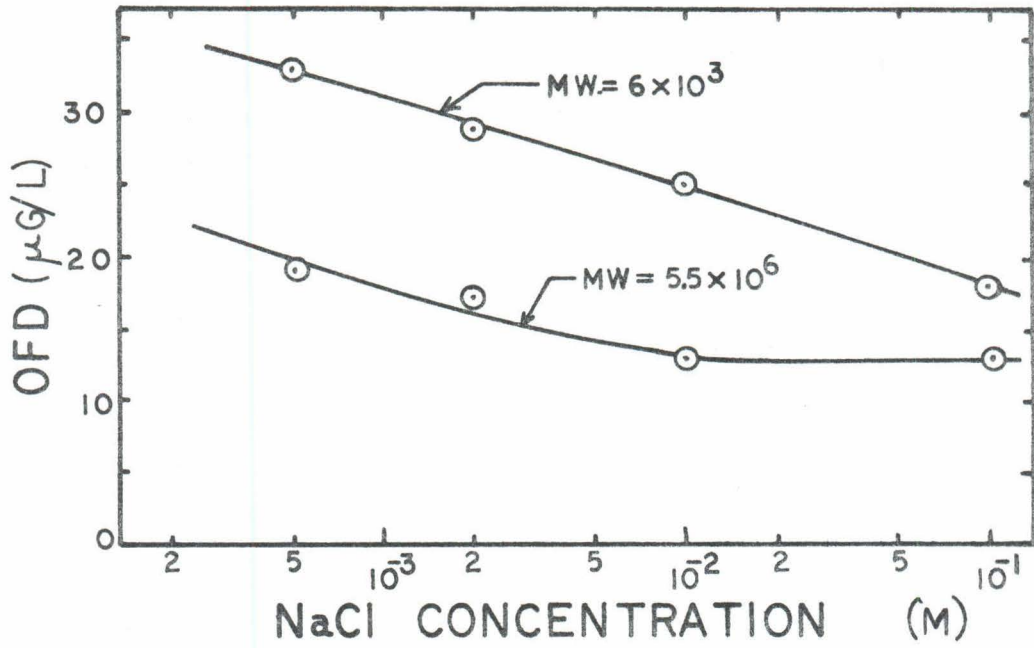


Fig. VII-10. Variation of OFD with polymer molecular weight and NaCl concentration. System: pH = 6.0 and PSL at 20 mg/l.

plane, it is valid only for systems in which the charge reversal is brought about by adsorption of potential determining ions or other ions which can be distributed over the surface uniformly. In the case of polyelectrolyte adsorption charged-patches occur and at zero mobility the surfaces are covered by two types of oppositely charged electrical double layers. Although the sum of the charges within the shear plane is zero at zero mobility, quantitative analysis is impossible without making some assumptions about the position of the shear plane.

Fig. VII-11 illustrates the observed relationship between particle mobility and polymer adsorption for Min-U-Sil and PSL particles at low ionic strengths. In both systems, at any given value of polymer adsorption, particle mobility is affected more by high molecular weight polymers than by low molecular weight polymers.

Values of adsorption at zero mobility are presented in Table VII-2 for polymers of various molecular weights at several different salt concentrations. There are definite differences in the behavior of the Min-U-Sil and PSL systems. Fig. VII-12 summarizes the general dependencies of polymer adsorption at zero mobility on solution ionic strength and polymer molecular weight. The observed decrease in zero-mobility-adsorption with increasing ionic strength in the constant surface potential Min-U-Sil system is unexpected since the Min-U-Sil surface charge increases at higher ionic strengths. This unexpected result might be due to the porous nature of the Min-U-Sil surfaces.

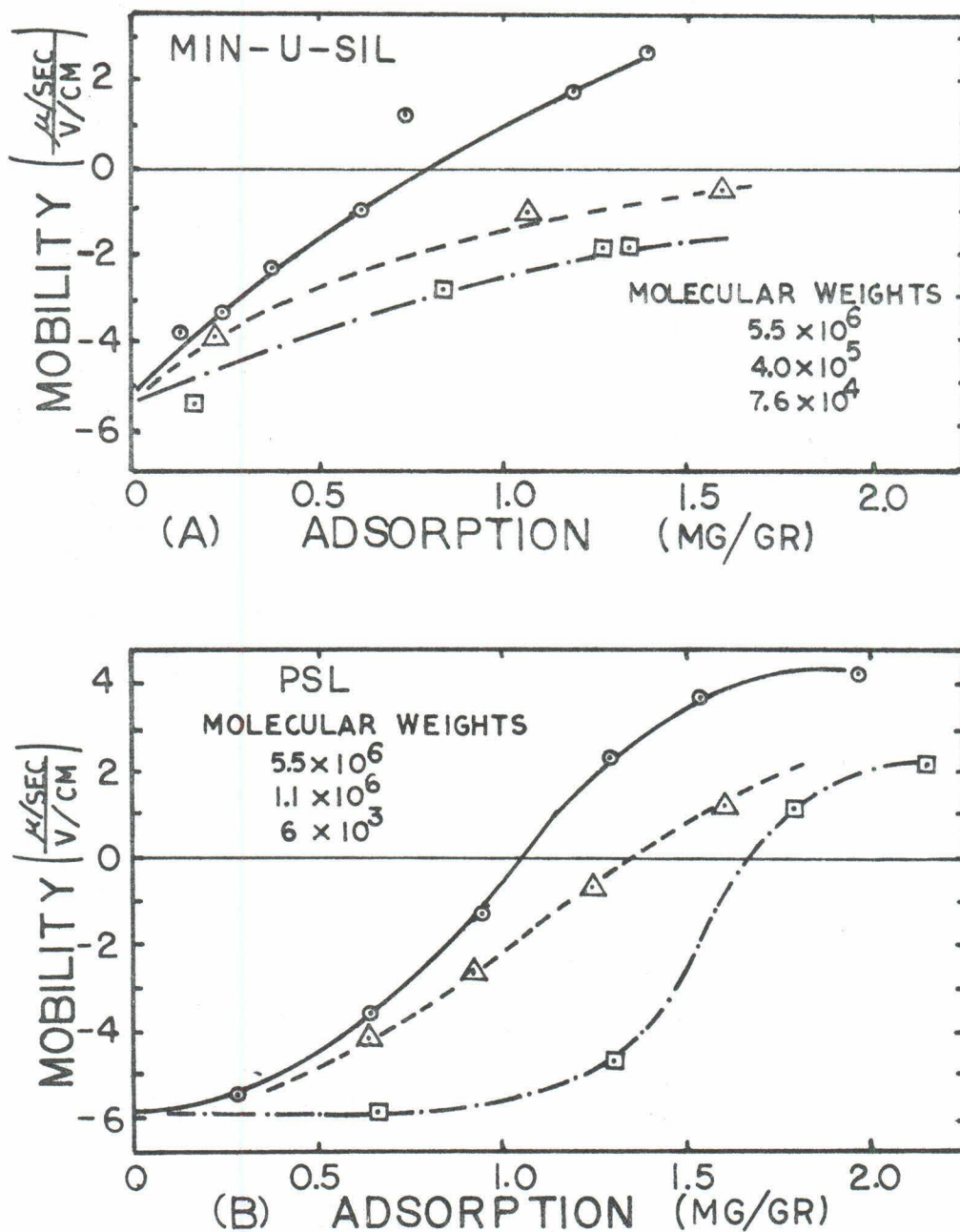


Fig. VII-11. Electrophoretic mobility versus polymer adsorption. (A) 50 mg/l Min-U-Sil in 5×10^{-5} molar NaHCO_3 . (B) 20 mg/l PSL in 5×10^{-4} molar NaCl .

Table VII-2. Values of polymer adsorption (mg/gr) at zero particle mobility.

(a) Min-U-Sil Particles, pH = 8.3

Molecular weight	NaHCO ₃ Concentration (moles/liter)		
	5x10 ⁻⁵	10 ⁻³	10 ⁻²
5.5x10 ⁶	0.80	0.80	0.72
1.1x10 ⁶	--	1.04	--
4.0x10 ⁵	--	1.14	--
7.6x10 ⁴	1.30	1.36	0.86
6x10 ³	2.12	2.20	1.64

(b) PSL Particles, pH = 6.0

Molecular weight	NaCl Concentration (moles/liter)			
	5x10 ⁻⁴	10 ⁻³	10 ⁻²	10 ⁻¹
5.5x10 ⁶	1.10	1.10	1.44	1.76
1.1x10 ⁶	1.36	--	--	--
7.6x10 ⁴	1.42	--	--	--
6.10 ³	1.76	1.80	1.70	1.76

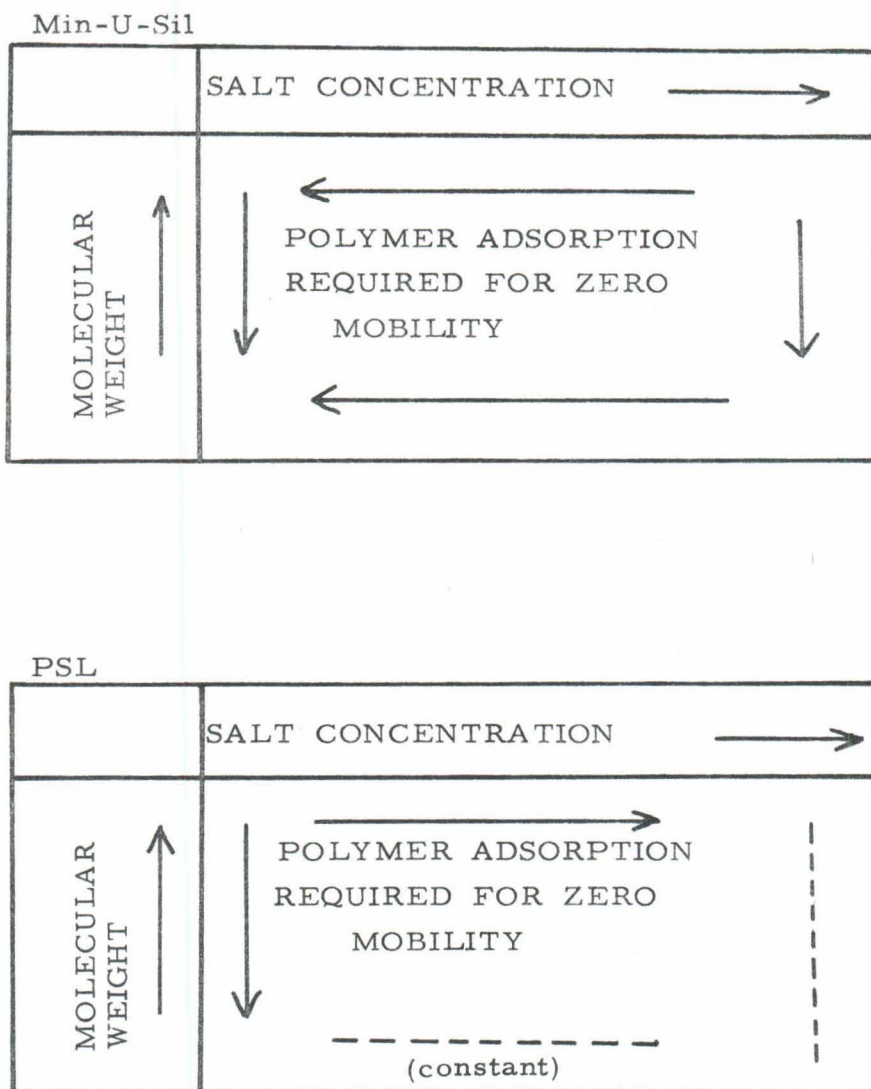


Fig. VII-12. Illustration of general trends in data of Table VII-3 showing the effects of salt concentration and polymer molecular weight on the polymer adsorption required for zero mobility.

The data in Fig. VII-11 and Table VII-2 can be interpreted in terms of the following processes which are consistent with the electrostatic patch model. The charges within the shear plane are due to the surface charge of the particles (Q_s), the Stern layer of the free surfaces (Q_{ss}), the adsorbed polyelectrolyte (Q_p), the Stern layer of the adsorbed polyelectrolyte (Q_{ps}), and the diffuse double layer around both free surface and adsorbed polyelectrolyte (Q_d).

That is

$$Q_{\text{total}} = Q_s + Q_{ss} + Q_p + Q_{ps} + Q_d \quad \text{VII-1}$$

(+or-) (-) (+) (+) (-) (+&-)

The symbols indicate the signs of the charges in the systems investigated. At zero particle mobility Q_{total} is zero.

For any given amount of adsorbed polyelectrolyte, Q_s and Q_p are independent of molecular weight with constant ionic conditions. Q_{ss} and Q_{ps} , on the other hand, are affected by polymer molecular weight.

Q_{ss} is directly proportional to the area of the free surfaces. Since the polymer density of an adsorbed patch increases with increasing molecular weight*, at constant adsorption Q_{ss} increases with increasing molecular weight.

* The area per patch is proportional to the 2/3 power of the molecular weight (see Eq. III-1). The polymer density is the ratio of the weight of polymer per patch to the area of the patch. Since the weight of polymer per patch is directly proportional to the molecular weight, the polymer density is proportional to the 1/3 power of the molecular weight.

Q_{ps} is equal to the product of the total area of polymer patches and the charge density of the polymer Stern layer. The increase in the polymer density of the adsorbed patches with increasing molecular weight is accompanied by an increase in the patch charge density which causes a relatively larger increase in the charge density of the polymer Stern layer. With increasing molecular weight the net effect of the decreasing area and increasing charge density of the polymer Stern layer is an increase in Q_{ps} .

For a given increase in molecular weight the increase in Q_{ps} is less than the increase in Q_{ss} . In a system of negatively charged particles and cationic polyelectrolyte the overall effect of increasing molecular weight is an increase in the number of cations within the shear plane. Higher molecular weight polyelectrolytes are, therefore, more efficient in reversing particle mobility.

2. OFD Mobility. The electrostatic patch model predicts that the amount of adsorbed polymer required for flocculation decreases with both increasing ionic strength and increasing molecular weight. The OFD mobility of originally negatively charged particles should therefore decrease with increasing ionic strength and molecular weight since less polymer is required for flocculation.

Values of particle mobilities at optimum flocculation conditions for polymers of various molecular weights at several ionic strengths are presented in Table VII-3. Two general trends are

Table VII-3. Electrophoretic mobility values ($\frac{\mu/\text{sec}}{v/\text{cm}}$) at optimum flocculation dose (OFD).

(a) Min-U-Sil Particles, pH = 8.3

Molecular weight	NaHCO ₃ Concentration (moles/liter)		
	5x10 ⁻⁵	10 ⁻³	10 ⁻²
5.5x10 ⁶	-3.6	-4.8	-3.5
4x10 ⁵	-3.0	-3.7	--
6x10 ³	-2.8	-3.8	-3.8

(b) PSL Particles, pH = 6.0

Molecular weight	NaCl Concentration (moles/liter)			
	Zero	5x10 ⁻⁴	2x10 ⁻³	10 ⁻²
5.5x10 ⁶	-1.2	-2.3	-3.0	-4.8
1.1x10 ⁶	-0.8	-2.5	--	--
7.8x10 ⁵	-0.4	--	--	--
4.0x10 ⁵	0	--	--	--
7.6x10 ⁴	+0.4	-2.2	--	--
6x10 ³	+0.6	-2.0	-2.8	-3.0

observed: (i) decreasing OFD mobility with increasing molecular weight; (ii) decreasing OFD mobility with increasing ionic strength. Both of these trends are in agreement with the predictions of the electrostatic patch model.

C. Adsorption Data

1. Saturation Adsorption. The values of polymer adsorption at saturation were all determined after one hour of mixing. See procedure in Sect. IV-E. The saturation values are not necessarily equilibrium values since, as shown in Sect. VI-B2, attainment of equilibrium may require several days. With the Min-U-Sil system there is additional uncertainty because of the porous nature of the surfaces. It is conceivable that the low molecular weight polymer molecules might be able to enter small pores which are inaccessible to high molecular weight molecules. In spite of the above complications the adsorption data are useful in qualitatively describing the effects of salt concentration and polymer molecular weight on the density of polymer molecules adsorbed to particles.

a. Ionic Strength Effects. In Table VII-4 values of adsorption at saturation and the areas per polymer segment are tabulated for high and low molecular weight polymers at various ionic strengths. The two sets of areas per adsorbed polymer segment for the Min-U-Sil particles are based on the two values of specific area presented in Sect. IV-C. The $6.9 \text{ m}^2/\text{gr}$ specific surface area value, measured by BET nitrogen adsorption, includes small pores which are unavailable to relatively large

Table VII-4. Saturation values of polymer adsorption and resulting areas per adsorbed segment.

(a) Min-U-Sil Particles pH = 8.3

NaHCO ₃ moles per liter	MOLECULAR WEIGHT					
	6x10 ³			5.5x10 ⁶		
	Sat. Ads. (mg/gr)	area/segment (Å ²)		Sat. Ads. mg/gr)	area/segment (Å ²)	
		SA = 6.9m ² /gr	SA = 2.1m ² /gr		SA = 6.9m ² /gr	SA = 2.1m ² /gr
5x10 ⁻⁵	3.0	81	25	1.4	173	52
10 ⁻³	4.6	53	16	2.1	118	36
10 ⁻²	6.4	38	11	2.8	86	26

(b) PSL Particles pH = 6.0

NaCl moles per liter	MOLECULAR WEIGHT			
	6x10 ³		5.5x10 ⁶	
	Sat. Ads. (mg/gr)	Area/ Seg. (Å ²)	Sat. Ads. (mg/gr)	Area/ Seg. (Å ²)
5x10 ⁻⁴	2.9	52	2.1	73
2x10 ⁻³	2.8	55	2.1	73
10 ⁻²	3.0	52	3.2	48

polymer molecules. The $2.1 \text{ m}^2/\text{gr}$ value, measured by an air permeability method, is the geometric surface area.

The true area per adsorbed polymer segment is between the two tabulated values which are the upper and lower limits for areas per segment. Some of the pore surfaces are definitely available to the low molecular weight polymer molecules since the 11 \AA^2 per pyridinium segment is too small. Shyluk⁶⁰ gives 32 \AA^2 as the area per pyridinium segment based on a vertically oriented Fischer-Hirschfelder model. The tabulated values indicate that the entire particle surface is not covered by polymer at saturation.

The large increase in saturation adsorption with increasing ionic strength in the Min-U-Sil system is attributed to the following phenomena:

- (ii) greater flexibility of polymers at higher ionic strengths which enables polymers to enter small pores.
- (ii) more compact adsorbed configurations at high ionic strengths which permit greater amounts of polymer to adsorb per unit surface area.
- (iii) lower degree of polyelectrolyte dissociation at high ionic strengths which enables more polyelectrolyte to adsorb before the surface becomes positively charged to the point where additional adsorption is prevented. The degree of

dissociation is reduced at high ionic strengths by adsorption of counterions into the Stern layer of the polyelectrolyte.

- (iv) increased particle surface charge at high ionic strengths for constant potential systems which enables adsorption of more oppositely charged polyelectrolyte.

The data in Table VII-4 agree with that of Peyser and Ullman⁵² who observed an increase in Poly-4-vinylpyridinium chloride adsorption onto glass with increasing ionic strength. These authors attributed the increase to coiling of the polyelectrolytes at higher ionic strengths.

The increase in saturation adsorption with increasing ionic strength for the PSL system is not as great as that for the Min-U-Sil system. The increase is smaller because the PSL system is influenced by only two of the four phenomena listed above: (ii) and (iii). The PSL particles are not porous, so that (i) does not come into play. The PSL particles have constant-charge surfaces rather than constant-potential surfaces and thus (iv) is not a consideration.

b. Molecular Weight Effects. With the Min-U-Sil system the increase in saturation adsorption with decreasing molecular weight is due to increased availability of surface area for the lower molecular weight polymer molecules. The large

size of the high molecular weight polymers excludes them from the surface pores.

The observed variation in saturation adsorption with molecular weight can also be a consequence of the relatively slow adsorption rate of the high molecular weight polymers. The process of adsorbed polymer reorientation is probably the rate limiting step. Reorientation of large molecules requires more time than reorientation of small molecules.

The absence of pores on the PSL particle surface causes the variation of saturation adsorption with molecular weight to be relatively less than in the Min-U-Sil system.

With the Min-U-Sil system it is not possible to determine the configuration of adsorbed polymer molecules by application of the relationship presented as Eq. II-7* since this relationship is limited to non-porous systems. Analyzing the PSL data in terms of Eq. II-7 yields the following β values: $\beta = 0$ in 10^{-2} M NaCl, $\beta = -0.05$ in 2×10^{-3} M NaCl, and $\beta = -0.07$ in 5×10^{-4} M NaCl. Since it is impossible for β to have negative values it is concluded that adsorption equilibrium does not exist after one hour of mixing in the PSL system. The true value of β is probably zero.

β is also zero for the adsorption of poly (DMVPB) to the non-porous silica glass surfaces. See Sect. VI-B1.

* $A_s = K M^\beta$ where A_s is polymer adsorption at saturation, K and β are constants, and M is the molecular weight.

Two types of adsorbed polymer configurations are possible in systems having zero β values: completely flat configurations and configurations with a constant fraction of segments in loops. Both of these configurations are compatible with the electrostatic patch model if the size of the loops is small.

2. Adsorption at Optimum Flocculation Conditions.

Analysis of polymer adsorption data for the OFD conditions has two main objectives, determination of the flocculation mechanism and determination of the residual polymer concentrations in solution. The residual polymer concentration is of interest because polyelectrolytes are used as flocculating agents in potable water supplies.

a. Flocculation Mechanism. In Table VII-5 the following parameters are tabulated for the Min-U-Sil and PSL systems: polymer adsorption at the OFD, the ratio (OFD adsorption/saturation adsorption), and the percent or degree of surface coverage at the OFD. The degrees of surface coverage are based on an area of 40 \AA^2 per polymer segment. This larger area per polymer segment was used rather than the value given by Shyluk⁶⁰ in order to account for steric hinderance. Again, as in Table VII-4, two sets of surface coverage values are listed for the Min-U-Sil system in light of the two different specific surface area values.

Several investigators have equated the (OFD/Sat.) ratio to the degree of surface coverage when describing polymer floccula-

Table VII-5 Values of polymer adsorption and degree surface coverage at OFD.
Area per segment = 40\AA^2 .

(a) Min-U-Sil Particles pH = 8.3

NaHCO ₃ (moles per liter)	MOLECULAR WEIGHT							
	6x10 ³				5.5x10 ⁶			
	Ads.@ OFD (mg/gr)	OFD Ads. Sat. Ads.	Surface Coverage SA = 2.1 m ² /gr	SA = 2 /gr 6.9m ² /gr	Ads.@ OFD (mg/gr)	OFD Ads. Sat. Ads.	Surface Coverage SA = 2.1m ² /gr	SA = 2 /gr 6.9m ² /gr
5x10 ⁻⁵	0.92	31%	49%	15%	0.36%	44%	19%	5.8%
10 ⁻³	0.64	14%	35%	10%	0.24%	11%	13%	3.9%
10 ⁻²	0.42	6.5%	23%	7.1%	0.24%	8.6%	19%	3.9%

(b) PSL Particles pH = 6.0

NaCl (Moles per liter)	MOLECULAR WEIGHT								
	6x10 ³				5.5x10 ⁶				
	Ads.@ OFD (mg/gr)	OFD Ads. Sat. Ads.	Surface Coverage	Ads.@ OFD (mg/gr)	OFD Ads. Sat. Ads.	Surface Coverage	Ads.@ OFD (mg/gr)	OFD Ads. Sat. Ads.	Surface Coverage
5x10 ⁻⁴	1.66	56%	43%	0.96	46%	25%	0.96	46%	25%
2x10 ⁻³	1.46	52%	37%	1.00	48%	26%	1.00	48%	26%
10 ⁻²	1.26	42%	32%	0.66	21%	17%	0.66	21%	17%

tion. This equality is true only when the surfaces are completely covered by polymer at saturation conditions. It should also be noted that neither of these parameters is directly related to the charge density of the particle surface.

Fig. VII-13, which includes the data of Table VII-5, illustrates the effect of molecular weight on the OFD degree of surface coverage for Min-U-Sil particles in 5×10^{-5} M and 10^{-2} M NaHCO_3 . The coordinate scales allow comparison of the experimental data with the theoretical results of the electrostatic patch model presented in Fig. III-8. This comparison assumes that the degree of surface coverage at the OFD is equal to the degree of surface coverage when the sum of the electrostatic interactions between two spherical particles is zero. That is, when the F parameter of the electrostatic patch model* is zero.

The two surface coverage scales in Fig. VII-13 are based on the Min-U-Sil surface areas determined by two different methods. In light of the assumed model surface conditions and the low (OFD/SAT.) ratios, it is more accurate to compare the surface coverage based on the geometric surface area with the theoretical results.

The agreement between the experimental data and the theoretical results is quite good, considering the shape differences between the Min-U-Sil particles and the spherical model. The irregular shapes and the polydispersity of the size distribution

* See Chapter III for complete description of the electrostatic patch model.

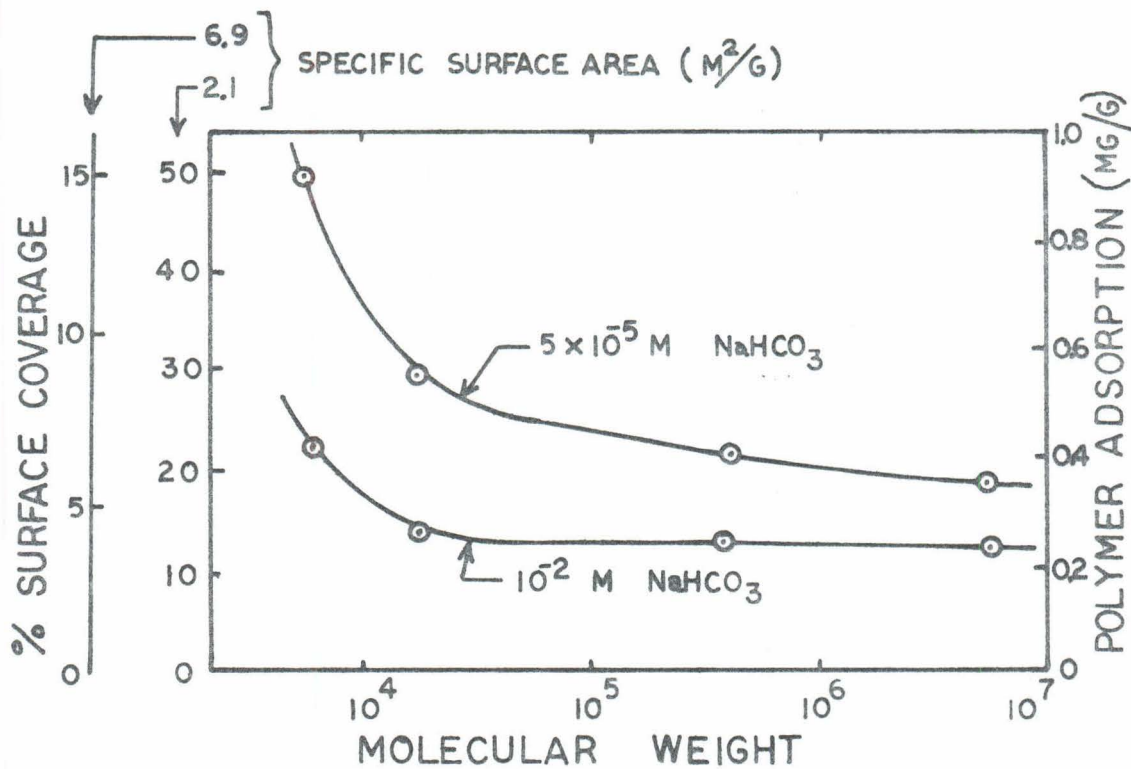


Fig. VII-13. Effect of molecular weight on polymer adsorption at the OFD for Min-U-Sil suspensions. Particle surface coverage values based on two specific surface area values of Min-U-Sil are illustrated.

cause the Min-U-Sil system to have greater degrees of curvature than the corresponding monodispersed, spherical system of equivalent particle volume. With increasing degrees of curvature the interactions between two particles are more localized since smaller areas of surface are separated by $2\kappa^{-1}$. No attempt was made in the theoretical analysis to account for the variation of the Min-U-Sil surface charge with ionic strength.

A comparison of the PSL experimental OFD surface coverage data (points) and the theoretical patch model results (solid lines) is made in Fig. VII-14. The agreement with the theoretical results is better with the PSL system than with the Min-U-Sil system. This is not surprising since the PSL system consists of non-porous, monodispersed spherical particles with constant surface charge; these are the assumed conditions of the electrostatic patch model.

b. Residual Polyelectrolyte Concentrations. Typical residual polymer concentration data from the systems investigated are compiled in Table VII-6. The residual or free polymer concentrations are tabulated for polymer doses equal to the OFD and equal to twice the OFD (i. e., $2 \times$ OFD). Investigation of residual concentrations at the OFD is not of primary interest since the operational polymer dose is usually larger. See Fig. VII-1.

Although no general trends other than the increase in residual polymer with increasing polymer dose are seen in the data of Table VII-6, it can be concluded that between 5 and 50 percent of the polymer remains unadsorbed in systems with conditions similar to those of industrial flocculation processes.

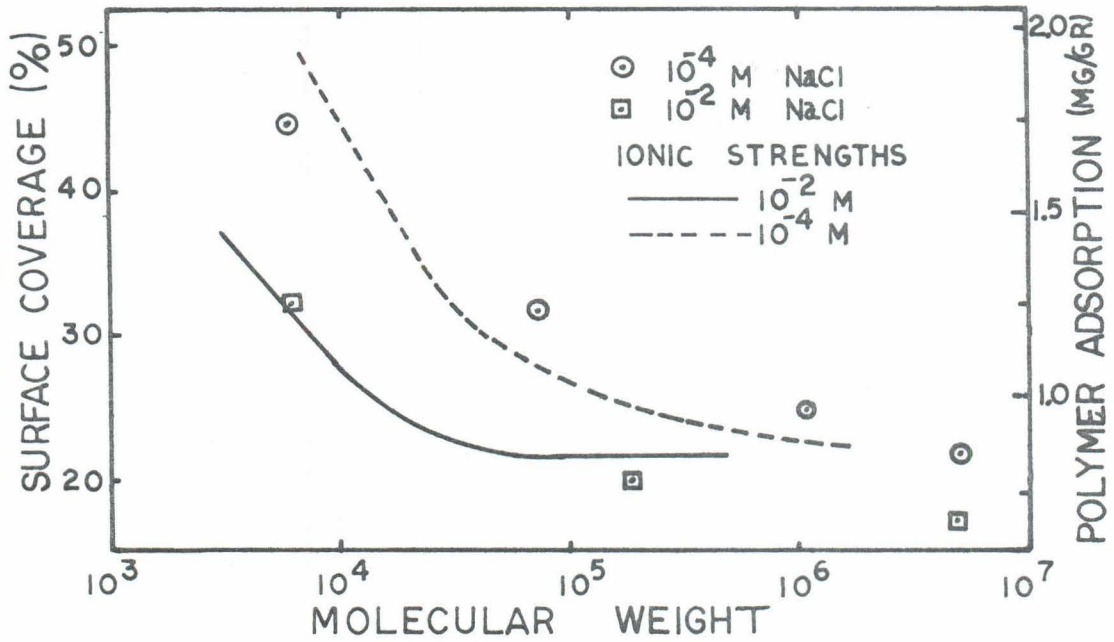


Fig. VII-14. Comparison of PSL experimental OFD surface coverage data (points) with theoretical patch model results (solid and dashed lines).

Table VII-6 Residual polymer in solution at OFD and at 2 x OFD.

System	Particle conc. (mg/l)	Salt	Salt conc. (molar)	Mol. weight	OFD ($\mu\text{g}/\text{l}$)	RESIDUAL POLYMER			
						OFD		2 x OFD	
						Conc. ($\mu\text{g}/\text{l}$)	percent free	Conc. ($\mu\text{g}/\text{l}$)	percent free
PSL	20	NaCl	5×10^{-4}	5.5×10^6	20	0.7	3.5%	8.4	21%
PSL	20	NaCl	5×10^{-4}	6×10^3	39	2.9	7.4	22	28
PSL	20	NaCl	5×10^{-4}	7.8×10^5	29	3.3	11	25	43
PSL	20	NaCl	10^{-1}	5.5×10^6	14	1.3	9.3	2.1	8
PSL	40	NaCl	5×10^{-4}	5.5×10^6	36	0.9	2.5	9.0	12
Silica	50	NaHCO_3	10^{-3}	5.5×10^6	14	2.2	16	3.2	12
Silica	50	NaHCO_3	10^{-3}	6×10^3	35	2.0	5.7	2.6	4
Silica	50	NaCl	10^{-2}	5.5×10^6	6.6	1.5	23	2.8	14
Silica	50	NaCl	10^{-2}	6×10^3	20	3.6	18	8.0	20

Chapter VIII

SUMMARY AND CONCLUSIONS

A. Rationale of this Research

Since the turn of the century the water treatment industry has concerned itself with the removal of particulate matter from public water supplies. Historically, removal of particulate matter has been carried out for aesthetic reasons. Recent studies, however, have shown that pesticides, herbicides, radionuclides, dissolved trace metals, and other substances potentially detrimental to human health are associated with particulate matter in natural waters. Particle removal can no longer be considered simply "aesthetically desirable".

The increased need of producing particle-free waters requires that the present techniques of particle removal be improved and that new methods be developed.

B. Research Objectives

The primary purposes of this research were twofold: (i) to establish the mechanism or mechanisms by which cationic polyelectrolytes flocculate dilute suspensions of negatively charged particles, and (ii) to determine the effects of polyelectrolyte molecular weight and solution composition on the flocculation of negatively charged particles by cationic polyelectrolytes. The investigation was limited to negatively charged particles and a cationic polyelectrolyte since the majority of particles in natural waters have negative surface charges and cationic polymers can be very effective flocculants.

C. Qualitative Description of the Flocculation Process

Polyelectrolyte molecules in aqueous solution have three-dimensional ellipsoidal or rod-like configurations, the compactness of which is controlled by the solution ionic strength. When the adsorption energy is large ($2 kT$), such as for the adsorption of cationic polyions onto negatively charged surfaces, the three-dimensional configuration of the polyelectrolyte molecule simply compresses into a two-dimensional patch upon adsorption. The adsorbed polyion patch has net positive charge, a consequence of the fact that its charge density is greater than the charge density of the negative surface. The rate of this polyelectrolyte adsorption process is relatively fast in comparison to the rate of particle collisions; adsorption is essentially complete before particle aggregation commences.

The existence of like-charged diffuse electrical layers, a result of the surface charges, causes repulsive interactions (interaction energy barriers) between particles. If the magnitude of the energy barrier is great enough, collisions between particles are prevented and the colloidal system is classified as stable. Particle collisions result from particle transport due to Brownian motion and/or velocity gradients, depending on particle size.

Interaction between a positively charged polyelectrolyte patch adsorbed to one particle with the negatively charged surface of another particle causes an attractive force between the particles. The magnitude of the attractive force is a function of the number, size, and charge density of the patches, the solution composition,

the shape and size of the particles, and the separation distances between the interacting surfaces. When enough polymer molecules adsorb, the attractive forces counteract the repulsive forces and coagulation occurs.

D. Principal Results

1. Improbability of Flocculation by Polymer Bridges.

A review of the statistical mechanical models of adsorbed polymer configurations in Sect. II-D leads to the conclusion that polyelectrolyte molecules adsorb to oppositely charged surfaces without forming large loops. By making reasonable assumptions about interaction energies between surfaces and polyion segments and about polyion segment lengths, a distance of 60 \AA is determined as the maximum loop extension away from a surface.

A theoretical analysis of the distances between stable or non-coagulating particles in terms of the Derjaguin-Landau, Verwey-Overbeek theory of particle stability is contained in Sect. II-C. A "distance of closest approach" (DCA) is defined which is characteristic of the smallest distance between stable particles.

The results of the DCA and adsorbed polymer configuration analyses are combined in Sect. II-E. The DCA's of stable particles are generally much greater than 60 \AA except (i) at ionic strengths greater than 10^{-2} moles/liter, and (ii) for surface potentials values lower than the values of most particles in natural waters.

It is thus very improbable that flocculation of charged

particles by polyelectrolytes of opposite charge occurs by the commonly accepted polymer-bridging mechanism.

2. Electrostatic Patch Model for Flocculation. An electrostatic flocculation mechanism based on the formation of positively charged polymer patches on the negative particle surfaces is presented in Chapter III. The effects of polyelectrolyte molecular weight and solution ionic strength on the amount of polymer required for flocculation are determined for the model by a computer program which calculates particle interaction energies. The agreement between experimental data (Chapter VII) and the theoretical predictions of the electrostatic patch model (Chapter III) is good.

3. Kinetics. The kinetics of polymer adsorption and particle aggregation are investigated theoretically and experimentally in Chapter VI. A theoretical analysis based on Smoluchowski's kinetic theories indicates that polymer adsorption is fast in comparison to the rate of particle aggregation in systems investigated, i. e., polyelectrolyte molecules and suspended particles of opposite charge. This theoretical analysis is experimentally verified.

In the non-aggregating poly(DMVPB)-pyrex glass system ultimate polyelectrolyte adsorption is dependent on the salt concentration of the solvent and independent of polymer molecular weight. The initial rate of polymer adsorption is, however, very dependent on molecular weight.

4. Experimental Effects of Polymer Molecular Weight and Solution Ionic Strength on Flocculation. The same dependency of the polymer dose at optimum flocculation (OFD) on polyelectrolyte molecular weight and solution ionic strength is found in both systems investigated (PSL and Min-U-Sil particles). Experimental data is presented in Chapter VII.

It was found that the OFD decreases with increasing molecular weight until a certain molecular weight value is reached; for molecular weights greater than this value ("limiting molecular weight") the OFD is independent of molecular weight. The value of the "limiting molecular weight" decreases with increasing ionic strength. In general, at high ionic strengths the OFD is independent of molecular weight while at low ionic strengths the OFD decreases with increasing molecular weight.

E. Applications

1. Treatment Plant Operation. In general, polymer costs and handling difficulties at the treatment plant (preparation of polymer feed solutions, pumping head losses and mixing of polymer feed solution with raw water) increase with increasing molecular weight. The results of the present research indicate that all polymers with molecular weights greater than the "limiting molecular weight" flocculate particle suspensions at the same minimum dose. Greater quantities of polymers having molecular weights lower than the "limiting molecular weight" are required to achieve this same degree of flocculation. In view of these dependencies of polymer cost and required flocculation dose on polymer molecular weight

the most economical polymer probably has a molecular weight on the order of the "limiting molecular weight".

It is possible for a polymer with a molecular weight lower than the "limiting molecular weight" to be economical if the greater dose requirement is outweighed by lower polymer costs per unit weight.

2. Polymer Manufactures. The present research indicates that there is a maximum desirable molecular weight (limiting molecular weight) for polyelectrolyte flocculants. The value of the "limiting molecular weight" depends on polyelectrolyte composition, the nature of the particulate matter, and the water composition.

The "limiting molecular weight" for waters with high salt concentrations is relatively low in comparison to the "limiting molecular weight" for waters with low salt concentrations. It therefore follows that low molecular weight polyelectrolyte flocculants are as effective as high molecular weight polyelectrolytes in many industrial and domestic wastewaters and some raw waters characterized by high salt concentrations. High molecular weight polyelectrolytes are more effective than low molecular weight polyelectrolytes in waters with low salt concentrations since the "limiting molecular weight" is greater.

The above facts should be considered in the development of polymeric flocculants.

F. Suggestions for Further Research

The present research is limited to certain types of particles and polyelectrolytes. There is a need to investigate the influence of the following parameters on the flocculation dose-molecular weight-solution composition relationships:

- (i) polymer composition, charge density and structure
- (ii) particle surface charge density and particle size
- (iii) solution temperature and composition, with special emphasis on the organic compounds present in wastewaters and the ions which interact specifically with particles and/or polymers
- (iv) mixing or agitation period and intensity

Additional verification of the electrostatic patch model should be possible by determining particle-particle collision efficiency factors from measurements of flocculation kinetics. According to the electrostatic patch model, the collision efficiency factor is that fraction of the total number of colliding particles which have net attractive orientations.

Further development and refinement of the electrostatic patch model is needed. An analysis of the interactions between the charged patches of two approaching particles based on diffuse double layer interactions instead of simple Coulombic interactions should be made.

The use of polymers to remove particulate matter in sand filters without a separate coagulation operation has great potential for waters with low concentrations of particles. The methods and techniques of polymer characterization and polymer adsorption used

in this research would be useful to determine the mechanism or mechanisms by which polymers act as filter aids.

APPENDICES

APPENDIX 1

Relationships Used to Calculate Electrical Double
Layers Properties According to Stern⁶⁷

n = ion concentration in number of ions/cm³

M_s = molecular weight of solvent

Other symbols defined on pages 187 and 188.

$$(i) \quad \sigma = \sigma_1 + \sigma_2$$

$$(ii) \quad \sigma = \frac{\epsilon'}{4\pi\delta} [\psi_0 - \psi_\delta]$$

$$(iii) \quad \sigma_2 = \frac{2n\epsilon kT}{\pi} \sinh\left[\frac{ze\psi_\delta}{2kT}\right]$$

$$(iv) \quad \sigma_1 = \frac{N_1 ze}{1 + \frac{N}{M_s h}} \exp\left[\frac{ze\psi_s + \phi}{kT}\right]$$

APPENDIX 2

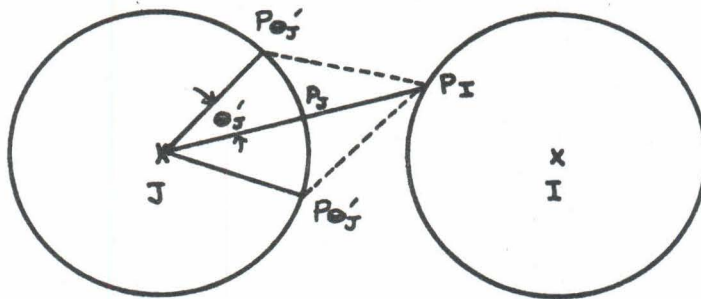
Additional Details of the Electrostatic Patch Model

The general approach used to evaluate the total interaction force between two spheres

$$F = \sum_I \sum_J \frac{S(a,b) S(c,d)}{[X(a,b:c,d)]^2} \quad \text{for } X(a,b:c,d) < d_{\max}. \quad (\text{III-4})$$

is described most easily by first examining a two-dimensional model.

Two-Dimensional Model



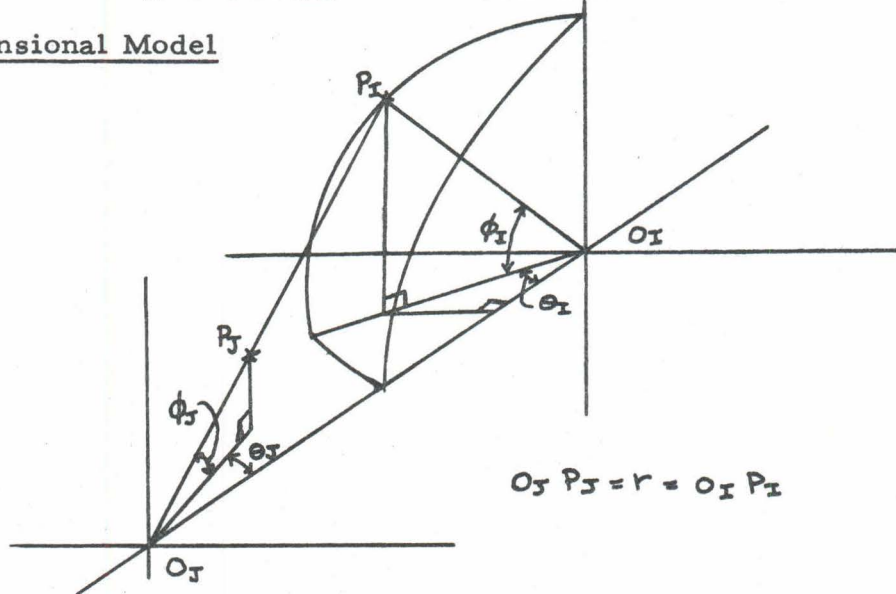
The force between a charged patch (P_I) on I and the closest patch (P_J) on J is first evaluated by the relationship

$$F(I,J) = \frac{S(P_I) S(P_J)}{D^2}$$

where $S(P_I)$ and $S(P_J)$ are the charges of the P_I and P_J patches, respectively, and D is the distance between P_I and

P_J . The forces between P_I and the patches (P_{O_J}) adjacent to P_J are then considered by varying θ'_J . θ'_J is increased in one-quarter degree increments until the distance $P_{O_J} - P_I$ is greater than d_{MAX} (d_{MAX} is defined and described in Section III-B2). All patches on I having $D < d_{MAX}$ are considered.

Three-Dimensional Model



The centers of two spheres with radii r are separated by a distance of $2r + S$. From any point P_I on the I sphere defined by the spherical coordinates (θ, ϕ, r) the shortest distance to the surface of the second sphere D is along the line which passes through the center of the J sphere. The equation for D , ($D = P_I P_J$) is

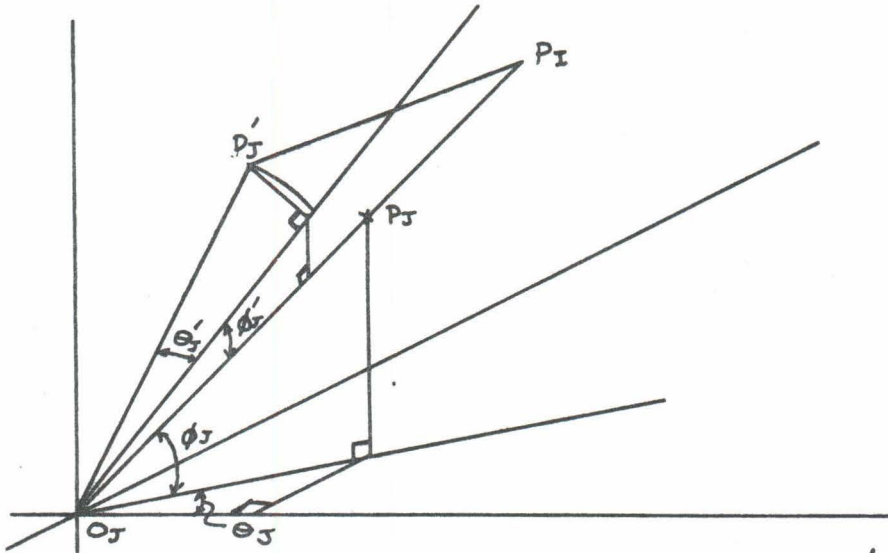
$$D = [r^2(5 - 4 \cos \phi_I \sin \theta_I) + 2rS(2 - \cos \phi_I \cos \theta_I) + S^2]^{1/2} - r$$

$$D = T - r$$

where T is the square root of the bracketed quantity and is equal to $P_I Q_J$. The angles Θ_J and ϕ_J are

$$\Theta_J = \text{Tan}^{-1} \left[\frac{r \cos \phi_I \sin \Theta_I}{r(2 - \cos \phi_I \cos \Theta_I) + X} \right]$$

$$\phi_J = \text{Tan}^{-1} \left\{ \left[T^2 + r^2 (\cos^2 \phi_I - 1) \right]^{1/2} [r \sin \phi_I] \right\}.$$



The patches around P_J are considered by varying Θ_J' and ϕ_J' in one-quarter degree increments. The distance between these (P_J') adjacent patches and P_I is $S(P_I, \Theta_J', \phi_J')$.

$$S(P_I, \Theta_J', \phi_J') = [r^2 + T^2 - 2Tr \cos \Theta_J' \cos \phi_J']^{1/2}$$

where Θ_J' and ϕ_J' are angles relative to Θ_J and ϕ_J . $S(P_I, \Theta_J', \phi_J')$ equals $X(a, b:c, d)$ (see Eq. III-2).

NOTATION

Symbols used only in one section are not included in this list.

A	Hamaker constant
C	ion concentration - molar
D	Einstein diffusion coefficient
DCA	distance of closest approach
F	total interaction parameter
f	Stokes' friction coefficient for a sphere
f(a, b:c, d)	force between grids on separate spheres
I	ionic strength - molar
k	Boltzmann constant
M	polymer molecular weight
M _o	monomer molecular weight
N	Avogadro's number
N ₁	adsorption site density in Stern layer
n	particle number concentration per cc or degree of polymerization
OFD	optimum flocculation dose
Q	particle charge
R	particle radius
R _G	radius of gyration
S	separation distance between particle surfaces
T	temperature
V _A	van der Waal's attractive energy
V _h	hydrodynamic volume of polymer molecule

V_R	energy of repulsion between two spheres
V_T	total interaction energy between two spheres
Z	ion valence
α	collision efficiency factor
δ	Stern layer thickness
ϵ	dielectric constant
ϵ'	dielectric constant in Stern layer
η	viscosity
$[\eta]$	intrinsic viscosity
κ^{-1}	double layer thickness = $\left[\frac{\epsilon kT}{8\pi n e^2 z^2} \right]^{1/2}$
σ	surface charge density
σ_1	Stern layer charge density
σ_2	diffuse layer charge density
τ	turbidity
ϕ	Stern specific interaction energy
ψ_0	surface potential
ψ_s	Stern potential

REFERENCES

1. Adamson, A. W. , Physical Chemistry of Surfaces, Interscience Publishers, New York (1967).
2. "Approved Coagulant Aids," The American City, 85, No. 8, 72 (1970).
3. Bailey, G. W. and White, J. L., "Factors Influencing the Adsorption, Desorption, and Movement of Pesticides in Soil," Residue Reviews, 32, 29 (1970).
4. Binford, J. S. and Gessler, A. M., "Multisegment Adsorption of Long Chain Polymers on Carbon Black," J. Phys. Chem., 63, 1376 (1959).
5. Birkner, F. B., The Destabilization of Dilute Clay Suspensions with Labelled Polymers, Ph.D. Thesis, University of Florida (1965).
6. Birkner, F. B. and Edzwald, J. K., "Nonionic Polymer Flocculation of Dilute Clay Suspensions," J. AWWA, 61, 645 (1969).
7. Birkner, F. B. and Morgan, J. J., "Polymer Flocculation Kinetics of Dilute Colloidal Suspensions," J. AWWA, 60, 175 (1968).
8. Black, A. P., "Challenges of Quality Water," J. AWWA, 56, 1279 (1964).
9. Black, A. P. and Smith, A. L., "Determination of the Mobility of Colloidal Particles by Microelectrophoresis," J. AWWA, 54, 926 (1962).

10. Black, A. P. and Vilaret, M. R., "Effect of Particle Size on Turbidity Removal," J. AWWA, 61, 209 (1969).
11. Botham, R. and Thies, C., "The Effect of Stereoregularity upon the Adsorption Behavior of High Molecular Weight Poly (Isopropyl Acrylate)," Preprints 43rd National Colloid Symposium Cleveland, Ohio (1969).
12. Brunauer, S., Emmett, P. H. and Teller, E., "Adsorption of Gases in Multimolecular Layers," J. Amer. Chem. Soc., 60, 309 (1938).
13. de Bruyn, P. L. and Agar, G. E., "Surface Chemistry of Flotation," a chapter in Froth Flotation, D. W. Fuerstenau, ed. (1962).
14. Corning Glass Works, "Properties of Selected Commercial Glasses," Publication B-83, Corning, New York (1965).
15. Davis, S. N. and DeWiest, R., Hydrogeology, Wiley, New York (1966).
16. Dickert, C. T., private communication to J. J. Morgan (1966).
17. DiMarzio, E. A., "Proper Accounting of Conformations of a Polymer Near a Surface," J. Chem. Phys., 42, 2101 (1965).
18. DiMarzio, E. A. and McCrackin, F. L., "One-Dimensional Model of Polymer Adsorption," J. Chem. Phys., 43, 539 (1965).

19. Dixon, J. K. and Zielyk, M. W., "Control of the Bacterial Content of Waters with Synthetic Polymer Flocculants," *Environ. Sci. Technol.*, 3, 551 (1969).
20. Dixon, J. K. et al, "Effect of the Structure of Cationic Polymers on the Flocculation and Electrophoretic Mobility of Crystalline Silica," *J. Colloid Interface Sci.*, 23, 465 (1967).
21. Felter, R. E. and Ray, L. N., Jr., "Polymer Adsorption Studies at the Solid-Liquid Interface Using Gel Permeation Chromatography," *J. Colloid Interface Sci.*, 32, 349 (1970).
22. Flory, P. J., Principles of Polymer Chemistry, Cornell University Press, Ithaca, New York (1953).
23. Fontana, B. J. and Thomas, J. R., "The Configuration of Adsorbed Alkyl Methacrylate Polymers by Infrared and Sedimentation Studies," *J. Phys. Chem.*, 65, 480 (1961).
24. Gregory, J., "Flocculation of Polystyrene Particles with Cationic Polyelectrolytes," *Trans. Faraday Soc.*, 65, 2260 (1969).
25. Hamaker, H. C., "The London-van der Waals Attraction Between Spherical Particles," *Physica*, 4, 1058 (1937).
26. Hara, K., Mizuhara, K. and Imoto, T., "Adsorption of Polymers at the Solution-Solid Interface," *Kolloid-Z. u. Z. Polmere*, 238, 438 (1970).

27. Hawkes, B. E., "Polyelectrolytes in Water Treatment,"
J. New England Water Works Assoc., 84, 189 (1970).
28. Higuchi, W. I., "Effects of Short Range Surface-Segment
Forces on the Configuration of an Adsorbed Flexible
Chain Polymer," J. Phys. Chem., 65, 488 (1961).
29. Hoeve, C. A., "Density Distribution of Polymer Segments
in the Vicinity of an Adsorbing Interface," J. Chem. Phys.,
43, 3007 (1965).
30. Howard, G. J. and McConnell, P., "Adsorption of Polymers
at the Solution-Solid Interface, 1. Polyethers on Silica,"
J. Phys. Chem., 71, 2974 (1967).
31. Hyde, A. J. and Taylor, R. B., "Light-Scattering Studies
on Model Polyelectrolyte Systems," in Solution
Properties of Natural Polymers, The Chemical Society,
Special Publication No. 23, London (1968).
32. Iler, R. K., The Colloid Chemistry of Silica and Silicates,
Cornell University Press, Ithaca, New York (1955).
33. Jellinek, H. H. G. and Northey, H. L., "Adsorption of
High Polymers from Solution on to Solids,"
J. Polymer Sci., 14, 583 (1954).
34. Jones, R. H., Liquid-Solids Separation in Domestic Waste
with a Cationic Polyelectrolyte, Ph.D. Thesis, University
of Florida (1966).
35. Kipling, J. J., Adsorption from Solutions of Non-Electrolytes,
Academic Press, New York (1965).

36. Kruyt, H. R., editor, Colloid Science Vol. I Irreversible Systems, Elsevier Publishing Co., Amsterdam (1952).
37. LaMer, V. K. and Healy, T. W., "Adsorption-Flocculation Reactions of Macromolecules at the Solid-Liquid Interface," *Rev. Pure Appl. Chem. (Australia)* 13, 122 (1963).
38. McCrackin, F. L., "Configuration of Isolated Polymer Molecules on Solid Surfaces Studied by Monte-Carlo Computer Simulation," *J. Chem. Phys.*, 47, 1980 (1967).
39. Miller, M. L., The Structure of Polymers, Reinhold Book Corp., New York (1966).
40. Motomura, K. and Matuura, R., "Conformation of Adsorbed Polymeric Chain," *Mem. Fac. Sci., Kyushu Univ.*, 6, 97 (1968).
41. Motomura, K. and Matuura, R., "Conformation of Adsorbed Polymeric Chain II," *J. Chem. Phys.*, 50, 1281 (1969).
42. Neihof, R., "Microelectrophoresis Apparatus Employing Palladium Electrodes," *J. Colloid Interface Sci.*, 30, 128 (1969).
43. O'Melia, C. R. and Stumm, W., "Aggregation of Silica Dispersions by Iron III," *J. Colloid Interface Sci.*, 23, 437 (1967).
44. Ottewill, R. H., Rastogi, M. C. and Watanabe, A., "The Stability of Hydrophobic Sols in the Presence of Surface Active Agents," *Trans. Faraday Soc.*, 56, 854 (1960).

45. Ottewill, R. H. and Shaw, J. N., "An Electrophoretic Investigation of the Behavior of Monodispersed Polystyrene Latices in Solutions of Lanthanum, Neodymium, and Thorium Nitrates," *J. Colloid Interface Sci.*, 26, 110 (1968).
46. Overbeek, J., Chapter VI in Colloid Science V.1, H. R. Kruyt, ed., Elsevier Publishing Co., Amsterdam (1952).
47. Parks, G. A., "Aqueous Surface Chemistry of Oxides and Complex Minerals," published in Equilibrium Concepts in Natural Water Systems, Adv. in Chem. Series, No. 67, ACS (1967).
48. Patat, F., Killmann, E. and Schliebener, C., "Adsorption of Macromolecules from Solution," *Fortschritte der Hochpolymeren Forschung* 3, 332 (1964); English translation in *Rubber Chem. and Tech.*, 39, 36 (1966)
49. Pennsylvania Glass Sand Corp., Min-U-Sil Data Sheet No. 1001-31167 MH, Pittsburg, Pa.
50. Perkel, P. and Ullman, R., "The Adsorption of Polydimethylsiloxanes from Solution," *J. Polymer Sci.*, 54, 127 (1961).
51. Peterson, C. and Kwei, T. K., "The Kinetics of Polymer Adsorption onto Solid Surfaces," *J. Phys. Chem.*, 65, 1330 (1961).

52. Peyser, P. and Ullman, R., "Adsorption of Poly-4-vinylpyridine onto Glass Surfaces," *J. Polymer Sci. Part A*, 3, 3165 (1965).
53. Riegel, B. and Prout, F. S., "The Synthesis of Progesterone-21-C¹⁴," *J. Org. Chem.*, 13, 933 (1948).
54. Roe, R. J., "Conformation of an Isolated Polymer Molecule at an Interface," *Proc. Natl. Acad. Sci.*, 53, 50 (1965).
55. Roe, R. J., "Conformation of an Isolated Polymer Molecule at an Interface. II Dependence on Molecular Weight," *J. Chem. Phys.*, 43, 1591 (1965).
56. Rubin, R. J., "A Random Walk Model of Chain Polymer Adsorption at a Surface. III Mean Square End-to-End Distance," *J. Res., Nat. Bureau Stds.*, B 70B, 237 (1966).
57. Sakaguchi, K. and Nagase, K., "The Flocculation of Kaolin and Precipitated Calcium Carbonate by Polymers," *Bull. Chem. Soc. Japan*, 39, 88 (1966).
58. Shaw, D. J., Introduction to Surface Chemistry, Butterworths, London (1966).
59. Shyluk, W. P., "Poly(1,2-dimethyl-5-vinylpyridinium Methyl Sulfate), Part I Polymerization Studies," *J. Polymer Sci., A* 2, 2191 (1964).
60. Shyluk, W. P., "Poly(1,2-dimethyl-5-vinylpyridinium Methyl Sulfate), Part II Polymer Properties," *J. Applied Polymer Sci.*, 8, 1063 (1964).

61. Shyluk, W. P., "Poly(1,2-dimethyl-5-vinylpyridinium Methyl Sulfate), III Adsorption on Crystalline Silica," J. Polymer Sci., A-2, 6, 2009 (1968).
62. Silberberg, A., "Adsorption of Flexible Macromolecules. III Generalized Treatment of the Isolated Macromolecule; The Effect of Self Exclusion," J. Chem. Phys., 46, 1105 (1967).
63. Silberberg, A., "Adsorption of Flexible Macromolecules. IV Effect of Solvent-Solute Interactions, Solute Concentration and Molecular Weight," J. Chem. Phys., 48, 2835 (1968):
64. Smith, L. E. and Stromberg, R. R., "Measurement of Optical Constants: Optical Constants of Liquid Mercury at 5461 Å," J. Opt. Soc. Am., 56, 1539 (1966).
65. Smoluchowski, M., "Versuch einer methematischen Theorie der Koagulations-kinetic kolloider Losungen," A. Physik. Chemie., XCII, 129 (1916).
66. Steinberg, G., "On the Configuration of Polymers at the Solid-Liquid Interface," J. Phys. Chem., 71, 292 (1967).
67. Stern, O., "Zur Theorie Der Elektrolytischen Doppelschucht," Z. Elektrochem., 30, 508 (1924).
68. Stromberg, R. R. and Smith, L. E., "Conformation of Polystyrene on Liquid Mercury," J. Phys. Chem., 71, 2470 (1967).
69. Stumm, W. and O'Melia, R., "Stoichometry of Coagulation," J. AWWA, 60, 515 (1968).

70. Tanford, C., Physical Chemistry of Macromolecules, Wiley, New York (1961).
71. Tilton, R. C. and Dixon, J. K., "Control of the Algae Content of Water with Synthetic Polymeric Flocculants," Amer. Chem. Soc. Preprints, Atlantic City (1968).
72. United States Geological Survey, The Industrial Utility of Public Water Supplies in the U. S., Water Supply Paper 1299 (1952).
73. van Olphen, H., An Introduction to Clay Colloid Chemistry, Interscience Publishers, New York (1963).
74. Verwey, E. J. W. and Overbeek, J., Theory of the Stability of Lyophobic Colloids, Elsevier Publishing Co., Amsterdam (1948).
75. Walles, W. E., "Role of Flocculant Molecular Weight in the Coagulation of Suspensions," J. Colloid Interface Sci., 27, 797 (1968).
76. Watillon, A. and Joseph-Petit, A. M., "Interactions Between Particles of Monodispersed Polystyrene Latices," Diss. Faraday Soc., 42, 143 (1966).
77. Zimm, B. H., "The Scattering of Light and the Radial Distribution Function of High Polymer Solutions," J. Chem. Phys., 16, 1093 (1948).